

Doctoral Thesis

**Indium nitride growth with in situ
surface modification by RF-MBE**

March 2019

Doctoral Program in Advanced Electrical, Electronic and Computer Systems
Graduate School of Science and Engineering
Ritsumeikan University

FAIZULSALIHIN BIN ABAS

Doctoral Dissertation Reviewed
by Ritsumeikan University

**Indium nitride growth with in situ
surface modification by RF-MBE**

(RF-MBE 法による in situ 表面改質を用いた窒化インジウム成長)

March 2019

2019 年 3 月

Doctoral Program in Advanced Electrical, Electronic and Computer Systems
Graduate School of Science and Engineering
Ritsumeikan University

立命館大学大学院 理工学研究科
電子システム 専攻 博士課程後期過程

FAIZULSALIHIN BIN ABAS

ファイズルサリヒン ビン アバス

Supervisor: Professor ARAKI Tsutomu

研究指導教員: 荒木 努 教授

Abstracts

Indium nitride (InN) has the smallest effective mass, the largest mobility, the smallest direct-band gap energy and a high Seebeck coefficient among III-nitride semiconductors. Thus, it is a very promising material for various applications including high-speed electronic, long-wavelength optoelectronic devices, high efficiency solar cells and thermoelectric devices. However, high crystalline quality InN is the most difficult to be obtained due to its low dissociation temperature and lack of lattice-matched substrate. The hetero-epitaxial InN films have an extremely high density of threading dislocations (10^{10} – 10^{11} cm⁻²). These threading dislocations contribute to non-radiative recombination centers, dominant scattering centers limiting electron mobility and probably one of the origins of residual electrons in InN. Therefore, the objective of this research is to reduce threading dislocation density in InN to clarify its material performance and pursue its applicability.

In this study, we propose a new approach which provides a simple but effective growth process for threading dislocation reduction in InN film with in situ surface modification by radio-frequency molecular beam epitaxy (RF-MBE). In this method, we apply nitrogen radical irradiation to modify surface morphology of InN template in situ in MBE growth chamber before regrowing InN film on the template.

Transmission electron microscopy (TEM) revealed that threading dislocation density in InN grown with this method reduced by a factor of 3 from 2×10^{10} cm⁻² to 6×10^9 cm⁻². We clarified that the mechanism of the threading dislocations reduction was due to the inclination, fusion, and annihilation of edge dislocations at the regrowth interface. In addition, the repeatability of this method was also investigated. TEM showed evidence that the threading dislocation density was successfully reduced step by step from $\sim 2.8 \times 10^{10}$ cm⁻² in the first irradiated layer to $\sim 2.0 \times 10^{10}$ cm⁻² in the second irradiated layer, and to $\sim 1.3 \times 10^{10}$ cm⁻² in the top regrown InN film. If this technology is established, high-quality InN with low threading dislocation density can be achieved with an easy, simple and repeatable growth process. Furthermore, this method might also be applicable for threading dislocation density reduction in other III-nitride semiconductors and contribute to the realization of future electronic and optoelectronic device applications.

Table of Contents

Title	
Abstract	
Chapter 1 Introduction	1
1.1 Research background.....	3
1.2 III-nitride semiconductors.....	5
1.3 Indium nitride.....	8
1.4 Threading dislocation	10
1.5 Research aim	15
1.6 Outline of thesis	16
Chapter 2 Crystal growth technology	21
2.1 Epitaxial growth.....	23
2.2 Molecular beam epitaxy (MBE).....	23
2.3 Configuration of RF-MBE system	24
2.4 Radio frequency (RF) plasma	26
2.5 Knudsen cell	27
2.6 Crystal growth technique in nitride semiconductors	28
2.7 InN crystal growth technique.....	29
Chapter 3 Characterization methods	35
3.1 Reflection high energy electron diffraction (RHEED).....	37
3.2 Scanning electron microscopy (SEM).....	39
3.3 Transmission electron microscopy (TEM).....	42
3.4 Atomic force microscopy (AFM).....	47
3.5 X-ray diffractometry (XRD)	48
3.6 Hall effect measurement	51
3.7 Photoluminescence (PL) spectroscopy	53
Chapter 4 InN growth with in situ surface modification by radical beam irradiation (1)	57
4.1 Introduction.....	59
4.2 In situ surface modification by N radical irradiation.....	62
4.2.1 Experimental method.....	63
4.2.2 Substrate temperature dependency	65
4.2.3 Plasma power dependency	68
4.2.4 Irradiation time dependency	72
4.2.5 Comparison between N radical beam irradiation and annealing.....	73
4.2.6 Summary.....	76

4.3 InN regrowth on N radical irradiated InN template	77
4.3.1 Experimental method.....	77
4.3.2 Threading dislocation behaviors by cross-sectional TEM observation	78
4.3.3 Mechanisms of threading dislocation reduction.....	80
4.3.4 Summary.....	84
4.4 Conclusion.....	85
Chapter 5 InN growth with in situ surface modification	
by radical beam irradiation (2).....	89
5.1 Introduction.....	91
5.2 InN regrown on templates irradiated with different N radical irradiation time	91
5.2.1 Experimental method.....	92
5.2.2 Effects on threading dislocation behaviors	93
5.2.3 Surface morphology, electrical characteristics and optical properties.....	96
5.2.4 Summary.....	99
5.3 Relationship between the thickness of irradiated template with crystallographic	
quality and electrical properties of InN film.....	100
5.3.1 Experimental method.....	100
5.3.2 Experimental results and discussion.....	102
5.3.3 Summary.....	107
5.4 Repeatability of in situ surface modification by radical beam irradiation	
to reduce threading dislocation density in InN	108
5.4.1 Experimental method.....	108
5.4.2 Experimental results and discussion.....	110
5.4.3 Additional experiments.....	115
5.4.4 Summary.....	122
5.5 Conclusion.....	123
Chapter 6 Summary	127
Research achievements.....	131
Acknowledgements	

- References are listed at the end of each chapter.

Chapter 1

Introduction

Chapter 1

Introduction

1.1 Research background ^[1-7]

We are living in a phenomenal time of hyper-network that is reshaping our cultures and societies. Furthermore, this has just barely started. The internet has turned into the ubiquitous cloud that is associating each part of our daily lives including communication, search engines, information gathering, e-commerce, and remote devices. The information and communication technologies support our modern society, and none of this would be conceivable without the most fundamental building block which is the core material of the modern world: the semiconductor ^[1]. The semiconductor is a standout amongst the most pervasive and ground-breaking creations in mankind's history. It has been positioned fourth in the rundown of “The 50 Greatest Breakthroughs Since the Wheel”, behind the printing press, electricity, and penicillin, but ahead of eyeglasses, paper, and the steam engine ^[2]. The properties of semiconductor materials make feasible various innovative technologies including transistors, microchips, solar cells and LED displays. Much of present modern life would be altogether different without transistors and integrated circuits made of semiconductors. No computers, smartphones and tablets would deal with undertakings tasks at work and home, nor would microprocessors control the operations of cars, planes, and space vehicles.

The revolution in electronics that made such wonders conceivable started in 1947, when the first transistor was invented by Walter H. Brattain, John Bardeen and William B. Shockley at Bell Labs ^[3]. Their invention prompted a smaller, lighter, and more durable substitution for the vacuum tube which were an innovation broadly adopted in the 1920s. Vacuum tubes could amplify electrical signals in radios and stereos, and fill in as the on-off switch necessary for the binary code utilized in computers ^[4]. The transistor which is ultimately more efficient and significantly smaller could do this and more. The first transistor was a point-contact transistor in which contact was made between a piece of germanium and three wires. Soon afterwards, the more reliable junction transistor which consists of two types of germanium (n-type and p-type) produced by adding small amount of impurities was invented by Shockley ^[5]. Silicon turned into the favored material for making transistors and its capacity to form a dioxide layer effectively also made the

present integrated circuits attainable.

Such silicon integrated circuit innovation has been driving development of today's advanced information and network society by miniaturizing the device size of metal-oxide-semiconductor field-effect transistor (MOSFET) which is the fundamental component, as according to the scaling principle [6]. Currently, devices with gate processing dimensions of MOSFET of 32 nm or less, and devices with a three-dimensional gate structure have been put into practical use. Later on, this miniaturization technology is yet vital for integrated circuit technology but in the current situation where the device size has been scaling down to nanometer scale, the aspect of the electronics field which has been developed mainly by silicon integrated circuits is rapidly changing.

We often hear the names of devices, for example, LSIs, DRAMs and CPUs when talking about semiconductors. These devices are mainly utilized for information and signal processing, and quietly operate in different sorts of applications such as cell phones, computers, cars, and control systems for huge plants [7]. Aside from this, there are likewise semiconductor devices utilized for energy processing, and such semiconductor devices are called power devices. These power devices perform a noteworthy role in hybrid vehicles and inverters. Besides, well-known solar cells are ones that convert sunlight into electrical energy. Conversely, devices transmitting or accepting energy through light, the so-called optical devices are equipped in numerous workaday things, for example, semiconductor lasers used in CD/DVD players, laser pointers, and light emitting diodes (LED). These are quickly spreading as a method for energy-saving illumination that convert electrical energy into light.

Accordingly, power and optical devices will turn out to be progressively indispensable in the future, and the enhancement of performance, adequate supply, and cost reduction will be essential. The basis of such new innovation improvement lies in material advancement. Silicon has been the standard material of sensor devices and power semiconductor devices since it exists in the surface layer of Earth and its availability is higher than oxygen, making it appropriate for large scale manufacturing and low-cost production. However, from the perspective of physical limitations and diversity of functions, it is required to acknowledge high performance and high function by acquainting new semiconductor materials to extend the field of electronics applications. Hence, the cutting-edge semiconductors called wide-gap semiconductors are drawing in consideration, and one of them is group III-nitride semiconductors.

1.2 III-nitride semiconductors [8-13]

Recently, advancement and ascendancy of III-nitride-based semiconductors have been phenomenal. Performance of the III-nitride devices enhanced very rapidly since the mid 1990s. Light emitting diodes (LED) in the blue and the green regions of the spectrum are also being made from III-nitride semiconductors and have been commercialized. The applications have already been applied to various fields such as large displays, traffic signals, cell phones, and so forth. Furthermore, accessing the ultraviolet (UV) and visible spectral ranges with semiconductors which requires a very large bandgap material is most commonly accomplished with the III-nitride compounds. These materials have fascinating potentials to revolutionize numerous industries, medicine, military, agriculture, communication, space exploration and scientific systems because of their high mechanical strength and durability.

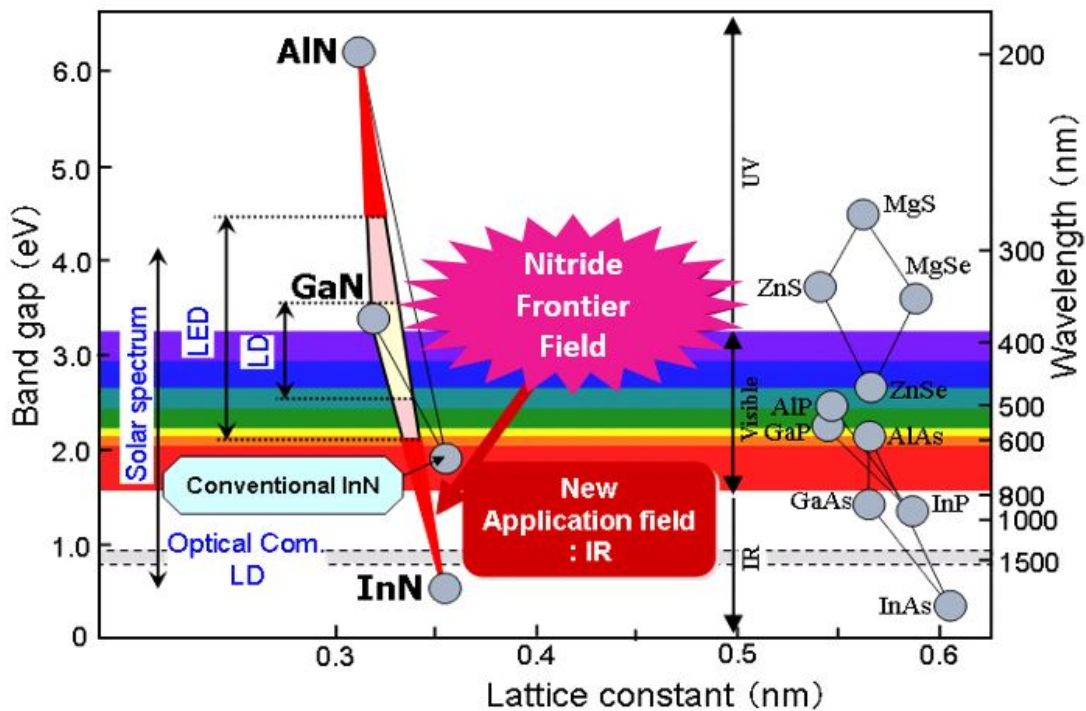


FIG. 1.1. Compound semiconductors lattice constant and bandgap energy [10]

As shown in Fig. 1.1, group III-nitride semiconductors consist of aluminum nitride (AlN), gallium nitride (GaN), indium nitride (InN) and their alloys. They are both direct transition semiconductors and have extremely wide band gaps. Their bandgap energy span from ~ 6.2 eV (AlN) to ~ 3.4 eV (GaN) and ~ 0.65 eV (InN). When InN or/and AlN

alloyed with GaN, it allows tuning of band gaps and emission wavelengths. They can also work at higher temperatures as well as in hostile environments. Moreover, they are robust, chemically, mechanically and thermally stable, and impervious materials to radiation. In this way, they have great astounding highlights for viable device applications. Table 1.1 shows the comparison of physical property constants of conventional semiconductor and III-nitride semiconductor materials.

TABLE 1.1. Physical property constants of conventional and III-nitride semiconductors ^[14-15]

Material	Band gap (eV)	Dielectric constant	Effective mass	Electron mobility (cm ² /Vs)	Breakdown electric field (10 ⁶ V/cm)	Saturated drift velocity (10 ⁷ cm/s)	Thermal conductivity (W/cm K)
InN	0.65 ^[11]	15.0	0.042 ^[12]	14000 ^[13]	2.0	5.0 ^[13]	0.8
GaN	3.39	9.0	0.22	900/1200	3.3	2.7	2.0
AlN	6.2	8.5	0.29	—	—	2.0	2.9
Si	1.12	11.8	0.19	1400	0.3	1.0	1.5
GaAs	1.43	12.8	0.067	8500	0.4	2.0	0.5
6H-SiC	2.93	9.7	0.42	80/400	2.8	1.9	4.9
Diamond	5.47	5.5	0.20	2200	10.0	2.7	20.0

By having nitrogen (N) which is a light element as a V-element constituting nitride semiconductor, they have strong interatomic forces of Al-N, Ga-N, and In-N, and their lattice constants are also smaller than that of conventional semiconductors. They have a large dielectric breakdown electric field and a high saturation drift velocity and thus, they are effective not only for optical devices but also as materials for high-frequency devices and environmental resistance power devices. Furthermore, since they contain no highly toxic materials such as phosphorus (P) and arsenic (As), it can be said that they are safe materials. Table 1.2 shows examples of applications of optical and electronic devices using nitride semiconductors. A wide range of applications from optical devices to electronic devices are expected by making full use of the features of nitride semiconductors.

TABLE 1.2. Examples of applications using III-nitride semiconductors
(Modified by the author) [8]

Device applications	System applications
Blue, green, white LED	Full color large display, signal light, illumination, agriculture, fishery, medicine
Blue-violet, ultraviolet laser	Blu-ray disk, high density optical recording, photo excitation process, chemical analysis
High output frequency device	4 th generation transition communication, satellite communication, multimedia wireless access, intelligent transportation system, home network
Environment resistant power device	High temperature operating device, engine control, space electronic system, high power high efficiency inverter/converter
Ultraviolet light detection device	Ozone layer detection, fire sensor, takeoff and landing induction, combustion control
Cold cathode field emission device	Flat display, vacuum microelectronic system
Intersubband transition light device	Next generation ultrahigh-speed optical communication system, wide band wavelength conversion system, trace gas detection and analysis system, mid-infrared laser

However, there are no suitable lattice-matched substrates for III-nitride semiconductors, and crystal growth of III-nitride semiconductors are considered to be difficult. While the way to great device quality epitaxy of the III-nitride semiconductors is far from simple, the infrastructure is currently across the board; blue LEDs and lasers are mass produced and cheap. We have to acknowledge that this is not yet a mature technology, but research endeavors are as yet in progress to create higher quality device templates, higher quality UV cameras, shorter wavelength laser diodes, and more efficient green emitters for full color displays and lighting. The III-nitride semiconductors can possibly get to a substantially more extensive scope of the spectrum, as discussed previously.

1.3 Indium nitride ^[16]

Indium nitride (InN) has pulled in much attention and has been extensively studied, especially since 2002. Its band gap energy was found to be about 0.65 eV ^[11, 17, 18], not 1.9 eV ^[19] which was accepted for more than 30 years. The improvement of metalorganic vapor phase epitaxy (MOVPE) and radio frequency molecular beam epitaxy (RF-MBE) growth technologies have made it achievable to obtain high-quality InN films and lead to the elucidation of its true band gap energy. This significant revelation implies that the wavelength ranges secured by nitride semiconductors is extended toward near infrared light, which also included optical communication wavelengths of 1300 nm and 1550 nm. InN has a bandgap energy smaller than Si and the smallest bandgap energy among III-nitride semiconductors. Its ternary alloys, for example, InGaN and InAlN cover a wide wavelength region and along these lines give the possibilities for creating numerous optoelectronic devices including high-efficiency solar cells and laser diodes in optical communication wavelength regions ^[20-21]. Besides, as shown in Table 1.1, InN has also the smallest electron effective mass among III-nitrides. This prompts a much higher electron mobility than that of GaN and makes InN potentially applicable in high-speed electronic devices. Moreover, some groups reported that InN has a high Seebeck coefficient ^[22] which is a crucial parameter for thermoelectric device applications ^[23, 24]. Different applications, for example, gas sensor ^[25], terahertz wave device ^[26] and so forth are additionally anticipated.

However, the epitaxy of high crystalline quality InN and its alloys are the most difficult compared to GaN and AlN mainly due to the low dissociation temperature of InN, high equilibrium vapor pressure of nitrogen molecules and the absence of suitable substrates for InN growth. Contrasted with GaN and AlN, the equilibrium vapor pressure of nitrogen of InN is larger as shown in Fig. 1.2 ^[27]. Since InN has an extremely low dissociation temperature and the equilibrium vapor pressure of nitrogen at its growth temperature is high, growth of InN at high temperature is troublesome. Consequently, it must be grown at low temperature which is around 500 °C. This prompts smaller surface migration and thus, it is difficult to obtain high quality InN crystals.

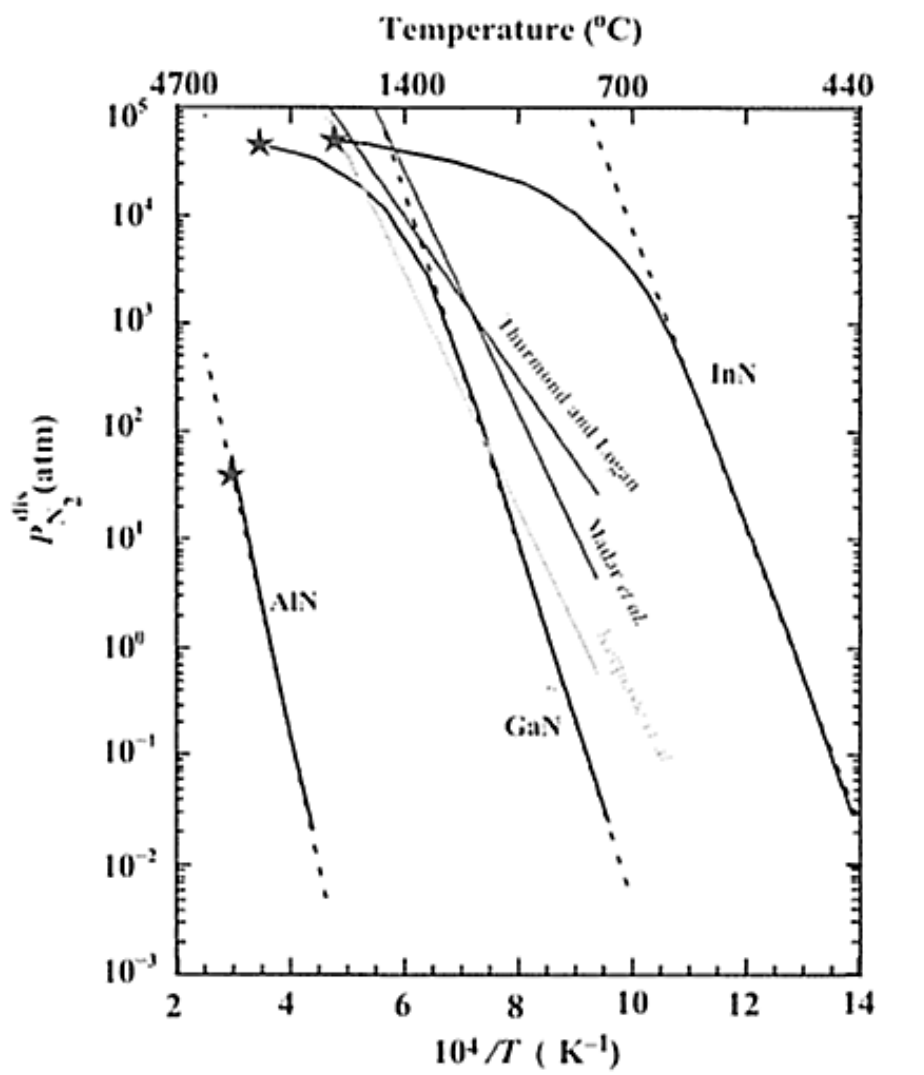


FIG. 1.2. Temperature dependence of equilibrium vapor pressure of N in nitride semiconductors [27]

In addition, control of V/III ratio is essential in crystal growth by MBE method. As a method to solve this issue, InN growth was carried out using droplet elimination by radical beam irradiation (DERI) method as proposed previously by our group [28]. By this method, high quality InN crystals can be obtained with high reproducibility without strict control of the V/III ratio. However, to date, almost all InN thin films are grown on foreign substrates such as sapphire, AlN and GaN because of the absence of substrate matching the lattice constant of InN. These substrates have large lattice mismatch with InN which are 25.4%, 14%, and 11% for sapphire, AlN and GaN, respectively. Thus, the heteroepitaxial InN films still have an extremely high density of threading dislocations, which is around 10^{10} to 10^{11} cm^{-2} .

1.4 Threading dislocation [27, 29-31]

A crystal imperfection can exist within crystal lattices and the movement of the imperfection at low stress levels prompts deformation. This imperfection is called threading dislocation (TD), as postulated by G. I. Taylor, E. Orowan, and M. Polanyi in 1934. Later on, in 1939, a concept of dislocation theory known as Burgers vector was presented by J. M. Burgers to portray the character of threading dislocation.

There are three sorts of threading dislocations: screw dislocation, edge dislocation, and mixed dislocation. In the wurtzite structure of the group III nitride semiconductors, the Burgers vector (\mathbf{b}) of these dislocations are $\langle 0001 \rangle$, $\langle 11\bar{2}0 \rangle/3$, and $\langle 11\bar{2}3 \rangle/3$ for screw dislocation, edge dislocation, and mixed dislocation, respectively. For example, Fig. 1.3 illustrates threading dislocations in GaN crystal; (a) unit lattice of GaN, (b) edge dislocation, (c) screw dislocation and (d) mixed dislocation. In the figures, “ \mathbf{b} ” denotes a Burgers vector, and “ \mathbf{l} ” denotes a dislocation line.

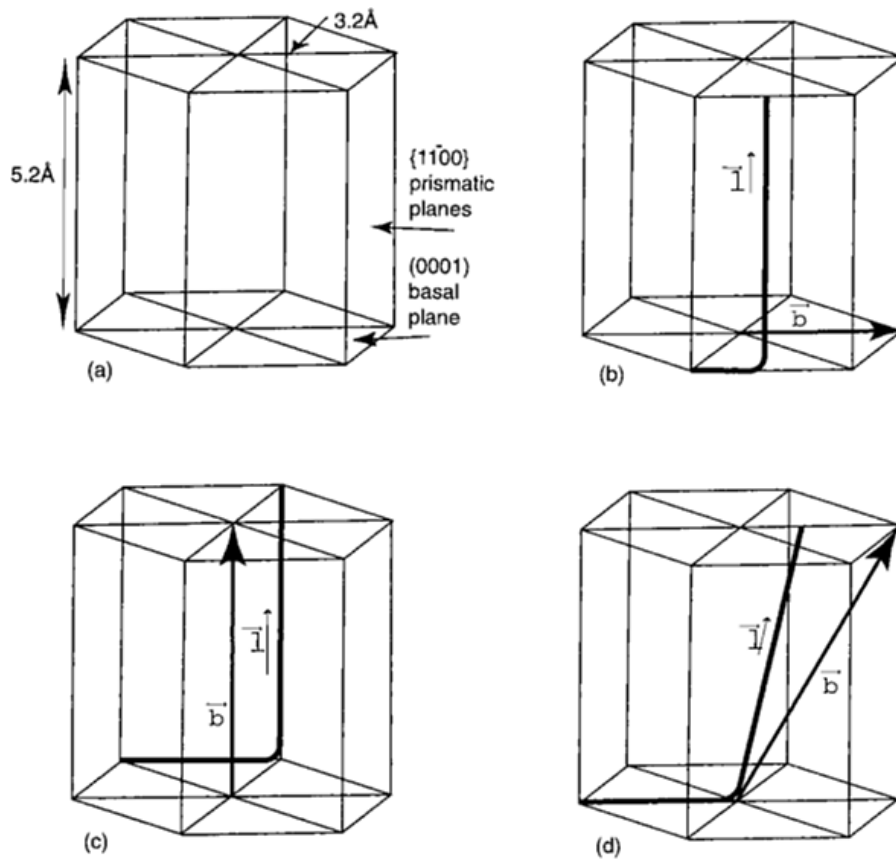


FIG. 1.3. Threading dislocations in GaN: (a) Unit lattice of GaN, (b) edge dislocation, (c) screw dislocation, and (d) mixed dislocation [31]

When a threading dislocation interacts with other threading dislocation, it will cause dislocations fusion and dislocations annihilation. The dislocations fusion occurs when two threading dislocations combine to form one resultant threading dislocation, and the Burgers vector becomes $\mathbf{b}_3 = \mathbf{b}_1 + \mathbf{b}_2$. On the other hand, when two threading dislocations with opposite Burgers vector ($\mathbf{b}_1 = -\mathbf{b}_2$) interact with each other, it will cause dislocations annihilation and the Burgers vector becomes $\mathbf{b}_1 + \mathbf{b}_2 = \mathbf{0}$. These two mechanisms are important concepts for reduction of threading dislocation density in a crystal.

There are a few different ways to observe and characterize these dislocations. If the dislocation appears on the surface of the crystal, it can be observed with an atomic force microscope (AFM). Besides, scanning electron microscope (SEM) can also be used to observe the pits appear at the surface which correspond to threading dislocation end after undergoing wet etching process. Additionally, in order to observe the threading dislocation inside the crystal, a transmission electron microscope (TEM) can be used and the dislocations can be characterized by using different diffraction vector, \mathbf{g} of the electron beam.

As mentioned previously, the density of threading dislocation in currently available InN film is very high due to large lattice mismatch with the foreign substrate used. Figure 1.4 shows an example of a cross-sectional TEM image of InN grown on GaN template with a diffraction vector, $\mathbf{g} = 1-100$. The dark lines observed are edge dislocations. The density of the threading dislocation in the sample is around 10^{10} cm^{-2} , and it is the common density for InN available at the present time [32, 33]. It was found that in InN film, the density of edge dislocation is about one to two orders higher than that of screw dislocation. More importantly, it is notable that these dislocations contribute to non-radiative recombination centers, carrier scattering centers, and probably one of the origins of residual electrons in InN.

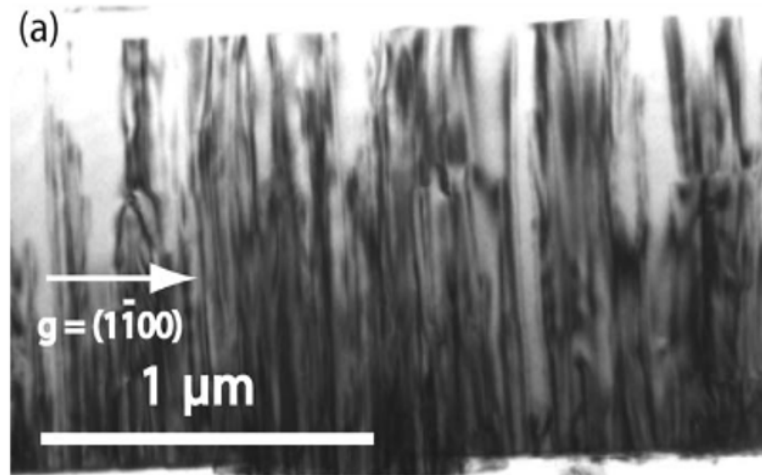


FIG. 1.4. A cross-sectional TEM image of InN grown on GaN ^[32]

(a) Non-radiative recombination centers ^[34]

The correlation between threading dislocations and non-radiative recombination centers in InN films was previously investigated by our group using infrared cathodoluminescence (CL). Panchromatic CL images of the InN films showed that a sample with a higher density of threading dislocations had a higher density of CL dark spots. As shown in Fig. 1.5, a correlation between threading dislocations and the non-radiative regions was also observed by cross-sectional panchromatic CL of the InN film regrown on micro-faceted InN template, in which the density of threading dislocation was dramatically reduced. Reduction of threading dislocation density is thought to lead to the improvement in optical characteristics on InN.

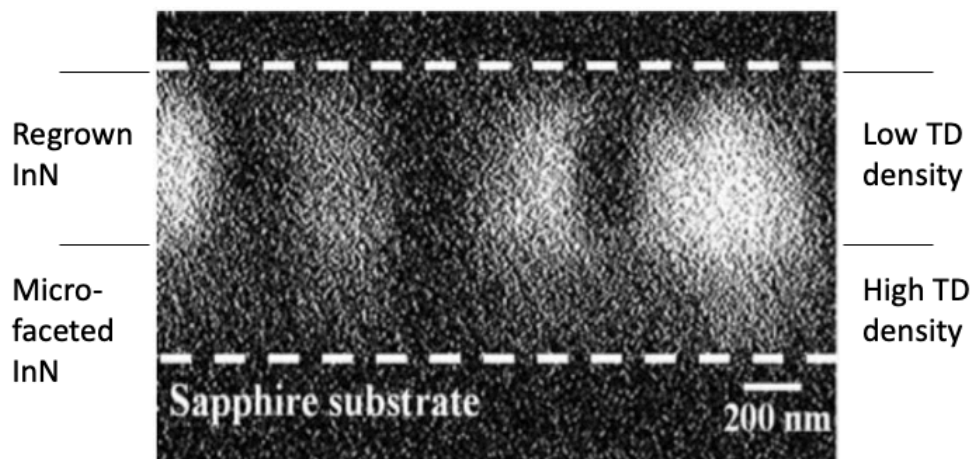


FIG. 1.5. Cross-sectional CL image of the InN film regrown on a micro-faceted InN template (Modified by the author) ^[34]

(b) Carrier scattering center ^[35-37]

It has been reported that threading dislocation is dominant in the electron scattering mechanism of InN. Look et al. first reported on the scattering of electrons by threading dislocations in InN ^[35]. Wang et al. reported that charged dislocation scattering limited the mobility of electrons in InN epilayers by a combined experimental and theoretical analysis ^[36]. They predicted that electron mobilities as high as 10000 cm²/Vs at room temperature can be achieved for InN with improvement in epitaxial growth techniques resulting in reduction of dislocation densities. Lebedev et al. analyzed microstructure and electron transport properties of heteroepitaxial InN films with varying thickness by variable temperature Hall-effect measurements and TEM ^[37]. They found that the threading dislocation density decay exponentially with epilayer thickness and observed exponential variations of both the carrier concentration and electron mobility with thickness. The relative insensitivity of the mobility with respect to the temperature suggests that a temperature-independent dislocation strain field scattering dominates over ionized impurity and phonon scattering, causing the increase of the mobility with rising layer thickness due to the reduced dislocation density ^[37]. Therefore, reduction of threading dislocation density is thought to lead to improvement in mobility.

(c) Origins of residual electrons in InN ^[37-41]

Some researchers suggested that threading dislocations with dangling bonds contribute electrons and might be the origin of the high electron concentration in all unintentionally doped InN films. Piper et al. showed that the formation of positively charged nitrogen vacancies at the cores of threading dislocations in InN are energetically favorable in the absence of impurities, suggesting that threading dislocations are the dominant donor in InN ^[39]. Lebedev et al. observed a relatively constant sheet density down to 100 K by variable temperature Hall measurements, and they suggested that as the evidence of direct carrier generation from threading dislocations ^[37]. They considered that edge dislocations have dangling bonds as shown in Fig. 1.6(a) and (b). Furthermore, Walukiewicz et al. suggested that dangling bonds in InN also release free electrons from the fact that Fermi level stabilization energy exists in the conduction band ^[40]. In addition, Fig. 1.7 shows the relationship between FWHM of (102) X-ray rocking curve and electrical characteristics in InN reported by Wang et al. ^[41]. The dotted line in the figure shows the electron concentration due to the dangling bond of edge dislocation which is almost similar to the carrier concentration, and it is considered that edge dislocation contributed to residual carriers in InN. However, a contrasting report of the need for negatively charged threading dislocations in InN for charge balance and no correlation

was observed between threading dislocation density and electron concentration were reported by Thakur et al. [42].

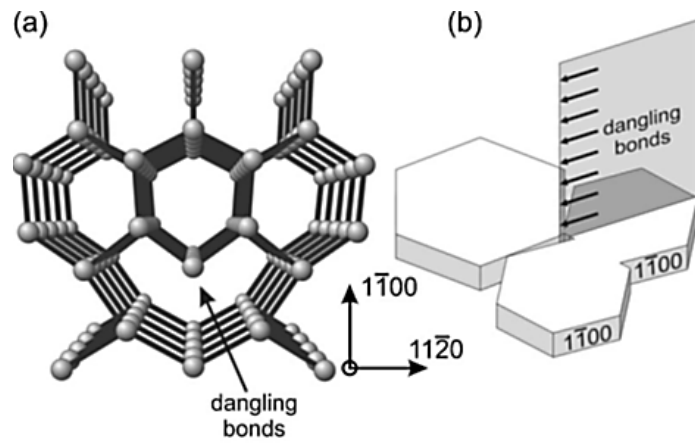


FIG. 1.6. Dangling bonds of edge dislocations [37]

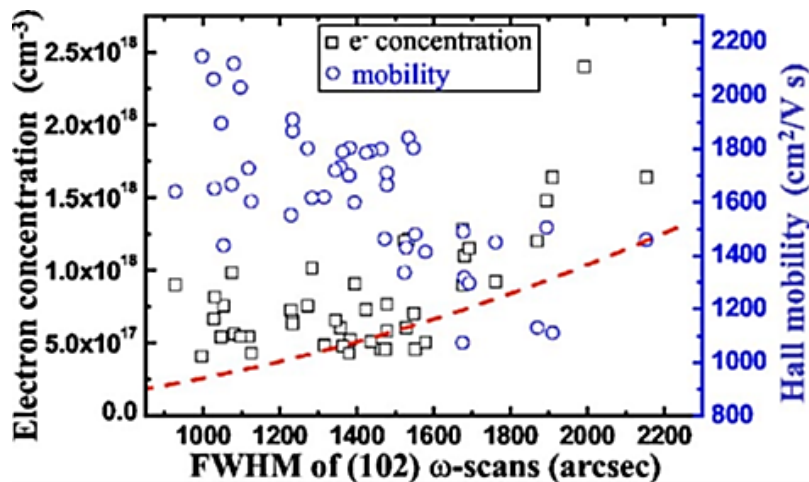


FIG. 1.7. Relationship between electrical characteristics and edge dislocation density [41]

Although there is no general agreement on the effect of threading dislocations on the carrier concentration in InN, there seems to be a consensus that threading dislocations contribute to non-radiative recombination centers, dominant scattering center limiting electron mobility and probably one of the origins of residual electrons in bulk InN. As described above, the high density of threading dislocations is considered to adversely affect the characteristics of InN. Therefore, a substantial study on the reduction of threading dislocation density is necessary to improve InN crystalline quality to utilize the full potential of InN for practical application of devices.

1.5 Research aim

The objective of this research is to improve InN crystalline quality in order to clarify its material performance and pursue its applicability for practical use. Since the presence of high threading dislocation density is one of the main issues that hindered the realization of high-quality InN, we put our efforts and focus on this fundamental issue to improve InN crystalline quality. Hitherto, nanocolumns growth^[43], selective-area lateral growth^[44] and regrowth on KOH-etched template^[45] have been reported as successful methods to reduce threading dislocation density in InN.

In this study, we propose an idea of InN growth with in situ surface modification by N radical beam irradiation. This method provides some advantages over the methods mentioned above such as:

- 1- Since this method is performed in situ during the growth process, there is no necessity to take the template out of MBE chamber compared to that in the regrowth on KOH-etched template method, and thus providing a repeatable growth process.
- 2- Furthermore, this method might be applicable to reduce threading dislocation density in a large area of InN film compared to nanocolumns growth method which only applicable to a very small area.
- 3- More importantly, this method requires no mask preparation before the InN growth compared to that in the selective-area lateral growth method and thus, providing a very simple growth process.

Therefore, if this technology is established, high-quality InN with low threading dislocation density can be achieved with an easy, simple and repeatable growth process. This will lead to the realization of various applications of InN and its related alloys such as high-speed electronic and long-wavelength optoelectronic devices. In this dissertation, the surface modification of InN by N radical beam irradiation, the threading dislocations behavior, crystallographic quality, electrical characteristics and luminescence properties of InN grown with this method are reported.

1.6 Outline of thesis

This dissertation comprises of all six chapters. The outline of each chapter will be described below.

Chapter 1 Introduction

In this chapter, we will describe the features of the III-nitride semiconductors, in particular, InN. We also describe the background, objectives and composition of this paper.

Chapter 2 Crystal growth technology

In this chapter, we will describe crystal growth technology of nitride semiconductors, in particular, InN. We will also describe the features of epitaxial growth and RF-MBE method used in this study.

Chapter 3 Characterization methods

In this chapter, we will describe the principles and configurations of RHEED, SEM, TEM, AFM, XRD, Hall effect measurement, and PL which are used for the evaluation and characterization of InN grown in this study.

Chapter 4 InN growth with in situ surface modification by radical beam irradiation (1)

In this chapter, we will describe the main idea of this dissertation. In situ surface modification of InN, threading dislocation behaviors and other results obtained from the experiments will be discussed.

Chapter 5 InN growth with in situ surface modification by radical beam irradiation (2)

In this chapter, we will describe further study on the InN growth with in situ surface modification by varying parameters such as irradiation time for the surface modification process and thickness of the template. The repeatability of the proposed method is also studied.

Chapter 6 Summary

In this chapter, we will summarize the contents of this research and conclude this dissertation.

References

- [1] M. Razeghi, *Vacuum* 146, 308 (2017).
- [2] J. Fallows, *The 50 Greatest Breakthroughs Since the Wheel* (The Atlantic, 2013).
- [3] J. Bardeen and W. H. Brattain, *Phys. Rev.* 71, 435 (1948).
- [4] J. E. Brittain, *Proceedings of the IEEE* 93, 1, 198 (2005).
- [5] W. Shockley, *The Bell System Technical Journal* 28, 3, 435 (1949).
- [6] R. H. Dennard, F. H. Gaensslen, V. L. Rideout, E. Bassous and A. R. LeBlanc, *IEEE J. Solid-State Circuits* 9, 256 (1974).
- [7] IHI Corporation, *IHI Engineering Review* 48, 1, 16 (2015).
- [8] K. Takasaki, *Kagoubutsu Handoutai No Saishin Gijutsu Daizenshuu* (The Latest Technology of Compound Semiconductors) (Technical Information Institute Co., Ltd., Tokyo, 2007) p. 14 [in Japanese].
- [9] S. C. Jain, M. Willander, J. Narayan, and R. Van Overstraeten, *J. Appl. Phys.* 87, 965 (2000).
- [10] Y. Nanishi, T. Araki, and T. Miyajima: *Oyo Buturi*, 72, 565 (2003) [in Japanese].
- [11] J. Wu, W. Walukiewicz, K. M. Yu, J. W. Ager III, E. E. Haller, H. Lu, W. J. Schaff, Y. Saito and Y. Nanishi, *Appl. Phys. Lett.* 80 3967 (2002).
- [12] A. A. Klochikhin, V. Yu. Davydov, V. V. Emtsev, A. V. Sakharov, V. A. Kapitonov, B. A. Andreev, Hai Lu and William J. Schaff, *Phys. Rev. B* 71, 195207 (2005).
- [13] V. M. Polyakov, and F. Schwierz, *Appl. Phys. Lett.* 88, 032101 (2006).
- [14] S. Takashi, *Toshiba Review* 59, 2 (2004) [in Japanese].
- [15] M. Hikita, M. Yanagihara, Y. Uemoto, T. Ueda, T. Tanaka, and D. Ueda, *Panasonic Technical Journal* 22, 2 (2009).
- [16] Y. Nanishi, Y. Saito and T. Yamaguchi, *Jpn. J. Appl. Phys.* 42, 2549 (2003).
- [17] V. Yu. Davydov, A. A. Klochikhin, R. P. Seisyan, V. V. Emtsev, S. V. Ivanov, F. Bechstedt, J. Furthmuller, H. Harima, A. V. Mudryi, J. Aderhold, O. Semchinova, and J. Graul, *Phys. Status Solidi B* 229, R1 (2002).
- [18] T. Matsuoka, H. Okamoto, M. Nakao, H. Harima, and E. Kurimoto, *Appl. Phys. Lett.* 81, 1246 (2002).
- [19] T. L. Tansley, and C. P. Foley, *J. Appl. Phys.* 59, 3241 (1986).
- [20] A. G. Bhuiyan, K. Sugita, A Hashimoto, and A. Yamamoto, *IEEE J. Photovolt.* 2, 276 (2012).
- [21] G. F. Brown, J. W. Ager III, W. Walukiewicz, and J. Wu, *Sol. Energy Mater. Sol. Cells* 94, 478 (2010).
- [22] N. Miller, J. W. Ager III, H. M. Smith III, M. A. Mayer, K. M. Yu, E. E. Haller, W.

- Walukiewicz, W. J. Schaff, C. Gallinat, G. Koblmüller, and J. S. Speck, *J. Appl. Phys.* 107, 113712 (2010).
- [23] S. Yamaguchi, R. Izaki, K. Yamagiwa, K. Taki, Y. Iwamura, and A. Yamamoto, *Appl. Phys. Lett.* 83, 5398 (2003).
- [24] H. Li, R. Li, J. Liu, and M. Huang, *Physica B* 479, 1 (2015).
- [25] H. Lu, W. J. Schaff, and L. F. Eastman, *J. Appl. Phys.* 96, 3577 (2004).
- [26] E. Starikov, P. Shiktorov, V. Gruzinskis, L. Reggiani, L. Varani, J. C. Vaissiere, and J. H. Zhao, *J. Phys. Condens. Matter* 13, 7159 (2001).
- [27] H. Morkoc, *Handbook of Nitride Semiconductors and Devices* (John Wiley & Sons Inc. 2008) Vol. 1.
- [28] T. Yamaguchi and Y. Nanishi, *Phys. Status Solidi A* 207, 19 (2010).
- [29] J. Weertman and J. R. Weertman, *Elementary of Dislocation Theory* (Oxford University Press, Oxford, 1992).
- [30] S. Takeuchi, *Kesshou Soseiron* (Theory of Crystal Plasticity) (Uchida Rokakuho Publishing Co., Ltd., Tokyo, 2013) p. 37 [in Japanese].
- [31] S. K. Mathis, A. E. Ramanov, L. F. Chen, G. E. Beltz, W. Pompe, and J. S. Speck, *Phys. Status Solidi A* 179, 125 (2000).
- [32] C. S. Gallinat, G. Koblmüller, Feng Wu, and J. S. Speck, *J. Appl. Phys.* 107, 053517 (2010).
- [33] S. M. Islam, V. Protasenko, S. Rouvimov, H. Xing, and D. Jena, *Jpn. J. Appl. Phys.* 55, 05FD12 (2016).
- [34] T. Akagi, K. Kosaka, S. Harui, D. Muto, H. Naoi, T. Araki and Y. Nanishi, *J. Electron. Mater.* 37, 5 (2008).
- [35] D. C. Look, H. Lu, W. J. Schaff, J. Jasinski, and Z. Liliental-Weber, *Appl. Phys. Lett.* 80, 258 (2002).
- [36] X. Wang, S. Liu, N. Ma, L. Feng, G. Chen, F. Xu, N. Tang, S. Huang, K. J. Chen, S. Zhou, and B. Shen, *Appl. Phys. Express* 5, 015502 (2012).
- [37] V. Lebedev, V. Cimalla, J. Pezoldt, M. Himmerlich, S. Krischok, J. A. Schaefer, O. Ambacher, F. M. Morales, J. G. Lozano, and D. Gonzalez, *J. Appl. Phys.* 100, 094902 (2006).
- [38] C. S. Gallinat, G. Koblmüller, and J. S. Speck, *Appl. Phys. Lett.* 95, 022103 (2009).
- [39] L. F. J. Piper, T. D. Veal, C. F. McConville, L. Hai, and W. J. Schaff, *Appl. Phys. Lett.* 88, 252109 (2006).
- [40] W. Walukiewicz, *Physica B* 302, 123 (2001).
- [41] X. Wang, S. B. Che, Y. Ishitani, and A. Yoshikawa, *Appl. Phys. Lett.* 90, 151901 (2007).
- [42] J. S. Thakur, R. Naik, V. M. Naik, D. Haddad, G. W. Auner, H. Lu, and W. J. Schaff, *J. Appl. Phys.* 99, 023504 (2006).

- [43] S. Harui, H. Tamiya, T. Akagi, H. Miyake, K. Hiramatsu, T. Araki, and Y. Nanishi, *Jpn. J. Appl. Phys.* 47, 5330 (2008).
- [44] J. Kamimura, K. Kishino, and A. Kikuchi, *Appl. Phys. Lett.* 97, 141913 (2010).
- [45] D. Muto, H. Naoi, T. Araki, S. Kitagawa, M. Kurouchi, H. Na, and Y. Nanishi, *Phys. Status Solidi A* 203, 1691 (2006).

Chapter 2

Crystal growth technology

Chapter 2

Crystal growth technology

2.1 Epitaxial growth [1-3]

Epitaxial growth is widely used not only for the fabrication of various semiconductor devices but also for polymer growth and so forth, and today it is an important technology being utilized in a wide range of fields from inorganic materials to organic materials. Epitaxial growth means to grow a crystal layer having the same orientation on a substrate crystal. Since the epitaxial growth is strongly influenced by the substrate, it is very important to determine the material properties of the substrate, the lattice constant, and the surface condition of the substrate. Additionally, nuclei formation during the epitaxial growth and the growth driving force also strongly depend on growth method.

Vapor phase growth method is mainly used in the epitaxial growth, and it is divided into chemical vapor deposition (CVD) which utilize chemical reaction and physical vapor deposition (PVD) which utilize physical adsorption. The CVD method is a method of decomposing or synthesizing raw materials containing thin film atoms vaporized at room temperature by chemical reaction and precipitating a thin film on the substrate. The CVD method includes metalorganic chemical vapor deposition (MOCVD) method and hydride vapor phase epitaxy (HVPE) method which use organic metal and halide, respectively, as the raw material. On the other hand, the PVD method includes molecular beam epitaxy (MBE) method which evaporates raw materials in an ultrahigh vacuum ($\sim \times 10^{-10}$ Torr) as molecular beams or atomic beams.

2.2 Molecular beam epitaxy (MBE) [2-5]

The history of the MBE method began in 1970 when Cho and Arthur of Bell Laboratories began their research on crystal growth in an ultrahigh vacuum for GaAs, and they named this method as molecular beam epitaxy (MBE) in 1975. This work was motivated by the eagerness to realize the superlattice which was advocated by Esaki et al. in 1970. Since then, the crystal growth research by MBE method have been progressed and it is being used for the growth of III-V compound semiconductors mainly GaAs.

The MBE method is performed by heating cells containing various constituent elements of crystals in an ultrahigh vacuum of about 10^{-10} to 10^{-11} Torr and releasing the overheated vapors in the form of molecular beams to the surface of substrate, and thus, a single crystal thin film or a desired heterostructure could be epitaxially grown on the substrate. In addition, although the MBE method is a kind of vacuum evaporation method, it differs from other ordinary vapor deposition methods in that it is performed in an ultrahigh vacuum and raw materials are supplied as atoms or molecules. In other words, crystal growth can be controlled at an atomic level in an environment with low impurities.

The characteristics of the MBE method can be listed as follows.

- ① Slow growth rate (1 ML/s) is possible
- ② Growth temperature can be lowered
- ③ Multiple raw materials can be selectively supplied
- ④ Evaluation using electron beams or ions as probes is possible during growth because of its ultrahigh vacuum environment.

Being able to supply a plurality of raw materials in addition to controlling the growth rate and growth temperature means that a steep heterointerface can be created in a non-equilibrium state. This technique is indispensable for fabrication of devices such as quantum structures, high electron mobility transistors (HEMT) and semiconductor lasers. Moreover, it is possible to monitor information on the growth layer surface in real time with reflection high energy electron diffraction (RHEED) equipped to the MBE system for in situ observation during crystal growth.

2.3 Configuration of RF-MBE system [2-4]

The MBE system used in this study is designed for InN and its related alloys growth, manufactured by EpiQuest, Inc. (EpiQuest RC2100NR). It uses radio-frequency (RF) plasma discharge to excite pure nitrogen gas for group V source and thus, it is called RF-MBE. The configuration of our RF-MBE system is as shown in Fig. 2.1. This system is composed of two chambers; a sample exchange chamber and a crystal growth chamber. Four substrate holders can be loaded into the sample exchange chamber at one time. Furthermore, a pre-baking apparatus is mounted in the sample exchange chamber and impurity gas can be released by heating the substrate or the substrate holder at 100 °C. Ultrahigh vacuum environment in the system is maintained by the turbo molecular pump (TMP) and rotary pump (RP) for the sample exchange chamber, and TMP, RP, ion pump

and titanium sublimation pump for the crystal growth chamber. The degree of vacuum in the crystal growth chamber is about 10^{-10} Torr. The two chambers are shut off by a gate valve between them and it is opened only during sample transportation. Therefore, although the sample exchange chamber is exposed to the atmosphere during the time of inserting the sample, the crystal growth chamber is not exposed to the atmosphere and thus, it is possible to fabricate plural number of samples with no necessity to retract to vacuum or to bake the growth chamber. In addition, the growth chamber is surrounded by a shroud cooled with liquid nitrogen to prevent impurities from being reflected or re-evaporated around the substrate holder and entering the substrate surface.

Furthermore, the crystal growth chamber is equipped with a heater for heating the substrate, thermocouples and a thermionic thermometer (pyrometer) to measure the substrate temperature, a substrate rotating mechanism, two RF radical cells for supplying group V source manufactured by SVT Associates Inc. and Veeco Inc., and five Knudsen cells for supplying group III sources (In, In, Ga, Al) and for supplying Mg for doping, beam flux monitor, quadrupole mass spectrometer (QMS), and reflection high energy electron diffraction (RHEED) for in situ monitoring of the surface during crystal growth.

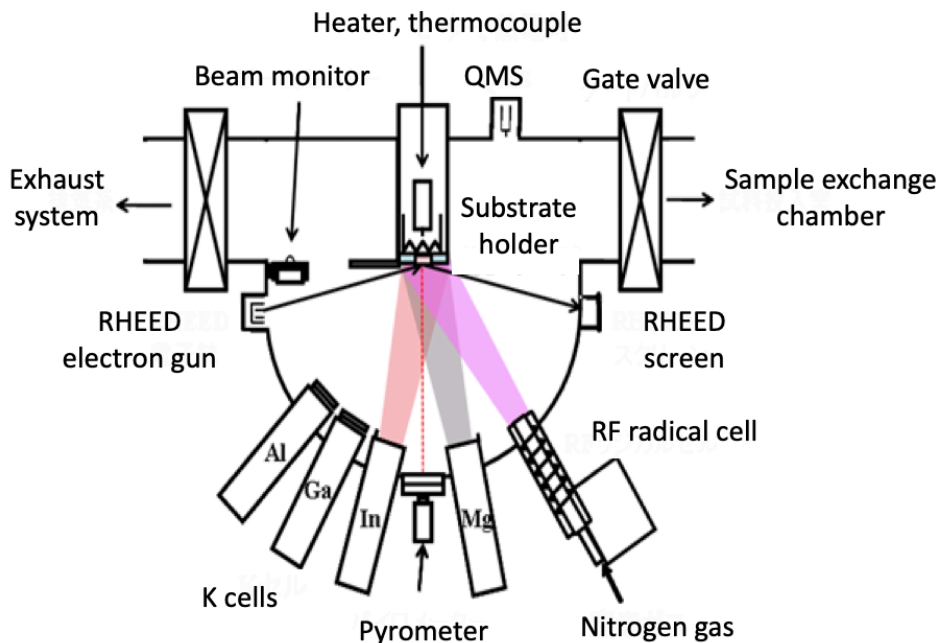


FIG. 2.1. Configuration of RF-MBE system (Araki Lab.)

2.4 Radio frequency (RF) plasma [1, 3, 6]

For MBE growth of nitride semiconductors, gases such as nitrogen (N_2) or ammonia (NH_3) are used as nitrogen source. For example, in the growth of GaN by MBE, when NH_3 is used as the nitrogen source, a substrate temperature of about 800 to 900 °C is required. On the other hand, when N_2 is used as the raw material, growth of GaN does not occur merely by supplying the N_2 gas and Ga to the substrate surface because the dissociation energy of nitrogen molecules is as large as 9.5 eV. Therefore, it is necessary to generate active nitrogen by electron cyclotron resonance (ECR) or RF plasma, or to generate atomic nitrogen. Atomic nitrogen is effective for crystal growth as it will bond to Ga and form crystal immediately. In the supply of active nitrogen molecules, when the sum of the energy of the active species and the energy corresponding to the binding energy released when Ga bonds with N exceeds the dissociation energy of the nitrogen molecule, nitrogen atoms decompose and the growth of GaN occur. In ECR and RF plasma, nitrogen plasma in the active state of active nitrogen N_2^* , nitrogen ion N_2^+ , N^+ , and atomic nitrogen N are generated. These generation ratios vary depending on the structure of the plasma source and discharge conditions such as input power and nitrogen flow rate.

In the RF plasma, nitrogen ions are less generated compared to the ECR plasma. The nitrogen ions generated in the RF plasma is around 10^{-4} to 10^{-5} , two orders of magnitude lower than that of ECR plasma which is around 10^{-2} . Figure 2.2 shows the comparison of emission spectroscopic analysis results of ECR plasma source and RF plasma source [7]. In the RF plasma, the first positive series and atomic N radicals are strong, whereas in the ECR plasma which has large excitation effect, the second positive series and ionized nitrogen are intensified. Since the ions are accelerated by the electric field in the plasma source, they are supplied to the substrate with a high energy and it might damage the growth layer surface. Therefore, the aperture of the gas discharge port is made as small as possible, and when the number of atomic N radical is increased, nitrogen ions are suppressed, and generation of atomic nitrogen is promoted.

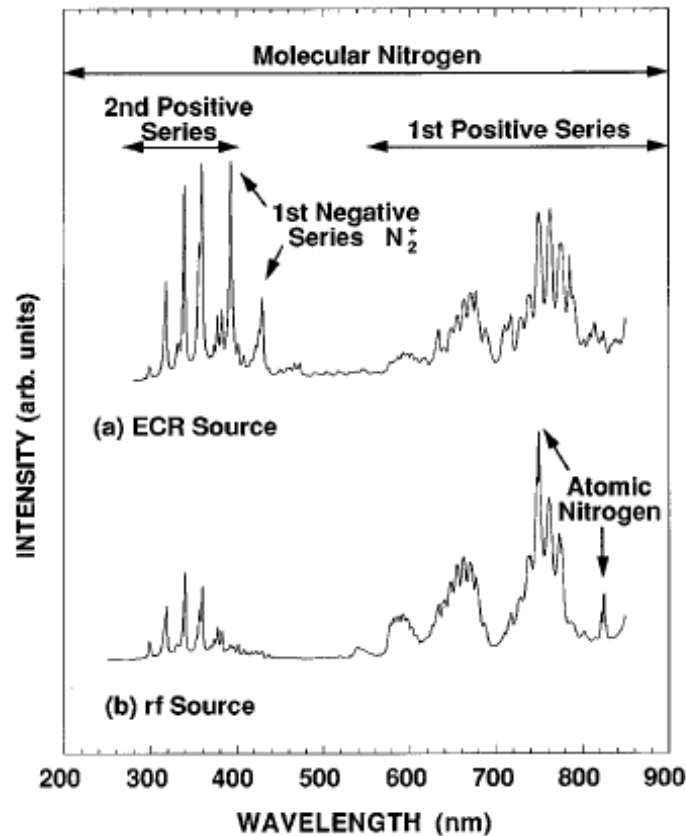


FIG. 2.2. Comparison of emission spectroscopic analysis results of ECR plasma and RF plasma [7]

2.5 Knudsen cell [3, 4]

Knudsen cell or also well known as K cell is used as a source cell for supplying a solid raw material such as In, Ga and Al. In order to obtain the necessary molecular beam of the group III elements, the K cell has to be heated to 800 to 1200 °C. For that reason, pyrolytic boron nitride (PBN) well degassed in an ultrahigh vacuum is used as the crucible. PBN is extremely low in reactivity to most materials and can withstand a high temperature up to about 1250 °C and thus, it is widely used as a crucible for various materials. Figure 2.3 shows an example of a standard K cell. The PBN crucible is heated by the surrounding resistive heating of tantalum (Ta) or tungsten (W) heater. The heater is surrounded by a multilayered heat shield made of tantalum. A thermocouple is attached to the bottom of the crucible so that the temperature can be controlled with a precision of 1 °C.

Depending on the raw material, stress on the crucible rises when the temperature is raised to the temperature at the time of crystal growth or when the temperature is lowered,

and also when the material transforms from solid phase to the liquid phase, from the liquid phase to the gas phase and vice versa. This possibly might damage the crucible. For this reason, the standby temperature of In and Ga cells are kept above the melting points of In and Ga. However, for the Al cell, temperature below the melting point is set as the standby temperature for safety precaution since the melting point of Al is high.

Besides, the vapor pressure in the cell changes depending on the shape of the crucible and amount of material left in the crucible. So, when it is desired to accurately determine the growth rate and mixed crystal composition, a vacuum gauge attached to the substrate holder side (beam monitor) is used to measure the flux accurately.

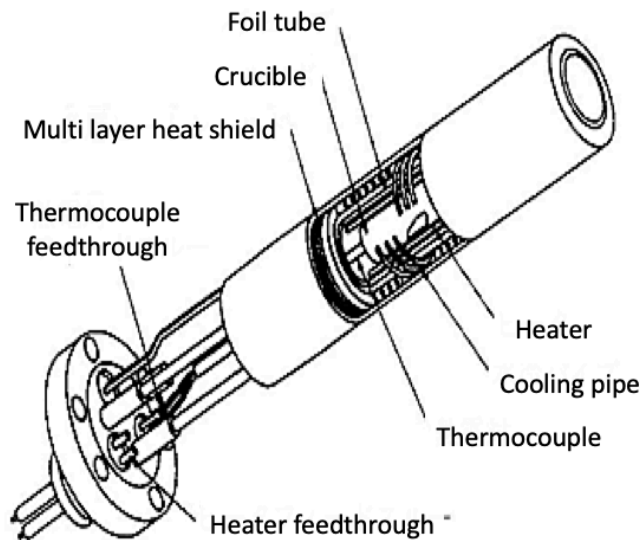


FIG. 2.3. Structure of K cell (Modified by the author) [4]

2.6 Crystal growth technique in nitride semiconductors [8-10]

With all epitaxial semiconductor devices, the substrate is a key factor in the production of high-quality films. Ideally the substrate should have the same crystal symmetry and lattice constant as the films being deposited. GaAs substrates, for example, are used for GaAs-based devices. However, it is extremely difficult to produce native III-nitride substrates with the Czochralski method due to the high temperatures required and high vapor pressure of nitrogen. Even after many years of development, direct growth in industry is still performed on material grown originally on sapphire or silicon substrates, both of which can be produced with low cost and high quality.

In the 1980's, there was no bulk crystal of GaN available as a substrate for crystal growth. Sapphire ($\alpha\text{-Al}_2\text{O}_3$) which has the same hexagonal structure as GaN but has lattice mismatch of 14% was mainly used as the conventional substrate. Despite such large lattice mismatch, high-quality GaN superior in surface flatness and crystallinity grown on the sapphire substrate was made possible by AlN buffer layer technology by metal organic vapor phase epitaxy (MOVPE) in 1986 [11]. As shown in Fig. 2.4, the threading dislocation in the GaN thin film has been reduced to $10^8\text{-}10^9\text{ cm}^{-2}$ by the low temperature buffer layer technology. However, it needs to be less than about 10^6 cm^{-2} in order to fabricate devices such as laser. Epitaxial lateral overgrowth (ELO) method has been introduced as an effective way to reduce the threading dislocations density to about $10^6\text{-}10^7\text{ cm}^{-2}$, and this has been realized by MOVPE [12] and HVPE [13] in 1997. In addition, the growth rate by HVPE method can be as high as several tens to 100 $\mu\text{m/h}$. The grown layer with thickness of several hundreds of μm is then peeled off from the sapphire substrate, and used as bulk crystal for GaN homoepitaxial growth [14]. In the other hand, the MOVPE method is used for a low dislocation base crystal growth for growing a laser structure [15].

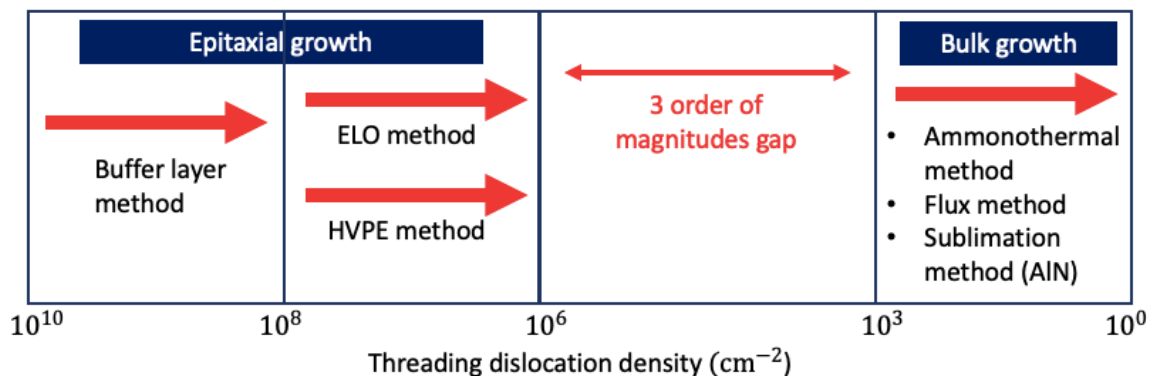


FIG. 2.4. Threading dislocation density by different growth methods
(Modified by the author) [9]

2.7 InN crystal growth technique [16]

An endeavor to grow bulk InN from a melt began in the early 20th century [17] but it was failed due to the low dissociation temperature and high vapor pressure of nitrogen molecules [18]. Single-crystalline InN was reported for the first time by Matsuoka et al. in 1989 utilizing MOVPE method [19]. However, growth by MOVPE need to fulfill the conditions for NH_3 pyrolysis while preventing InN dissociation, which impose conflicting

temperature requirements. Conversely, molecular beam epitaxy (MBE) outfitted with a RF plasma source has an essential preferred standpoint over MOVPE for obtaining high-quality InN. In this growth method, neutral and ionized excited-state nitrogen atoms and molecules can be produced independently by plasma sources as mention in Section 2.2. In this way, the crystal growth temperature can be set independently without considering the temperature requirement for nitrogen source. The primary endeavor to develop single-crystalline InN by the RF-MBE was made by Hoke et al. in 1991 ^[20].

Since InN has extremely low dissociation temperature and equilibrium vapor pressure at growth temperature is high, growth at high temperature is difficult. In addition, control of V/III ratio is important in growth by MBE method. Growth at N-rich condition forms a rough surface and results in low-crystalline quality of InN films, while growing in the In-rich condition yields high-quality films but droplets of In form on the film surface ^[21]. In the case of GaN, the droplets of Ga can be removed by heat treatment. However, in the case of InN, the droplets of InN cannot be removed by the heat treatment because the decomposition temperature of InN is lower than the evaporation temperature of In droplets ^[22]. Therefore, strict control of V/III ratio is required to obtain high quality InN films without droplets.

As a method to solve these issues, our group proposed the droplet elimination by radical beam irradiation (DERI) method ^[23] for InN growth. In the DERI method, high quality crystals can be obtained with high reproducibility without strict control of the V/III ratio. It consists of two processes which are metal-rich growth process (MRGP) where InN is grown under In-rich condition and droplet elimination process (DEP) where the excess In droplets are eliminated by supplying only N radical to the surface. The change in RHEED diffraction intensity during the DERI process is shown in Fig. 2.5. During MRGP, excess droplets of In are formed on the surface, and the RHEED intensity decreases. Thereafter, during DEP, the In droplets are eliminated and flat InN is obtained on the surface, and thus, the RHEED intensity gets increases and recovers. In this manner, the DERI method can solve the narrow window of V/III ratio for InN growth by monitoring the RHEED patterns. Figure 2.6 shows the surface morphology of InN film grown under In-rich condition and after subsequent droplet elimination. We use this DERI method in each experiment described in this dissertation.

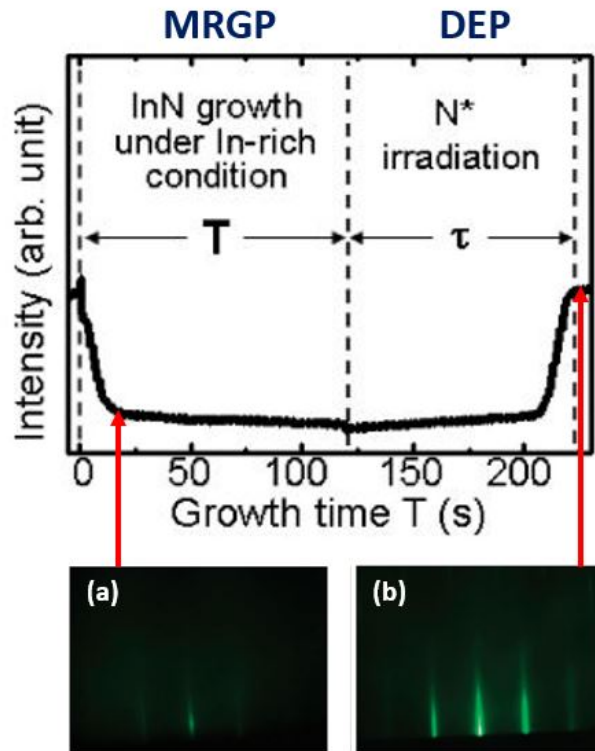


FIG. 2.5. Changes of RHEED patterns in InN growth process by DERI method (Modified by the author) ^[23]

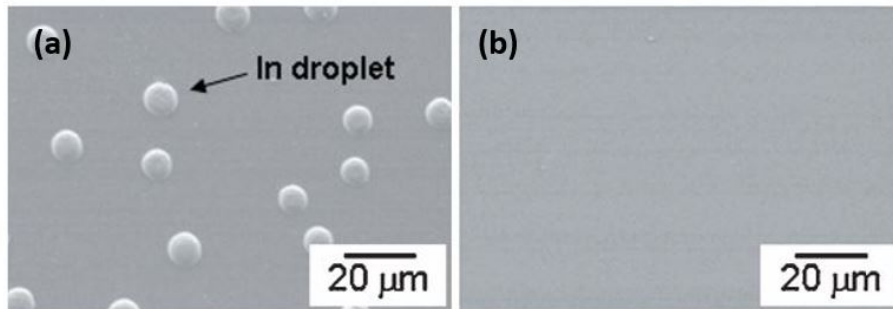


FIG. 2.6. SEM images of (a) InN grown under In-rich condition (b) After subsequent droplet elimination ^[23]

References

- [1] K. Nakajima, *Epitakisharu Seichou No Mekanizumu* (Mechanism of Epitaxial Growth) (Kyoritsu Shuppan Co., Ltd., Tokyo, 2002) [in Japanese].
- [2] A. Kinbara, *Hakumaku Kougaku* (Thin Film Technology) (Maruzen Publishing Co., Ltd., Tokyo, 2011) p. 43 [in Japanese].
- [3] *Kesshou Kougaku Suku-ru Tekisuto (Dai 12-ban), Kesshou Kougaku No Kisou* (Text book of Crystal Engineering School Vol. 12, Basic of Crystal Engineering) (The Japan Society of Applied Physics, Tokyo, 2014) [in Japanese].
- [4] S. Gonda, *Bunshisen Epitakishii* (Molecular Beam Epitaxy) (Baihukan Co., Ltd., Tokyo, 1994) [in Japanese].
- [5] K. Takahashi, *Bunshisen Epitakishii Gijutsu* (Molecular Beam Epitaxy Technology) (Kogyo Chosakai Publishing Co., Ltd., Tokyo, 1984) p. 5 [in Japanese].
- [6] I. Akasaki, *III-zoku Chikkabutsu Handoutai* (Group III Nitride Semiconductors) (Baihukan Co., Ltd., Tokyo, 1999) [in Japanese].
- [7] W. C. Hughes, W. H. Rowland, Jr, M. A. L. Johnson, S. Fujita, J. W. Cook, Jr, J. F. Schetzina, J. Ren, and J. A. Edmond, *J. Vac. Sci. Technol. B*, 13, 1571 (1995).
- [8] M. Razeghi, *Vacuum* 146, 308 (2017).
- [9] K. Hiramatsu, *Oyo Buturi*, 82, 422 (2013) [in Japanese].
- [10] T. Yoshida, *Posuto Shirikon Handoutai Nano Seimaku Dainamikusu To Kiban Kaimen Kouka* (Post Silicon Semiconductor, Nano Film Deposition Dynamics and Substrate/Interface Effect) (NTS Inc., Tokyo, 2013) p. 116 [in Japanese].
- [11] H. Amano, N. Sawaki, I. Akasaki, and Y. Toyoda, *Appl. Phys. Lett.* 48, 353 (1986).
- [12] O. H. Nam, M. D. Bremser, T. S. Zheleva, and R. F. Davis, *Appl. Phys. Lett.* 71, 2638 (1997).
- [13] A. Usui, H. Sunakawa, A. Sakai, and A. Yamaguchi, *Jpn. J. Appl. Phys.* 36, L899 (1997).
- [14] Y. Oshima, T. Eri, M. Shibata, H. Sunakawa, K. Kobayashi, T. Ichihashi, and A. Usui, *Jpn. J. Appl. Phys.* 42, L1 (2003).
- [15] S. Nakamura, M. Senoh, S. Nagahama, T. Matsushita, H. Kiyoku, Y. Sugimoto, T. Kozaki, H. Umemoto, M. Sano, and T. Mukai, *Jpn. J. Appl. Phys.* 38, L226 (1999).
- [16] Y. Nanishi, Y. Saito and T. Yamaguchi, *Jpn. J. Appl. Phys.* 42, 2549 (2003).
- [17] F. Fischer and F. Schroter, *Ber. Dtsch. Keram Ges.* 43, 1465 (1910).
- [18] J. B. MacChesney, P. M. Bridenbaugh and P. B. O'Connor, *Mater. Res. Bull.* 5, 783 (1970).
- [19] T. Matsuoka, H. Tanaka and A. Katsui, *Int. Symp. on GaAs and Related Compounds, Karuizawa, Japan 1989, Inst. Phys. Conf. Ser.* 106, p. 141 (1990).
- [20] W. E. Hoke, P. J. Lemonias and D. G. Weir, *J. Cryst. Growth* 111, 1024 (1991).
- [21] C. S. Gallinat, G. Koblmüller, J. S. Brown, S. Bernardis, J. S. Speck, G. D. Chern, E. D.

- Readinger, H. Shen, and M. Wraback, *Appl. Phys. Lett.* 89, 032109 (2006).
- [22] S. V. Ivanov, T. V. Shubina, V. N. Jmerik, V. A. Vekshin, P. S. Kop'ev, and B. Monemar, *J. Cryst. Growth* 269, 1 (2004).
- [23] T. Yamaguchi, and Y. Nanishi, *Appl. Phys. Express* 2, 051001 (2009).

Chapter 3

Characterization methods

Chapter 3

Characterization methods

Our group use a wide variety of characterization methods to determine the surface morphology, crystallographic quality, electrical characteristics, and optical properties of InN films. The methods include in situ reflection high-energy electron diffraction (RHEED), scanning electron microscopy (SEM), transmission electron microscopy (TEM), atomic force microscopy (AFM), X-ray diffractometry (XRD), Hall effect measurement and photoluminescence (PL) spectroscopy. These typical characterizations are described below.

3.1 Reflection high energy electron diffraction (RHEED) ^[1, 2]

Reflection high energy electron diffraction (RHEED) is an indispensable technique for monitoring surface morphology in situ during growth process of thin film by vacuum evaporation method including MBE used in this study. High speed electrons with kinetic energy of 10 to 50 keV are irradiated onto the sample surface at a specular angle of 1 to 6° and the angular distribution of the reflected electrons are observed as a diffraction pattern on the fluorescence screen as shown in Fig. 3.1.

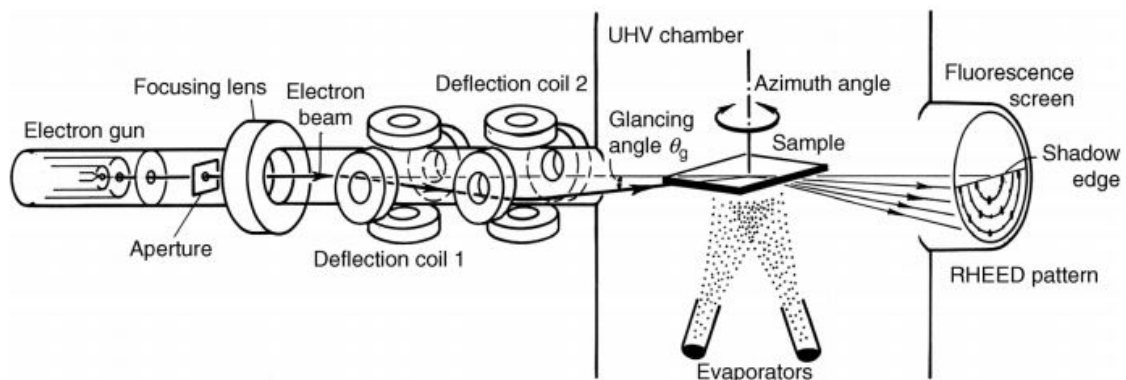


FIG. 3.1. RHEED schematic diagram ^[1]

In RHEED, electron beam is directed at low angles, and thus, most of the atoms involved in electron beam scattering are the atoms on the sample surface. Therefore, when considering the diffraction image of RHEED, it is possible to consider a two-dimensional lattice as a reciprocal lattice, that is, the reciprocal lattice of the single crystal surface layer. When the width of the atomic layer step presents on the crystal surface is L , the reciprocal lattice rod becomes a sheet-like rod having a width of $2\pi/L$ as shown in Fig. 3.2. Since the wavelength of the electron beam is very short, the radius of the Ewald sphere becomes very large, the intersection point with the rod becomes approximately an elongated bar-like intersection point, and thus, the diffraction image becomes an elongated long rod-like (streak) pattern.

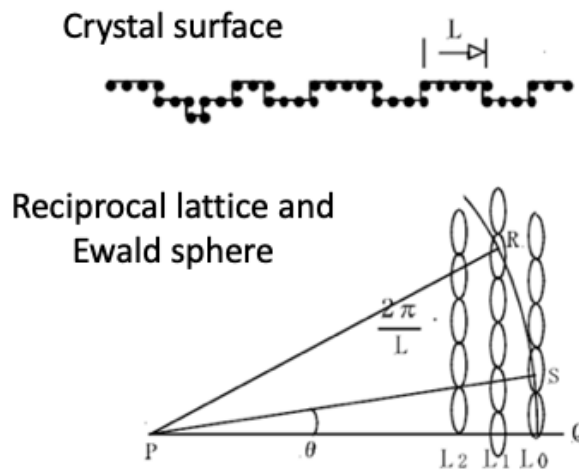


FIG. 3.2. (Top) Crystal surface (Bottom) reciprocal lattice and Ewald sphere
(Modified by the author) [2]

The RHEED patterns depending on surface morphology are as shown in Fig. 3.3. As illustrated in the figure, the RHEED pattern of a completely flat or atomically flat surface is streak pattern. In contrast, when the crystal has uneven surface, the RHEED pattern becomes spotty pattern. Furthermore, in the case of poor crystallinity and polycrystalline, the RHEED pattern becomes a ring pattern, while in the case of amorphous, it becomes a halo pattern. From these facts, it can be concluded that if the RHEED pattern during crystal growth is streak, the growth is a two-dimensional growth, while if the pattern is spotty, the growth is a three-dimensional growth. Therefore, the flatness of the crystal surface can be evaluated by observing the RHEED pattern in situ during the growth process.

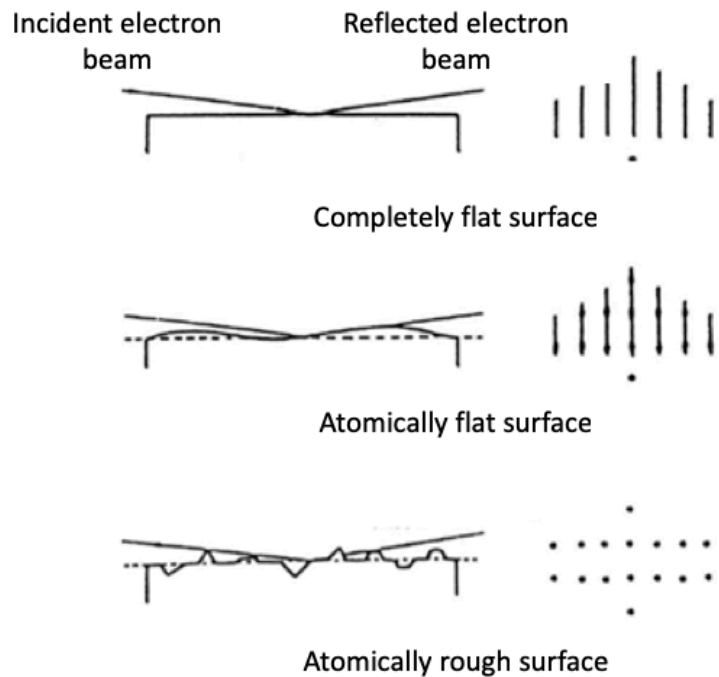


FIG. 3.3. Surface condition and RHEED pattern (Modified by the author) ^[2]

3.2 Scanning electron microscopy (SEM) ^[3, 4]

Scanning electron microscope (SEM) is used to study the surface morphology of crystal after the growth. SEM irradiates narrowed electron beams onto the bulk sample surface while scanning it in the two-dimensional (X, Y) direction, detects the electrons emitted from the sample, and detects the unevenness information of the sample surface (secondary electrons image) and composition difference information (backscattered electron image) and displays the images on a monitor. Furthermore, it is possible to obtain element information of the sample, crystal information and so forth by attaching various detectors to the SEM.

Figure 3.4 shows the electrons and electromagnetic waves emitted from the sample by the interaction between the incident electrons and the sample. Detection of each signal requires a unique detector. For the investigation of the surface morphology of crystal, secondary electrons (SE) are extremely advantageous. As shown in Fig. 3.5, secondary electrons are electrons that generated when free electrons in a sample receive static electricity from incident electrons and scattered electrons, and escape from the sample surface. Since the energy that the free electrons receive is about several tens of eV regardless of the energy of the incident electrons, the energy of secondary electrons is as

low as several tens of eV or less. Therefore, it can be said that secondary electrons generation depth is as shallow as 10 nm from sample surface and they are rich in sample surface information.

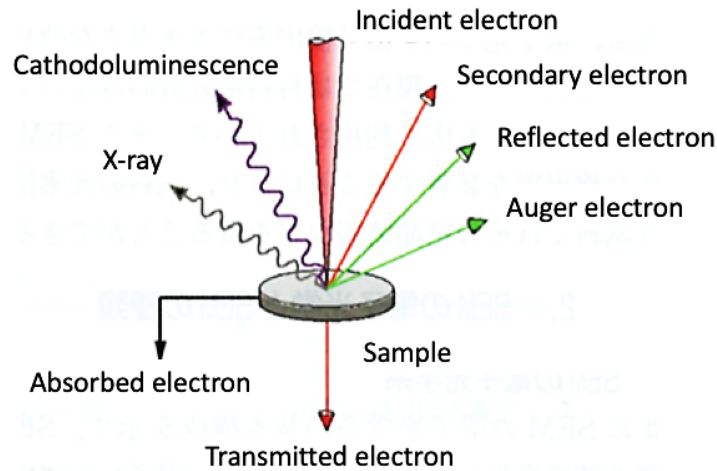


FIG. 3.4. Different types of signal obtained by SEM (Modified by the author) ^[3]

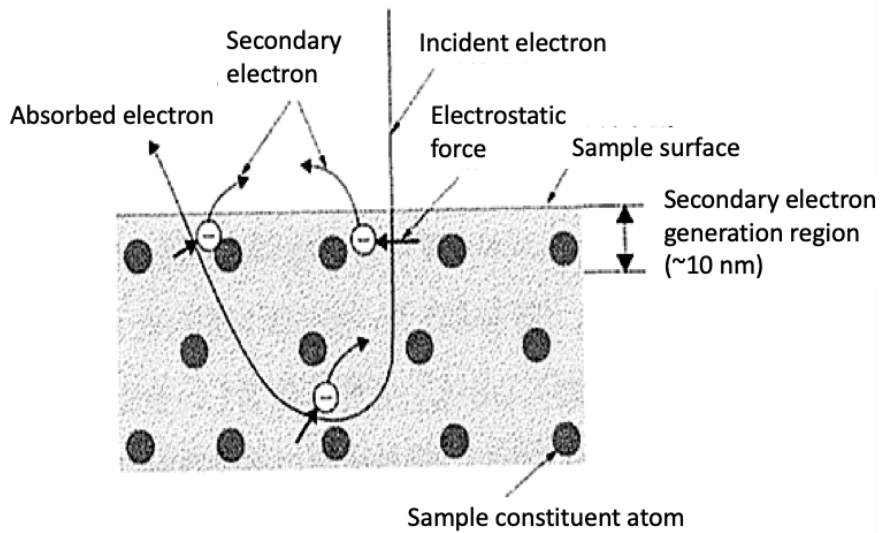


FIG. 3.5. Schematic diagram of generation of secondary electrons (Modified by the author) ^[4]

Figure 3.6 shows the configuration of the SEM. The main body comprises an electron gun, condenser lens, deflection coil, and objective lens. Furthermore, the electron beam passage and the sample chamber in the main body are always kept at a high vacuum

by a vacuum pump. The electron beam emitted from the electron gun is squeezed narrowly via the condenser lens and the objective lens, and the electron beam scans the sample surface in two dimensions by the deflection coil. The narrowed electron beam has a deep focal depth compared to the optical microscope, because the irradiation angle at the time of sample irradiation is very small. The signal generated from the sample by the electron beam is converted and amplified into an electric signal by the detector and projected on the display.

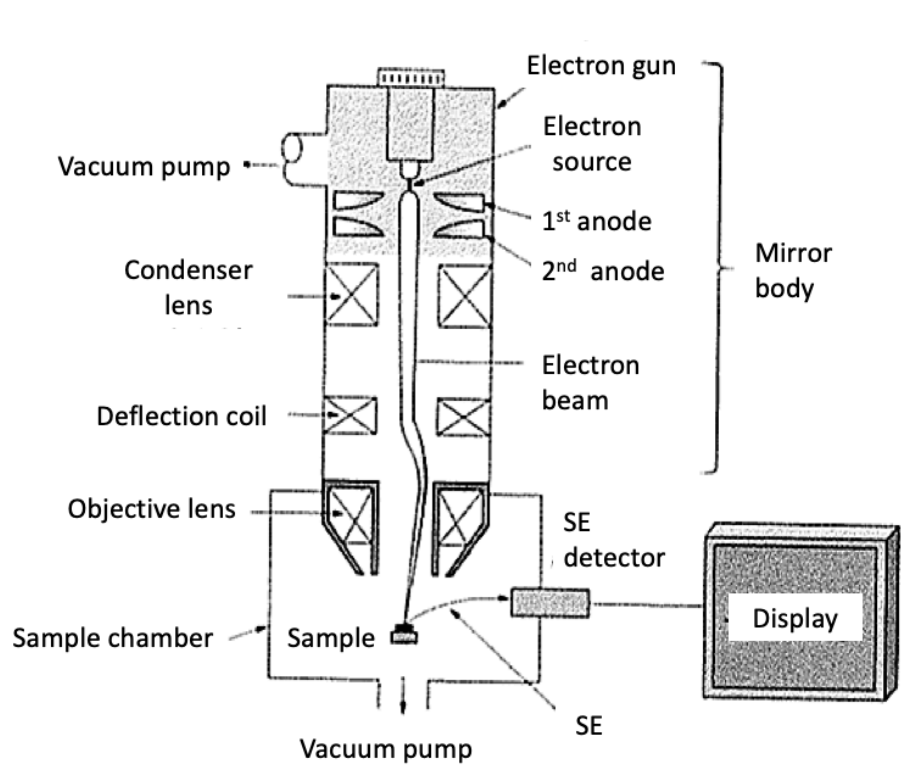


FIG. 3.6. Configuration of SEM (Modified by the author) [4]

The electron gun plays a role of extracting and accelerating electrons from a filament which is the electron source. Currently, the electron gun adopted in SEM is roughly divided into thermionic emission (TE) type and field emission (FE) type. Although it is difficult to obtain a thin electron probe due to the large electron source of the thermo-electron gun, stable electron beam and a probe current of about $1 \mu\text{A}$ at maximum can be obtained, and it is inexpensive. Therefore, it is mainly used as an electron gun in SEM. On the other hand, the field emission electron gun is effective for obtaining a thin electronic probe because the electron source is extremely small and it is used as an electron gun for high-resolution SEM.

3.3 Transmission electron microscopy (TEM) [5, 6]

Transmission electron microscope (TEM) is the only tool that can observe and analyze the structure of material at the atomic level. We mainly use TEM for obtaining electron microscopic image with high resolution and to study the properties of crystal defects. To obtain high resolution image, it is necessary not only to simply observe the enlarged image of the sample, but also to keep in mind that images with different information are photographed according to diffraction phenomena, sample thickness, and so forth. Therefore, it is important to examine carefully what kind of image to be observed before the TEM observation and what kind of information is extracted from the TEM image. Figure 3.7 shows TEM (Model JEM2010) manufactured by JEOL used in this study.



FIG. 3.7. TEM JEM2010

In contrast to SEM which usually detect secondary electrons and backscattered electrons, TEM detect transmitted electrons which provide information on the inner structure of the crystal. Configuration of TEM is as shown in Fig. 3.8. Electrons are emitted from the uppermost electron gun to the vacuum evacuated lens barrel, and accelerated by the accelerating voltage tube. The accelerated electron passes through the sample and the electrons transmitted through the sample are enlarged and focused by the lens of the imaging system and reach the large screen of the viewing chamber. TEM mode

with parallel incidence is used for observation of enlarged image and diffraction pattern of crystal. By changing the diffraction vector, \mathbf{g} to 0002 and 1-100, type of threading dislocations observed could be characterized to screw dislocation, edge dislocation or mixed dislocation.

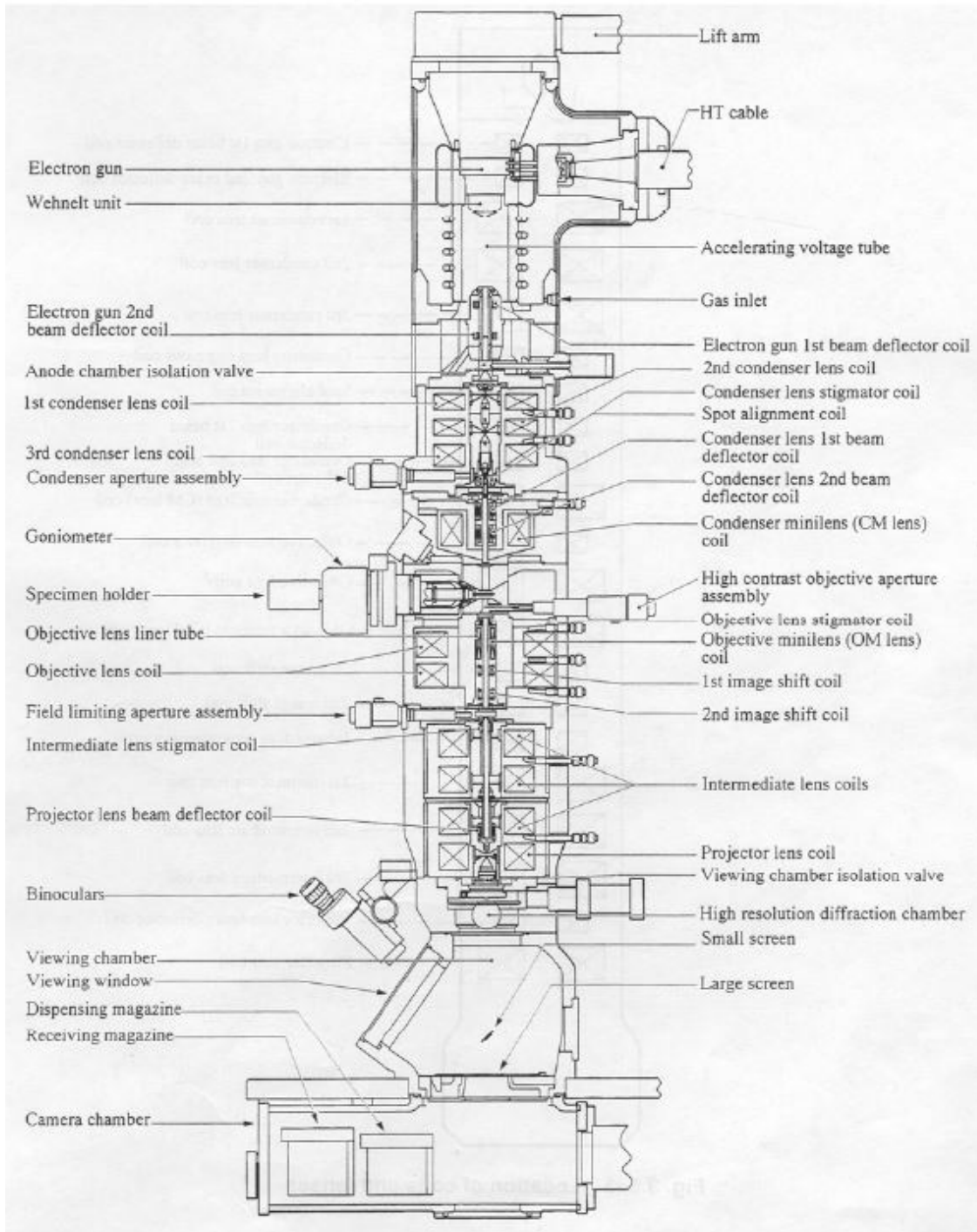


FIG. 3.8. Cross section of TEM column [6]

TEM specimen preparation

TEM specimen preparation is important to obtain a clear image in TEM observation. To date, various methods have been used for fabrication of TEM specimen such as mechanical polishing, focused ion beam (FIB) etching, ion milling, chemical etching and so forth. In any of the preparation methods, it is necessary to satisfy the following conditions to obtain a clear image in TEM observation:

- a) The specimen should be sufficiently thin and transparent for electrons, specifically, with the thickness of ~ 100 nm or less. Furthermore, the specimen thickness is required to be at least 50 nm or less, and ideally 10 nm or less for high resolution observation.
- b) The specimen surface must be flat.
- c) The damage to the specimen must be small even when irradiated by the electron beam.
- d) The specimen must exist stably in vacuum.
- e) The specimen must be conductive.

For nitride semiconductors, the requirements of (a), (b), (c) and (d) are not problematic, but as for (e), there is a problem that the charge up of the specimen occurs and the TEM observation image is disturbed since sapphire which is an insulator, is often used as the growth substrate. In this laboratory, we have traditionally prepared the TEM specimen using mechanical polishing and ion milling method, but in this study, focused ion beam (FIB) etching method is used since the specimen preparation time is shorter as shown in Table 3.1.

TABLE 3.1. Comparison of TEM specimen preparation methods

Comparison	Mechanical polishing and ion milling method	FIB method
Total preparation time	2-3 days	0.5 - 1 day
Slicing specific parts	Not possible	Possible
Observable field of view	Several μm	10~15 μm
Specimen thickness	Very thin but wedge shaped	Thick but uniform
Specimen damage	Small	Large
Multilayer structure observation	Preferable	Difficult
Lattice image observation	Preferable	Difficult
Other features	At least 5 mm square sample required	Very small sample is also possible and multiple specimens can be installed on the same mesh

TEM specimen preparation by FIB is as illustrated in Fig. 3.9. Firstly, after determining the part for TEM observation from the bulk sample, a protective film is deposited on the sample surface by tungsten (W) deposition. Then, the periphery of the protective film is scraped off with a strong Ga ion beam and only a small part of the area is left to support the TEM specimen. Next, the sample is tilted at 45 degrees and the specimen bottom part is scraped off by sputtering. After that, the sample is repositioned back to normal and microprobe for specimen extraction is adhered to the specimen using W deposition. When the adhesion is completed, the remaining part left for supporting the specimen is cut with the ion beam and now the specimen is completely separated from the original bulk sample. The specimen is then lifted by the microprobe and deposited to a mesh which will be used for TEM observation as shown in Fig. 3.10. Finally, after the unnecessary microprobe is cut, the thinning process of the specimen is started. The center part of the specimen is thinned gradually while weakening the ion beam until its thickness becomes 100 nm or less.

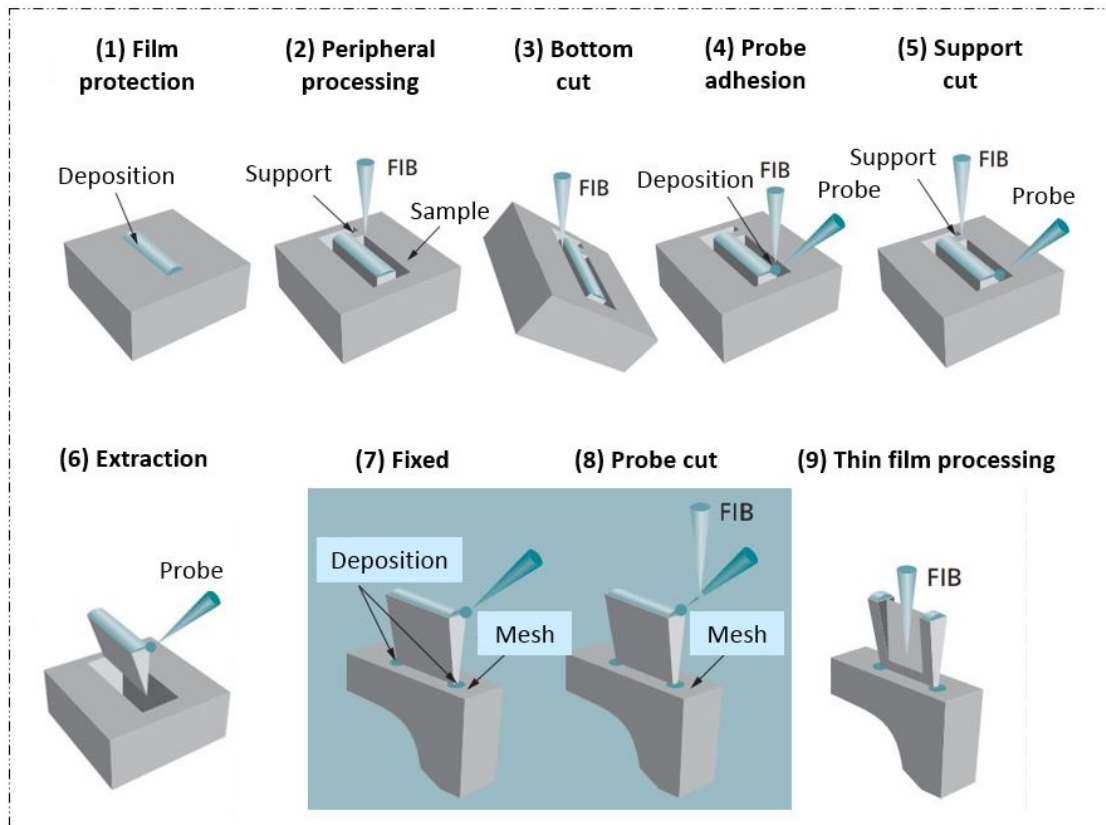


FIG. 3.9. TEM specimen preparation by FIB etching method
(Modified by the author) [7]

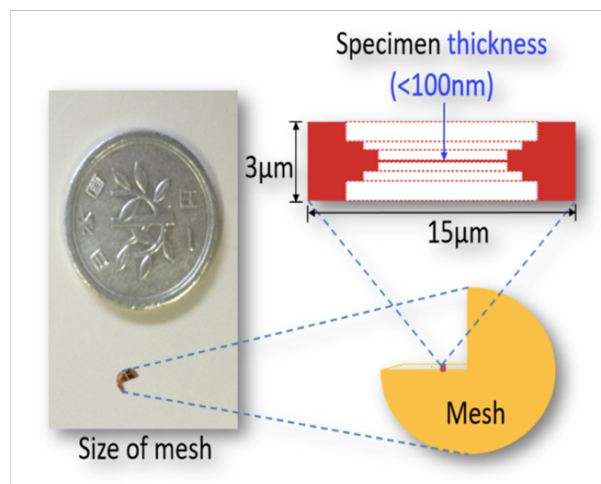


FIG. 3.10. A mesh used for TEM observation

3.4 Atomic force microscopy (AFM) ^[8,9]

Atomic force microscope (AFM) is a type of microscope that detects interatomic forces acting on a probe and a sample. It is synonymous with scanning probe microscope (SPM), sometimes called contact mode or contact AFM. Since AFM is not a current measurement, it can be used even with an insulator thin film. Figure 3.11 shows the configuration of AFM. The AFM probe is attached to the tip of a cantilever, and this probe is brought into contact to the sample surface with a small force. Scanning is performed in the horizontal (X, Y) while controlling the distance between the probe and the sample (Z) so that the amount of deflection of the cantilever is constant in order to perform the surface topology imaging. The pushing force of the cantilever (deflection signal) is detected by the optical lever system. The semiconductor laser is irradiated to the back surface of the cantilever, and the reflected laser light is detected by two position sensors vertically upward and downward, and four position sensors vertically and laterally. Resolution in the vertical direction can be realized at atomic level (0.01 nm). In general, it is possible to evaluate concavities and convexities of sizes up to about 2 μm . On the other hand, when the radius of curvature (R) of the probe tip is larger than the mobility (z) in the height direction, the horizontal resolution depends on R. The tip curvature radius of cantilever which is generally used is about 50 nm.

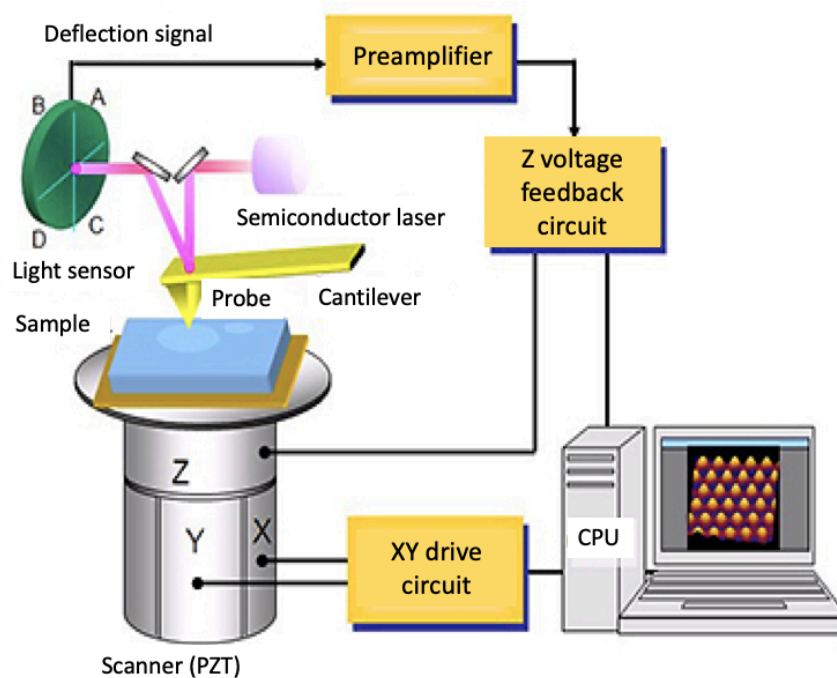


FIG. 3.11. Configuration of AFM (Modified by the author) ^[9]

In addition to the surface morphology and surface roughness, AFM is also used for observing threading dislocations [10]. Screw dislocation forms a spiral step or a hillock on the sample surface. On the other hand, edge dislocations are thought to form pits at locations away from the center of the step.

3.5 X-ray diffractometry (XRD) [8, 11-13]

In the case of heteroepitaxial growth such as nitride semiconductors, the lattice constant of the thin film changes variously as the result of distortion due to the influence of the substrate lattice and relaxation of the strain during growth. In addition, there are cases where lattice is partially deformed due to lattice defect (threading dislocation) which is generated into the film due to strain relaxation, in particular, it becomes a slightly inclined crystal aggregation (mosaic crystal). As shown in Fig. 3.12, the mosaic crystal has four parameters which are vertical coherence length, lateral coherence length, tilt, and twist. X-ray diffractometry is an effective technique for the analysis of these structures.

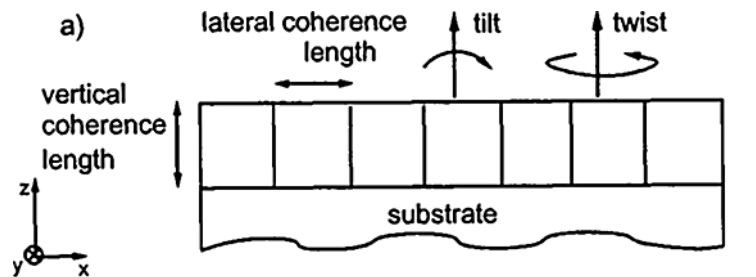
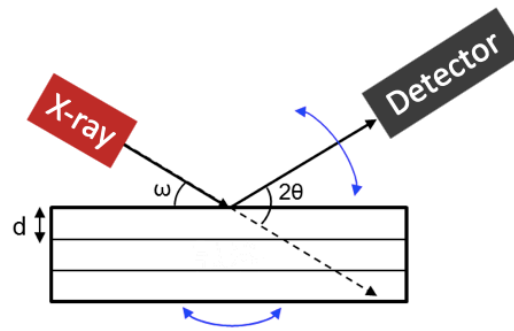
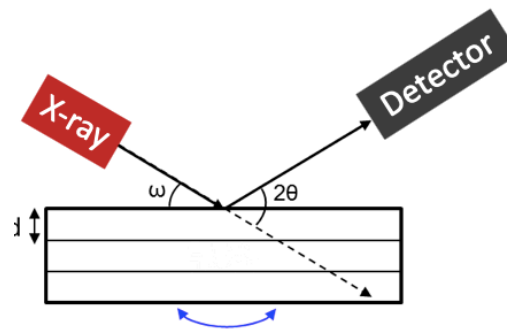


FIG. 3.12. Mosaic crystal [11]

The basic measurement of X-ray diffractometry is as shown in Fig. 3.13. X-ray diffraction can be divided into ω - 2θ measurement and X-ray rocking curve (XRC) measurement. In ω - 2θ measurement, the lattice spacing can be measured, which is often used to determine the composition of alloy semiconductor. As shown in Fig. 3.13(a), when the sample is rotated with respect to the incident X-ray, the detector is moved at an angle of twice the sample rotation angle. In the measurement, ω and 2θ are changed to satisfy the relationship of $\Delta\omega = \Delta\theta$. The full width at half maximum (FWHM) of the diffraction peak represents the variation in lattice spacing due to nonuniform distortion.

(a) ω - 2θ measurement

(b) XRC measurement

FIG. 3.13. Basic measurement of X-ray diffraction

On the other hand, XRC measurement is used to evaluate crystal orientation like a mosaic crystal. As shown in Fig. 3.13(b), angle of the detector (2θ) is fixed with respect to the X-ray incident direction and X-ray incident angle ω is changed. In practice, the sample is rotated to rock it against X-ray incident. The FWHM of the diffraction peak represents the fluctuation degree of lattice plane orientation and it is influenced by threading dislocation. For example, tilt shown in Fig. 3.12 is the fluctuation with respect to normal direction of the crystal surface and it is caused by screw dislocation with Burgers vector of $\langle 0001 \rangle$. It can be measured by symmetrical reflection measurement, and in this study, it is performed on (002) reflection. On the other hand, twist is the fluctuation with respect to in-plane inclination and it is caused by edge dislocation with Burgers vector of $\langle 11-20 \rangle/3$. Reflection of (100) is necessary for twist measurement, but diffraction intensity cannot be obtained sufficiently. Therefore, in this study, we measure several asymmetric surfaces and estimate the value of (100) reflection, as proposed by Gallinat et al. [12].

Gallinat et al. estimated threading dislocation density in InN from FWHM of XRC. From XRC, twist fitting is performed by the function in equation (3.1). Figure 3.14 shows an example of the XRC fitting.

$$\Gamma = \sqrt{(\Gamma_y \cos \chi)^2 + (\Gamma_z \sin \chi)^2} \quad (3.1)$$

Γ is FWHM, χ is the angle between the Bragg surface and (0002) surface. Γ_y and Γ_z are tilt and twist, respectively. Since χ used here is the angle ϕ between (hkl) and (h'k'l') as shown in Fig. 3.15, it could be obtained using formula in equation (3.2). The interplanar distance, d is expressed by the equation (3.3). However, it should be noted that these equations are valid only in the wurtzite structure [13].

$$\cos \phi = d_{hkl} d_{h'k'l'} \left\{ \left[hh' + kk' + \frac{1}{2}(hk' + kh') \right] \frac{4}{3a^2} + \frac{l'l'}{c^2} \right\} \quad (3.2)$$

$$d_{hkl} = \sqrt{\frac{1}{(h^2 + k^2 + hk) \frac{4}{3a^2} + \frac{l^2}{c^2}}} \quad (3.3)$$

Here, c and a represent lattice constants, and in this study $c = 5.693 \text{ \AA}$ and $a = 3.533 \text{ \AA}$ are used. Furthermore, threading dislocation density can be obtained by equation (3.4) and (3.5) using Γ_y and Γ_z .

$$\rho_s = \frac{\Gamma_y^2}{1.88c^2} \quad (3.4)$$

$$\rho_e = \frac{\Gamma_z^2}{1.88a^2} \quad (3.5)$$

Here, ρ_s and ρ_e represents the density of screw dislocation and edge dislocation, respectively. The threading dislocation density obtained from these equations is in good agreement with the density obtained from the TEM observation and it is considered to be effective for evaluation in InN film.

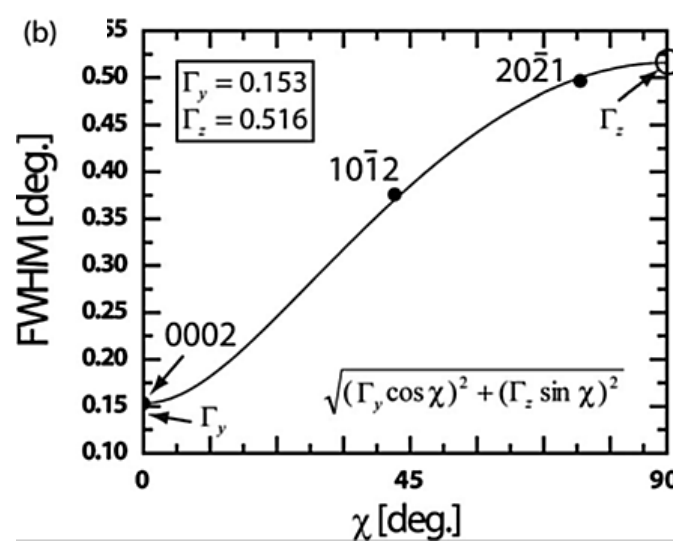


FIG. 3.14. XRC fitting example [12]

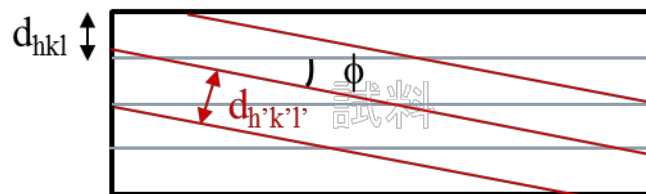


FIG. 3.15. Angle between two planes

3.6 Hall effect measurement [14]

Hall effect measurement is used to study electrical properties such as resistivity, conduction type, majority carrier concentration and majority carrier mobility of semiconductors and epitaxial films. Furthermore, in the Hall effect measurement, the scattering mechanism can also be obtained from temperature dependency of the mobility, and impurity density can be obtained from temperature dependency of the carrier concentration.

In Fig. 3.16(a), the resistivity ρ can be obtained from the current I flowing when the voltage V is applied between the electrodes AB. Next, when I flows and the magnetic flux density B is applied, from Fleming's left hand rule, majority carriers are accumulated on the upper side and a Hall voltage V_H is generated. The p-type or n-type determination is made from the sign of V_H , and the carrier concentration n is obtained using equations (3.6) and (3.7).

$$V_H = R_H \cdot \frac{IB}{D} \quad (3.6)$$

$$R_H = \frac{r_H}{qn} \quad (3.7)$$

Here, R_H is the hole coefficient, q is the elementary charge, r_H is the scattering factor, and D is the thickness of the sample in the magnetic flux direction.

In this study, measurements are made using the van der Pauw method which is suitable for the measurement of epitaxial film as shown in Fig. 3.16(b). The resistivity can be obtained by passing the current I_{AB} between the electrodes AB as shown in equation (3.8) and measuring the voltage V_{DC} between the electrodes DC.

$$R_{AB,DC} = \frac{V_{DC}}{I_{AB}} \quad (3.8)$$

Similarly, $R_{BC,AD}$ is obtained, and ρ can be obtained from equations (3.9) and (3.10) using $R_{BA,DC}$ and $R_{BC,AD}$.

$$\rho = \frac{\pi D}{\ln 2} \cdot \frac{(R_{AB,DC} + R_{BC,AD})}{2} \cdot f \quad (3.9)$$

$$\left| \frac{R_{AB,DC} - R_{BC,AD}}{R_{AB,DC} + R_{BC,AD}} \right| = \frac{f}{\ln 2} \cosh^{-1} \left[\frac{\exp(\ln 2/f)}{2} \right] \quad (3.10)$$

Here, f in equation (3.9) is obtained by creating a program that can calculate f such that the value on the right side is close to the value on the left side as shown in equation (3.10).

Next, a current I_{AC} flows from the electrode A to the electrode C, and the voltage V_{DB} generated between the electrodes DB when the magnetic field (+B) is applied from the top to the bottom is measured. Ideally, since V_{DB} is V_H and I_{AC} is I , the carrier concentration can be estimated from the equations (3.6) and (3.7). The mobility, μ can be obtained from equation (3.11) from n and ρ .

$$\rho = \frac{1}{qn\mu} \quad (3.11)$$

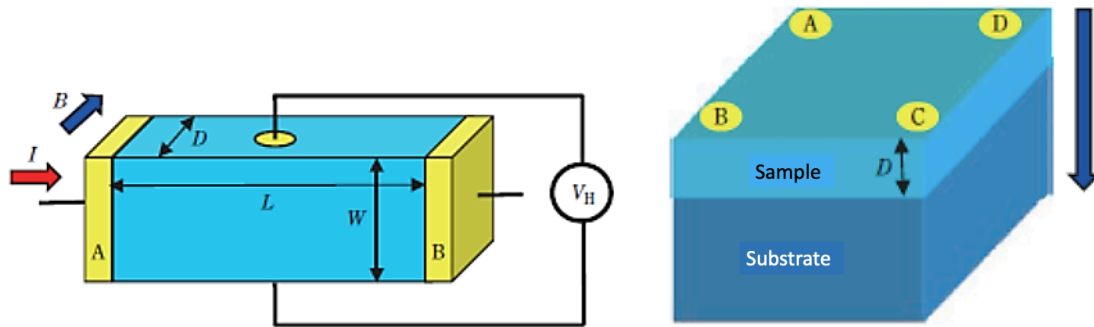


FIG. 3.16. (a) Basic of Hall effect measurement, (b) van der Pauw method
(Modified by the author)^[14]

3.7 Photoluminescence (PL) spectroscopy^[15, 16]

Photoluminescence (PL) spectroscopy is used to study luminescence properties of InN in this study. When electrons which are excited to high energy state by absorption of light or by some other methods return back to the low energy state and emit energy as photons, it is called radiative recombination. Light emission due to the radiative recombination is called luminescence, and the one that emits light after excitation of electrons by light irradiation is called photoluminescence.

PL has been widely used not only as a means of studying physical properties related to the band structure, luminescent center, and so forth but also as a convenient means of evaluation in crystal growth and device process. As the excitation light source, one having energy higher than the band gap is used. In this study, samples are optically excited using an argon (Ar) ion laser line at 514 nm. A liquid nitrogen cooled InGaAs photodiode and a lock-in amplifier are used for phase sensitive detection. The samples are set in a cryostat coupled with a He compressor. The penetration depth of the excitation light is determined by the absorption coefficient of the semiconductor at the excitation light wavelength. In general, the shorter the wavelength, the higher the absorption coefficient and thus, the light can penetrate only near the surface. Figure 3.17 shows the absorption coefficient of InN^[17]. The penetration length of light is the reciprocal of the absorption coefficient. In this study, since the Ar ion laser (514.5 nm=2.41 eV) is used, the penetration length is considered to be about 200 nm from the sample surface.

It is known that light-emitting energy of InN changes depending on carrier concentration^[18]. This is considered as a Burstein-Moss effect, and the relationship

between absorption edge energy and carrier concentration in InN is as shown in Fig. 3.18. The experimental data have shown that the band gap varies from 0.65 eV to about 2.0 eV.

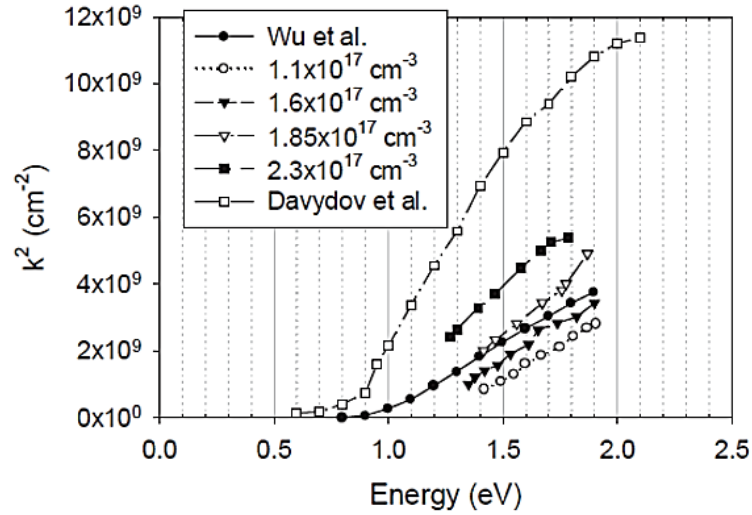


FIG. 3.17. InN absorption coefficient [17-19]

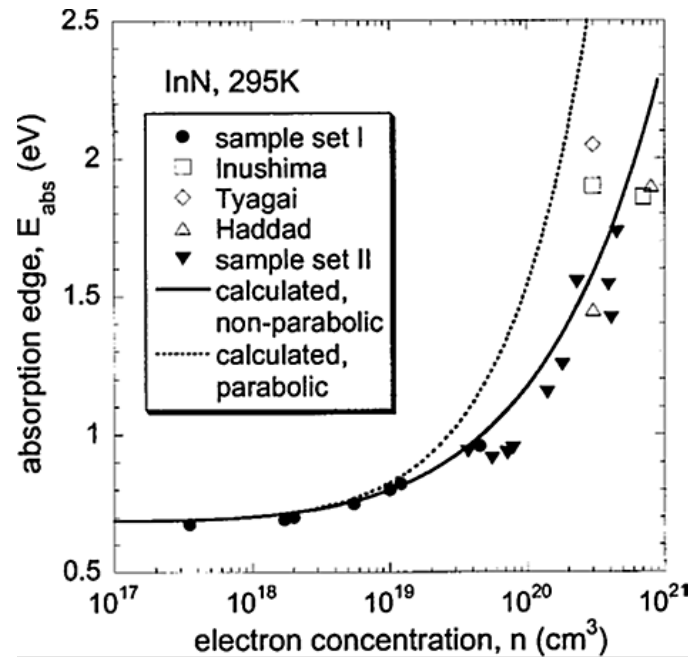


FIG. 3.18. Relationship between absorption edge energy and carrier concentration [20]

References

- [1] S. Hasegawa, *Charact. Mater.* 3, 1925 (2012).
- [2] Y. Okamoto, Dr. Thesis, Graduate School of Engineering, University of Tsukuba, Ibaraki (2000) [in Japanese].
- [3] K. Ogura, *Oyo Buturi* 81, 333 (2012) [in Japanese].
- [4] H. Ito, *Handoutai Denshi Zairyou Bunseki* (Analysis of Semiconductors and Electronic Materials) (The Japan Society for Analytical Chemistry, Tokyo, 2013) p. 94 [in Japanese].
- [5] K. Saka, *Kesshou Denshi Kenbikyogaku* (Electron Microscopy of Crystal) (Uchida Rokakuho Publishing Co., Ltd., Tokyo, 1998) p. 85 [in Japanese].
- [6] EM Facility CMSE-SEF: *JEOL JEM 2010 Training Transmission Electron Microscope User Manual* (Massachusetts Institution of Technology, Massachusetts, 2009) Ver. 5.1, p. 4.
- [7] S. Tomimatsu, I. Sekihara, M. Aizawa, T. Nanri, and T. Onishi, *Hitachi Hyoron* 94, 184 (2012) [in Japanese].
- [8] A. Kinbara, *Hakumaku Kougaku* (Thin Film Technology) (Maruzen Publishing Co., Ltd., Tokyo, 2011) p. 93 [in Japanese].
- [9] *SPM (Sousa-gata Puroubu Kenbikyou) Yu-za Tekisuto* (Scanning Probe Microscope User Text) (Hitachi High-Tech Science Co., Tokyo, 2010) [in Japanese].
- [10] Z. Chen, L. W. Su, J. Y. Shi, X. L. Wang, C. L. Tang, and P. Gao, *AFM Application in III-nitride Materials and Devices* (Intech Open, London, 2012).
- [11] R. Chierchia, T. Böttcher, H. Heinke, S. Einfeldt, S. Figge, and D. Hommel, *J. Appl. Phys.* 93, 8918 (2003).
- [12] C. S. Gallinat, G. Koblmüller, Feng Wu, and J. S. Speck, *J. Appl. Phys.* 107, 053517 (2010).
- [13] P. Kidd, *XRD of Gallium Nitride and Related Compounds: Strain, Composition and Layer Thickness* (PANalytical, 2009).
- [14] H. Matsuura, *Oyo Buturi*, 85, 601 (2016) [in Japanese].
- [15] T. Katouda, *Handoutai Hyouka Gijutsu* (Semiconductor Evaluation Technology) (Sangyou Tosho Kabushikigaisha, Tokyo, 1989) p. 256 [in Japanese].
- [16] *Kesshou Kougaku Suku-ru Tekisuto (Dai 12-ban), Kesshou Kougaku No Kisou* (Text book of Crystal Engineering School Vol. 12, Basic of Crystal Engineering) (The Japan Society of Applied Physics, Tokyo, 2014) [in Japanese].
- [17] K. S. A. Butcher, M. Wintrebert-Fouquet, P. P. -T. Chen, H. Timmers, and S. K. Shrestha, *Mat. Res. Soc. Symp. Proc.* 6, 351 (2003).
- [18] J. Wu, W. Walukiewicz, K. M. Yu, J. W. Ager III, E. E. Haller, H. Lu, W. J. Schaff, Y.

- Saito and Y. Nanishi, *Appl. Phys. Lett.* 80, 3967 (2002).
- [19] V. Yu. Davydov, A. A. Klochikhin, V. V. Emtsev, D. A. Kurdyukov, S. V. Ivanov, V. A. Veksin, J. Furthmuller, J. Aderhold, J. Gaul, A. V. Mudryi, H. Harima, A. Hashimoto, A. Yamamoto, and E. E. Haller, *Phys. Status Solidi B*, 234, 787 (2002).
- [20] J. Wu, W. Walukiewicz, S. X. Li, R. Armitage, J. C. Ho, E. R. Weber, E. E. Haller, Hai Lu William, J. Schaff, A. Barcz, and R. Jakiela, *Appl. Phys. Lett.* 84, 2805 (2004).

Chapter 4

InN growth with in situ surface modification by radical beam irradiation (1)

Chapter 4

InN growth with in situ surface modification by radical beam irradiation (1)

4.1 Introduction

As mentioned previously, InN is a very attractive material for various applications but the realization of InN-based devices has been hindered by the difficulty in obtaining high-quality InN film. The density of threading dislocation in currently available InN film is very high due to large lattice mismatch with the foreign substrate used. In this study, we will discuss a technique to reduce the threading dislocation density in InN film. Up until now, nanocolumns growth^[1-3] and selective-area lateral growth^[4-6] have been reported as successful methods to reduce threading dislocation density in InN. From TEM observation, no threading dislocation was detected in the InN nanocolumns as shown in Fig. 4.1(a). However, this nanocolumns growth method only applicable to reduce threading dislocation density in a very small area which is around ~100 nm. It is very difficult to develop InN-based devices with this small area of InN nanocolumns. For selective-area lateral growth, although high density of threading dislocations (10^{10} cm⁻²) was generated at the interface of InN and sapphire substrate, the threading dislocations propagated only into the center of the InN microcrystals and the laterally grown InN sides areas were nearly dislocation-free, as shown in Fig. 4.1(b). Unfortunately, this method requires ex-situ mask preparation before the InN growth.

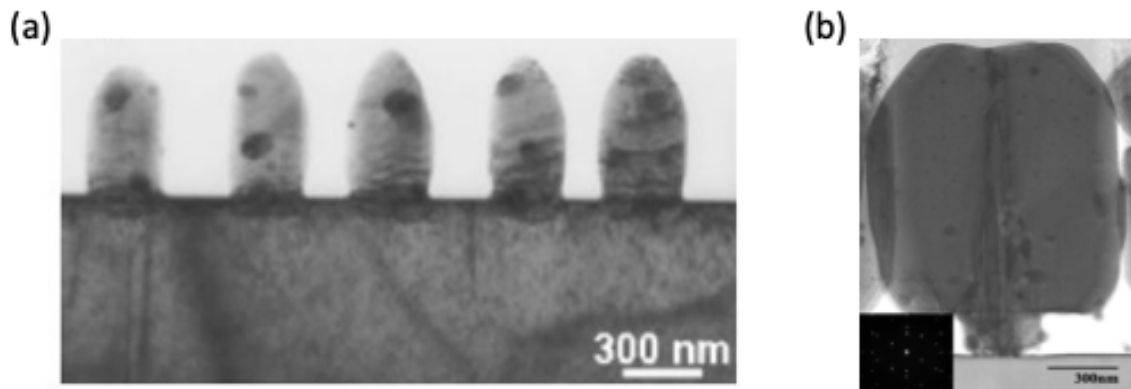


FIG. 4.1. (a) Nano-columns growth method^[2] (b) Selective-area lateral growth method^[6]

Furthermore, our group has previously succeeded in growth of high-quality InN film with low threading dislocation density on micro-faceted InN template wet etched by KOH [7]. Figure 4.2(a) shows the surface morphology of the N-polar InN after wet etching by KOH aqueous solution. After the KOH etching, InN was regrown on the template. Figure 4.2(b) shows a cross-sectional TEM image of the sample grown by this method. As can be seen, a high density of threading dislocations (10^{10} cm^{-2}) existed in the InN template, but these dislocations propagated to the regrown InN layer only through the apexes of the pyramids, then merged and terminated at the regrowth interface. As a result, threading dislocation density reduced by an order of magnitude in the regrown InN region (10^9 cm^{-2}). The effect of reducing these threading dislocations is also reflected in the FWHM of XRC shown in Table 4.1. FWHM of (0002) reflection which is influenced by screw dislocation density showed almost similar result, but FWHM of (10-10) reflection which is influenced by edge dislocation density was found greatly reduced to almost half. Therefore, this method is assumed to be effective for reducing edge dislocation density in InN. It is expected that the threading dislocation density will be further reduced by using this method repetitively. However, since it is necessary to take the sample out of the MBE growth chamber for KOH etching process and the sample need to be transferred back to the growth chamber for the regrowth of InN film, there is a disadvantage that it takes much time and effort to repeatedly perform further reduction of threading dislocation density by this method.

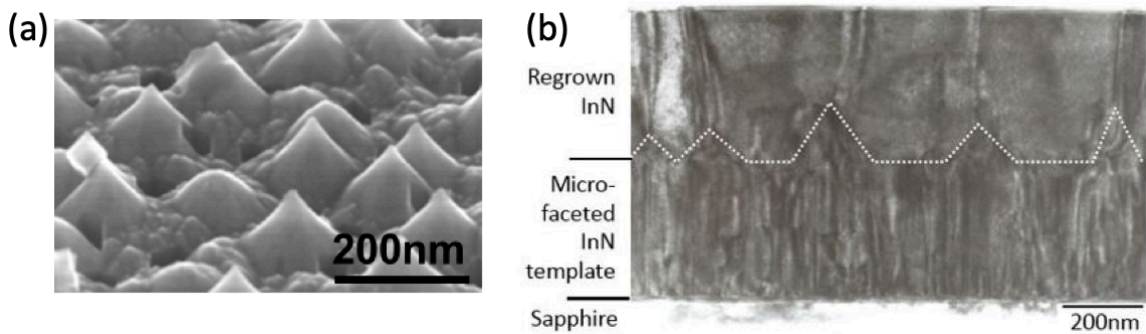


FIG. 4.2. (a) N-polar InN surface morphology after KOH etching (b) Cross-sectional TEM image of InN regrown on the micro-faceted InN template [7]

TABLE 4.1. XRC-FWHM of InN regrown on micro-faceted InN and InN regrown on flat InN [7]

Sample structure	XRC-FWHM (arcmin)			
	(0002) tilt	(10-12)	(30-32)	(10-10) twist
InN/micro-faceted InN	1.1	25.2	34.5	36.5
InN/flat InN	1.2	35.3	45.7	50.6

In this study, we propose an idea of InN film growth with in situ surface modification by radical beam irradiation as a new method to reduce threading dislocation density in InN. Instead of KOH etching, InN template is irradiated in situ by nitrogen radical beam in the MBE growth chamber, then, InN film is regrown on the irradiated template as shown in Fig. 4.3. The surface morphology of the InN template is expected to change from atomically flat surface to three-dimensional shaped surface after irradiated by the nitrogen radical beam as shown in Fig. 4.3(c). On the onset of InN regrowth, threading dislocations are expected to be bent, merged and terminated at the regrowth interface, and thus, threading dislocation density in the regrown InN layer might be reduced as illustrated in Fig. 4.4.

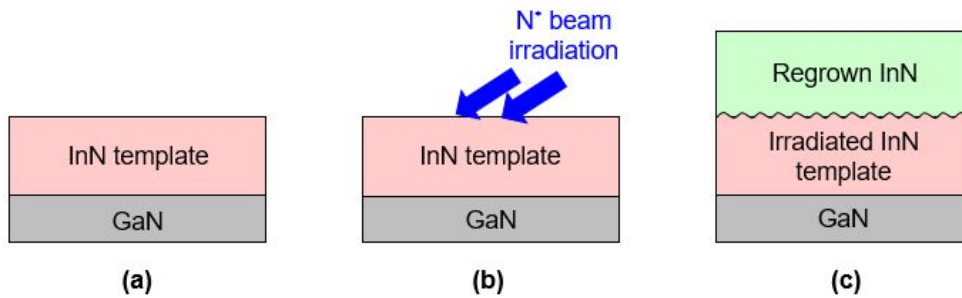


FIG. 4.3. Growth of InN film with in situ surface reformation by radical beam irradiation method: (a) Growth of InN template (b) N radical irradiation on InN template (c) Regrowth of InN film [8]

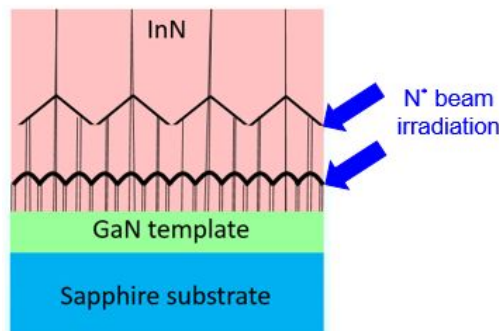


FIG. 4.4. Illustration of threading dislocation density reduction in regrown InN

In this method, there is no necessity to take the sample out of MBE growth chamber, and thus providing an in situ and easily repeatable growth process. Furthermore, this method is applicable to reduce threading dislocation density in a large area which consists of the whole crystal compared to nanocolumns growth method which only applicable for a very small area. More importantly, this method requires no mask preparation before the InN growth compared to selective-area lateral growth method.

Our goal is first to understand the effect of in situ nitrogen radical beam irradiation on the InN template surface morphology under various nitrogen radical beam irradiation conditions including different plasma power, substrate temperature and irradiation time. Then, we focus on how these different irradiation conditions affect the dislocation behavior at the interface of regrown InN and irradiated InN template, and finally, how these dislocation behaviors lead to the reduction of threading dislocation density in the regrown InN. If this technology is established, high quality InN with low threading dislocation density can be achieved with a very easy, simple and repeatable growth process. This will open up new possibilities for the realization of various applications of InN and its related alloys.

4.2 In situ surface modification by N radical beam irradiation

In the growth of III-nitrides, the MBE reactor is equipped with an RF plasma generator to supply active nitrogen radical as a nitrogen source. Besides, there are several other applications of N radical irradiation have been reported. For example, Gangopadhyay et al. applied the N radical beam irradiation to remove the oxide layer on the surface of GaN film [9]. They observed a transition from a streak to a spotty RHEED pattern, which indicates a roughening of the GaN surface due to active-nitrogen exposure at a high substrate temperature of 700 °C. Furthermore, Xue et al. made use of in situ annealing and N radical irradiation for nucleation of self-induced InGaN nanocolumn by MBE [10]. Figure 4.5 shows the SEM images of the sample surface that was irradiated with N radical beam and the sample surface that was annealed reported for InGaN. From this result, it can be seen that the surface morphology was changed by the irradiation with the N radical beam as shown in (c), and it has a different morphology from that of after annealing as shown in (b). It can be seen that the surface modification is possible by in situ N radical beam irradiation in this way. In this section, we report the change in surface morphology together with other experimental results and considerations of in situ N radical beam irradiation on InN film.

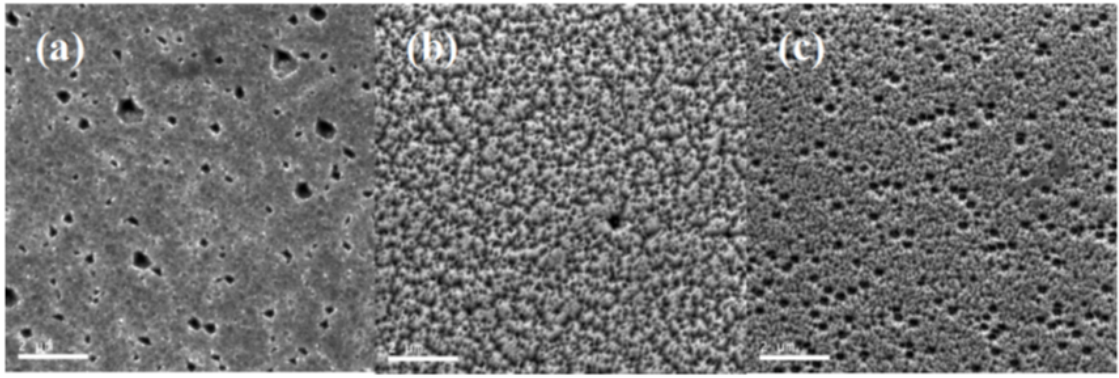


FIG. 4.5. SEM images of InGaN surfaces (a) As-grown, (b) After annealing, (c) After N radical beam irradiation ^[10]

4.2.1 Experimental method

All InN templates in this study were grown on MOCVD-grown (0001) GaN/sapphire substrates in a conventional RF-MBE system (EpiQuest RC2100NR) equipped with a nitrogen plasma source (SVT Associates 6.03) as described in Section 2.3. Prior to growth, the substrate was cleaned with acetone, methanol, hydrochloric acid and purified water. The details of these InN growth are described in Table 4.2. The InN growth rate in this experiment was 450 nm/h. Figure 4.6 shows the growth time chart. DERI method was used in each InN samples growth in this study as mentioned in Section 2.7.

TABLE 4.2. InN growth condition

Substrate temperature (°C)	435
In beam flux (Torr)	$1.36 \sim 1.40 \times 10^{-6}$
N ₂ flow (sccm)	2.0
Plasma power (W)	200

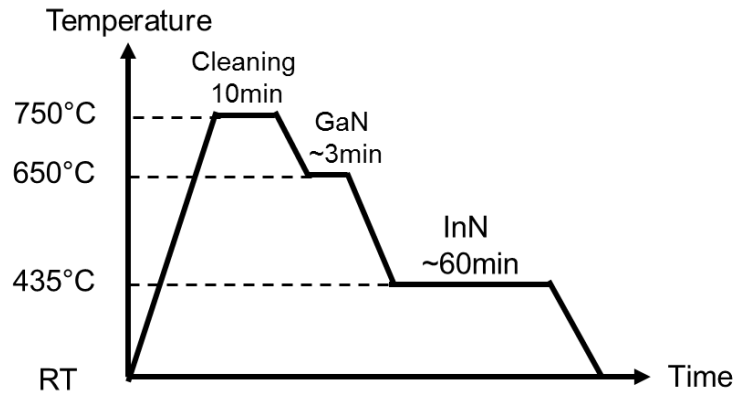


FIG. 4.6. InN template growth time chart

After the InN growth, the templates were taken out from the MBE system and evaluated. Then, the templates were transferred back to the MBE growth chamber and N radical beam irradiation was performed. In this study, we examined (1) substrate temperature dependency, (2) plasma power dependency, and (3) irradiation time dependency for N radical beam irradiation conditions. The conditions of N radical beam irradiation are shown in Table 4.3. The substrate temperature dependency experiments were performed at substrate temperature of 330 °C and 435 °C, while the plasma power dependency experiments were performed with plasma power of 200 W and 600 W. For irradiation time dependency experiments, the sample was first irradiated with N radical beam for 60 minutes and evaluated, then the same sample was irradiated for another 60 minutes and evaluated again for comparison with the previous result. Furthermore, another experiment with in situ annealing (without N radical irradiation) was also performed as for comparison, to study the differences between in situ N radical beam irradiation and in situ annealing of InN film. This comparison experiments were performed under the conditions shown in Table 4.4. The samples evaluation was carried out with RHEED, AFM, XRD and Hall effect measurement.

TABLE 4.3. N radical beam irradiation on the InN templates conditions

	Substrate temperature (°C)	Plasma power (W)	Irradiation time (min)
S2139	330	200	60
S2140	330	600	60
S2155	435	200	60~120
S2156	435	600	60~120

TABLE 4.4. Comparison with annealing

	Substrate temperature (°C)	Plasma power (W)	N radical irradiation/ Annealing time (min)
S2155	435	200	60
S2241	435	—	60
S2302	435	—	10

4.2.2 Substrate temperature dependency

In this section, we discuss the N radical irradiation on InN template with the same plasma power but at different substrate temperature. The plasma power was kept constant at 200 W. Figure 4.7 shows the RHEED patterns during N radical beam irradiation at substrate temperatures of 330 °C (left) and 435 °C (right). It can be seen that streak patterns are obtained on both samples before the N radical irradiation. However, for the substrate temperature of 435 °C, the RHEED pattern changed to a spotty streak pattern after 20 minutes, and the spotty pattern became more obvious after 60 minutes. On the other hand, for the substrate temperature of 330 °C, the RHEED pattern also changed to a spotty streak pattern but only after 40 minutes. The change in RHEED pattern from streak to spotty pattern indicates that the InN template morphology has changed from atomically flat surface to three-dimensional rough surface structure. In both samples, the RHEED patterns have changed, but the change in the pattern was faster and more remarkable for the substrate temperature of 435 °C, indicating that the change in surface morphological structure by N radical beam irradiation is affected by the substrate temperature.

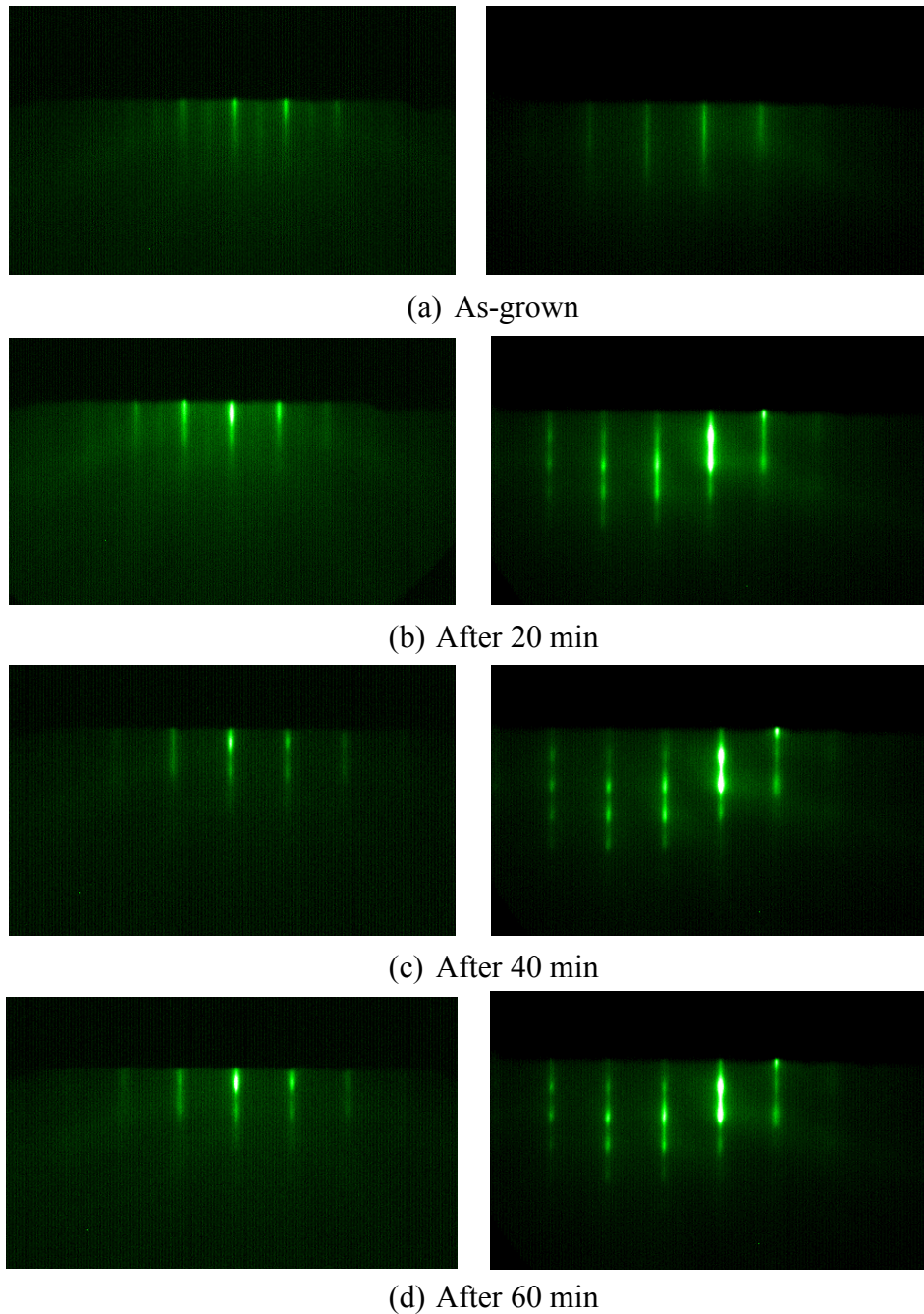


FIG. 4.7. RHEED patterns during in situ N radical beam irradiation on InN templates at substrate temperature of 330 °C (left) and 435 °C (right)

Figure 4.8 shows AFM images of the templates before and after the N radical beam irradiation with plasma power of 200 W at substrate temperatures of 330 °C and 435 °C. Both templates showed increase in RMS values indicating larger surface roughness after the N radical irradiation compared to the as-grown templates. However, the surface morphology of both templates obtained after the N radical irradiation were different. The

change in surface morphology at the substrate temperature of 330 °C was hardly to be seen, but for the higher substrate temperature of 435 °C, it can be seen clearly that the surface morphology changed to a three-dimensional rough structure. These results suggest that at substrate temperature of 330 °C, where thermal decomposition of InN is unlikely to occur, the change in surface morphology might be affected only by N radical beam irradiation. On the other hand, at substrate temperature of 435 °C where InN thermal decomposition is more likely to occur, the change in surface morphology might also be affected by thermal decomposition of InN in addition to the N radical beam irradiation. However, since the In peak was not detected in the XRD ω -2 θ scan measurement for both before and after the N radical irradiation, it is considered that the decomposition of InN might be only slightly occurred. We will describe about the thermal decomposition of InN later in Section 4.2.5.

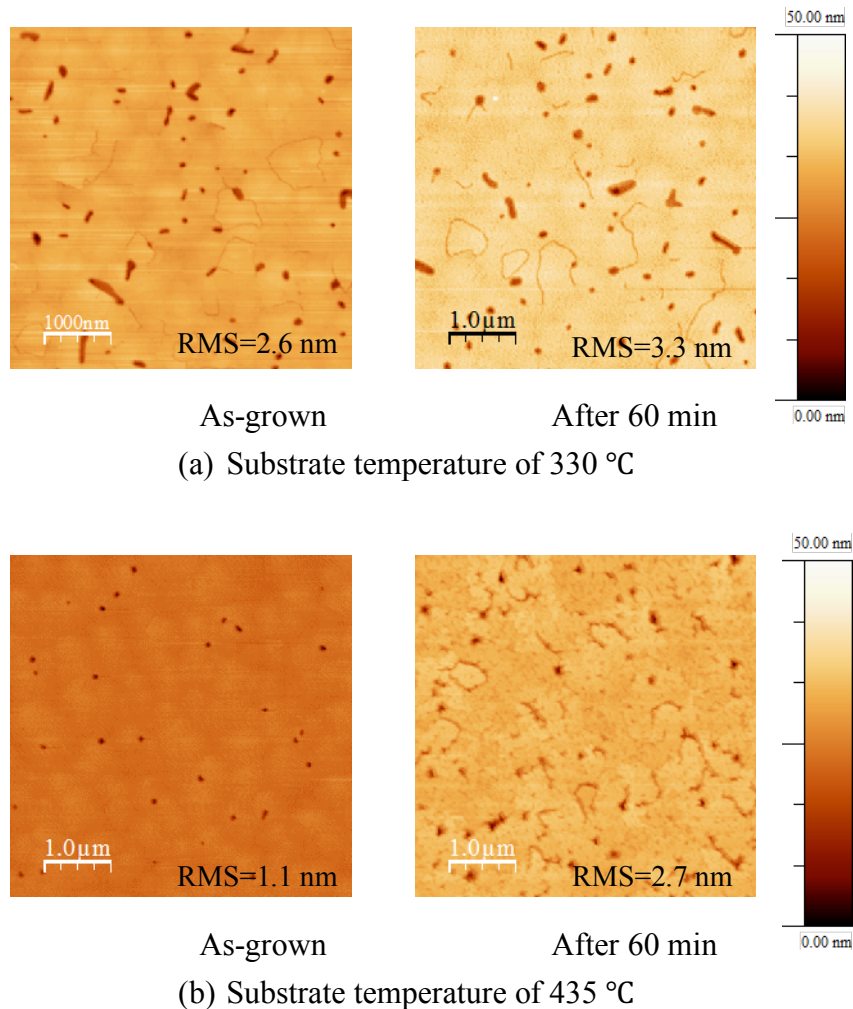


FIG. 4.8. Surface morphology of InN templates after N radical irradiation at different substrate temperature

4.2.3 Plasma power dependency

In this section, we discuss the N radical irradiation on InN templates at the same substrate temperature but with different plasma power. Figure 4.9 shows the RHEED patterns during N radical beam irradiation at substrate temperature of 330 °C with plasma power of 200 W (left) and 600 W (right). It can be seen that both templates had streak RHEED patterns before the N radical irradiation and the streak patterns were maintained even after irradiation for 20 and 30 minutes. Furthermore, there was almost no change in the surface morphology on both templates before and after the N radical irradiation as shown in Fig. 4.10. The RMS values also showed no significant difference. From this result, it is considered that at the low substrate temperature which was 330 °C, there was almost no change in surface morphology of InN template although the N radical irradiation was performed with a higher plasma power which was 600 W.

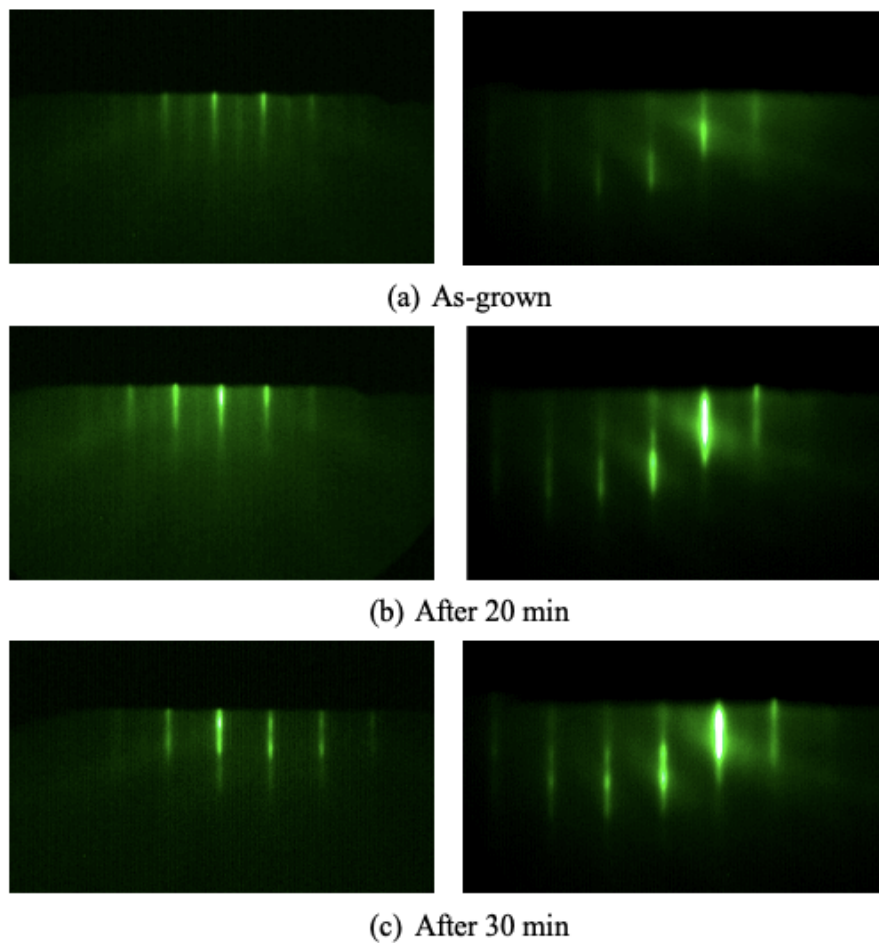


FIG. 4.9. RHEED patterns during in situ N radical beam irradiation on InN templates with plasma power of 200 W (left) and 600 W (right)

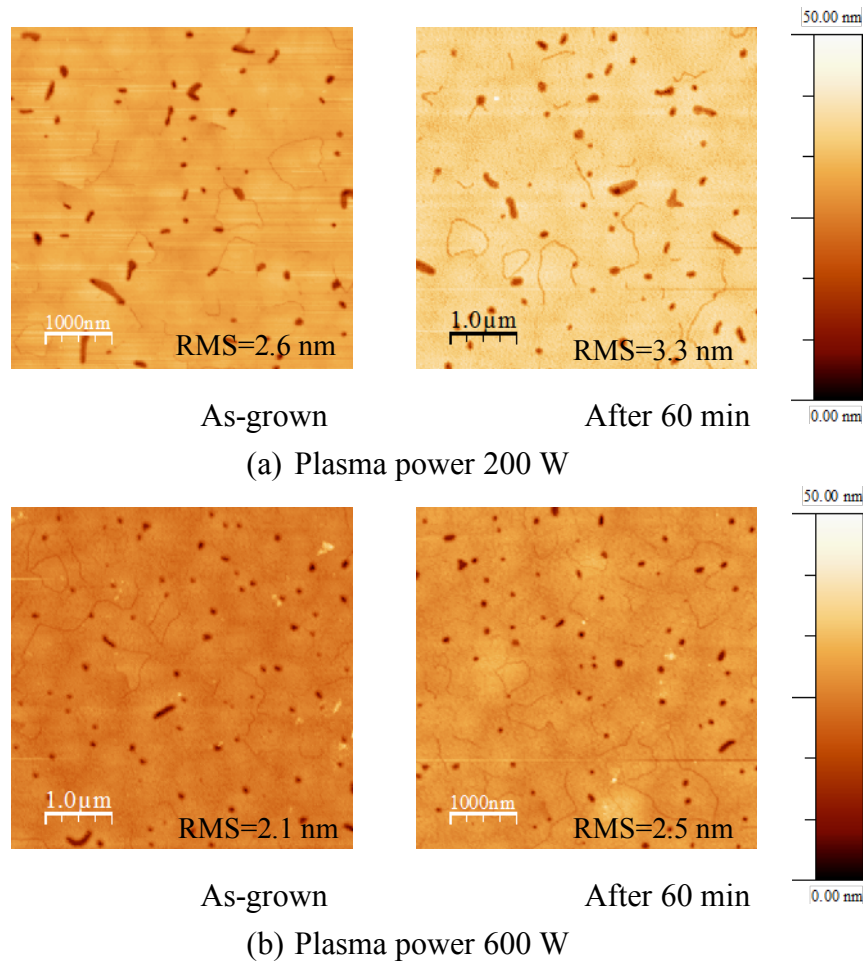


FIG. 4.10. Surface morphology of InN templates after N radical irradiation with different plasma power (substrate temperature of 330 °C)

Figure 4.11 shows the surface morphology of the InN templates before and after the N radical beam irradiation at substrate temperature of 435 °C with plasma power of 200 W and 600 W. It can be seen that at this temperature, when the template was irradiated with a higher plasma power, the surface morphology changed to small grains structures as shown in Fig. 4.11(b). It is assumed that this was due to the increase of ions irradiated to the template with a higher plasma power supplied [11, 12]. The difference in surface morphology regarding the substrate temperature is as described in the previous section 4.2.2.

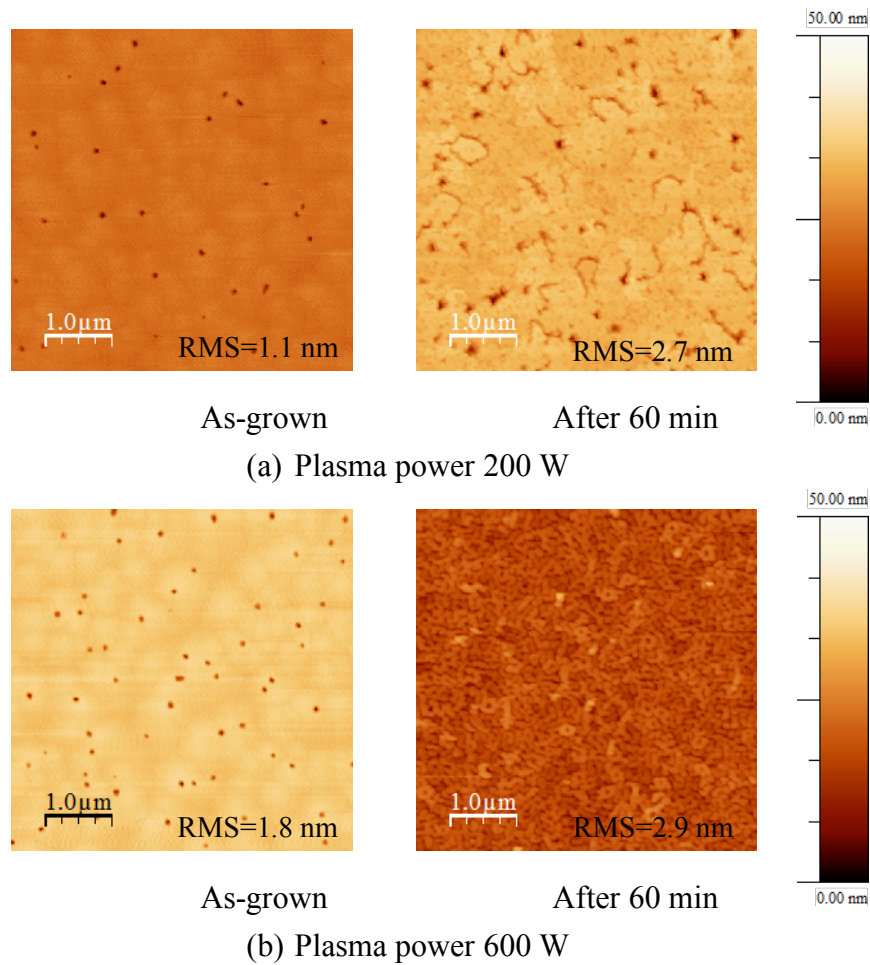


FIG. 4.11. Surface morphology of InN templates after N radical beam irradiation with different plasma power (substrate temperature of 435 °C)

Next, the electrical properties of the InN templates before and after the N radical beam irradiation at substrate temperature of 330 °C and 435 °C with plasma power of 200 W and 600 W will be described. The results of carrier concentrations and mobilities of these templates measured by Hall effect measurement are as shown in Figs. 4.12 and 4.13, respectively. The carrier concentration showed an increasing tendency after the N radical beam irradiation. In particular, it was found that the carrier concentration was remarkably increased with a higher plasma power of 600 W on both substrate temperature of 330 °C and 435 °C. This is considered to be due to an increase in damages to the crystal when the plasma power increased^[12]. It is reported that the point defects introduction increases when a higher plasma power is applied^[13], and leads to the increase in the carrier concentration^[14]. On the other hand, it can be seen that there was almost no change in the mobility for all templates as shown in Fig. 4.13. This is in an agreement with the report^[15] that the mobility limitation factor of InN is the threading dislocation. In other

words, although point defects increased due to the N radical beam irradiation, there was no influence on threading dislocation density and thus, change in mobility is not considered to have occurred.

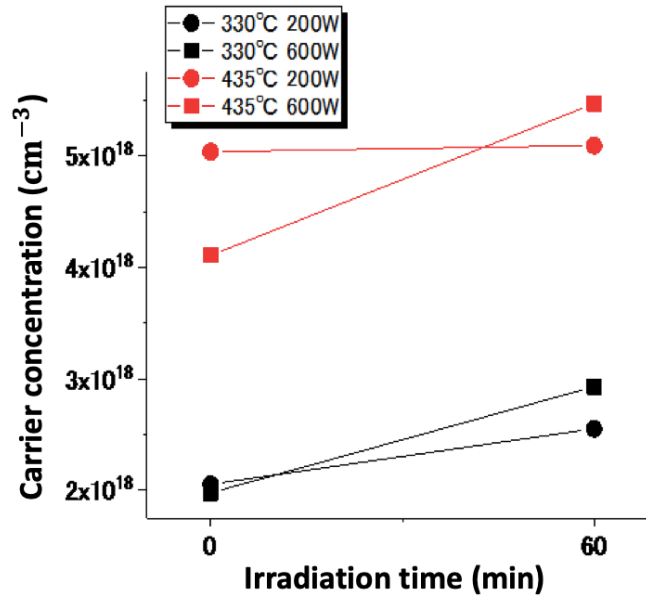


FIG. 4.12. Carrier concentration of InN templates before and after N radical beam irradiation with different plasma power and substrate temperature

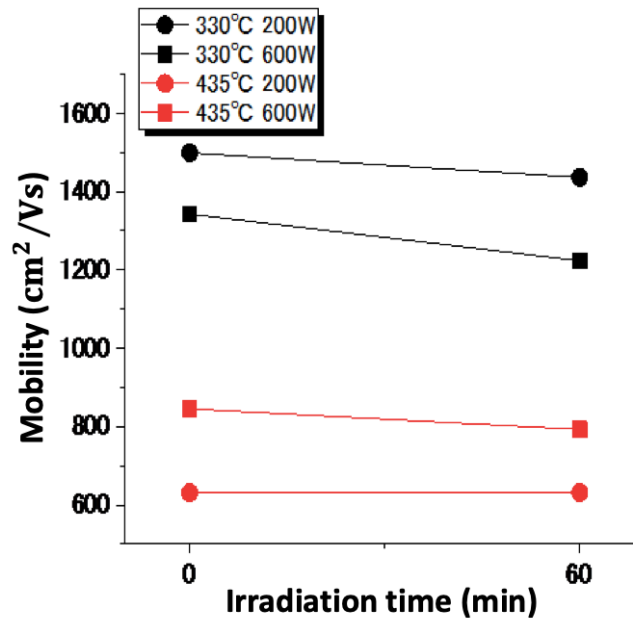


FIG. 4.13. Electron mobility of InN templates before and after N radical beam irradiation with different plasma power and substrate temperature

4.2.4 Irradiation time dependency

In this section, we discuss the N radical irradiation on InN template with different irradiation time. The substrate temperature and plasma power were kept constant at 435 °C and 200 W, respectively and the N radical irradiation was performed for 60 and 120 minutes. No further change was observed in RHEED pattern, even after the N radical irradiation was performed over 60 to 120 minutes, and the spotty streak pattern was maintained as shown in Fig. 4.7(right). The surface morphology by AFM and SEM are as shown in Fig. 4.14. As can be seen, the surface morphology changed from atomically flat surface as shown in Fig. 4.14(a) to three-dimensional structure after 60 minutes of irradiation as shown in Fig. 4.14(b), and further changed to smaller three-dimensional structure after 120 minutes as shown in Fig. 4.14(c). Figure 4.14(d) shows SEM image correspond to Fig. 4.14(c). To put it briefly, it was found that the surface morphology of the InN template changed to smaller three-dimensional structure by lengthening the irradiation time, and the surface became rougher.

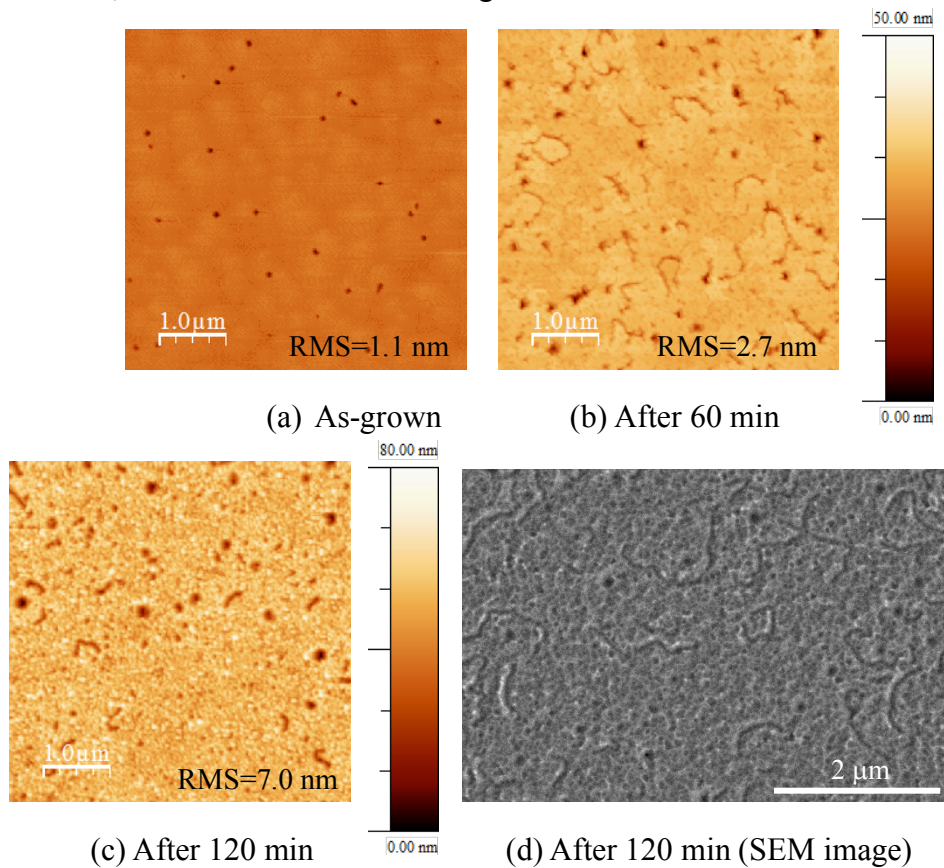


FIG. 4.14. Surface morphology of InN templates after N radical beam irradiation after 60 and 120 minutes

Next, the electrical properties of the InN templates before and after the N radical beam irradiation at substrate temperature of 435 °C with plasma power of 200 W for 60 to 120 minutes will be described. The results of carrier concentrations and mobilities of these templates measured by Hall effect measurement are as shown in Fig. 4.15. As in the previous section 4.2.3, the carrier concentration showed an increasing tendency after the N radical beam irradiation especially when the template was irradiated for 120 minutes, but no significant change in mobility was observed. Therefore, it was found that as the irradiation time increased, the electric characteristics deteriorated.

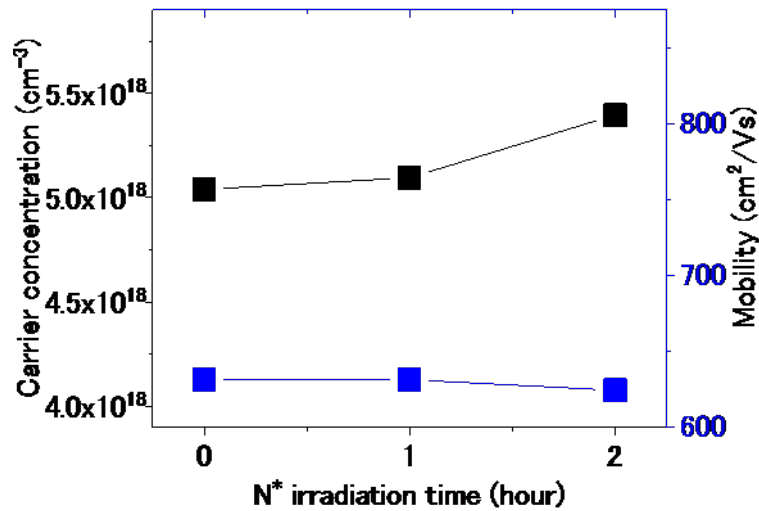


FIG. 4.15. N radical beam irradiation time dependence on electrical characteristics of InN templates

4.2.5 Comparison between N radical beam irradiation and annealing

In this section, we compare the changes in surface morphology between after N radical beam irradiation and after annealing of InN templates. Figure 4.16 shows the RHEED patterns during N radical beam irradiation with plasma power of 200 W (left) and annealing (right) at substrate temperature of 435 °C. Both templates had streak RHEED patterns before the process as shown in Fig. 4.16(a). After 10 minutes, the RHEED patterns for the template under N radical irradiation still maintained the streak pattern while the template under annealing process changed to spotty streak pattern as shown in Fig. 4.16(b). Furthermore, after 60 minutes, the RHEED patterns of the sample irradiated with N radical beam changed to spotty streak pattern, and for the annealed template, completely spotty pattern was observed as shown in Fig. 4.16(c). From this

result, it was expected that the surface morphology obtained from these two templates were greatly differs from each other.

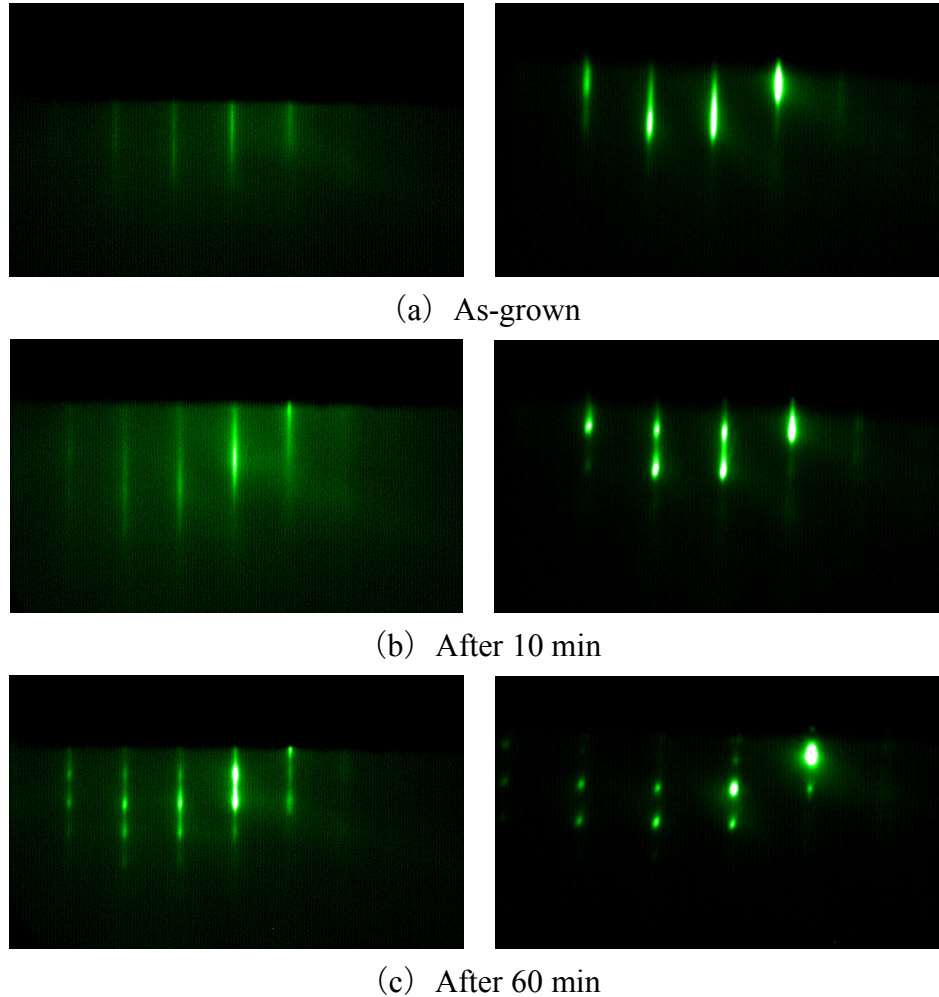


FIG. 4.16. RHEED patterns during N radical beam irradiation (left) and annealing (right)

Figure 4.17 shows AFM images of the templates after the N radical beam irradiation for 60 minutes (a), and after annealing for 10 minutes (b) and 60 minutes (c). Compared to the template irradiated with N radical for 60 minutes, the template annealed for 10 minutes already showed a larger RMS value. In addition, the surface morphology of the annealed template also had small grains structures. Furthermore, the template annealed for 60 minutes showed a more remarkable changes in the surface morphology. The surface morphology changed greatly and it is considered that the InN template was thermally decomposed. XRD ω - 2θ measurement was performed to confirm this consideration and the results are as shown in Fig. 4.18. As can be seen, a peak of In was

found only in the template annealed for 60 minutes and no In peak was observed in the template irradiated with N radical for 60 minutes and the template annealed for 10 minutes. Therefore, it means that thermal decomposition of InN differed between the cases of annealing in vacuum and N radical beam irradiation although both experiments were performed at the same substrate temperature. This was also confirmed by other groups. Fernández-Garrido et al. reported that the thermal decomposition rate of GaN in the MBE chamber is different between in vacuum state and N radical beam irradiation state [16]. In addition, Loitsch et al. reported that high temperature growth can be achieved in the N-rich state in InN growth [17]. From these facts, it can be said that the irradiation of the N radical beam could suppress the thermal decomposition of InN during the surface modification of the InN template.

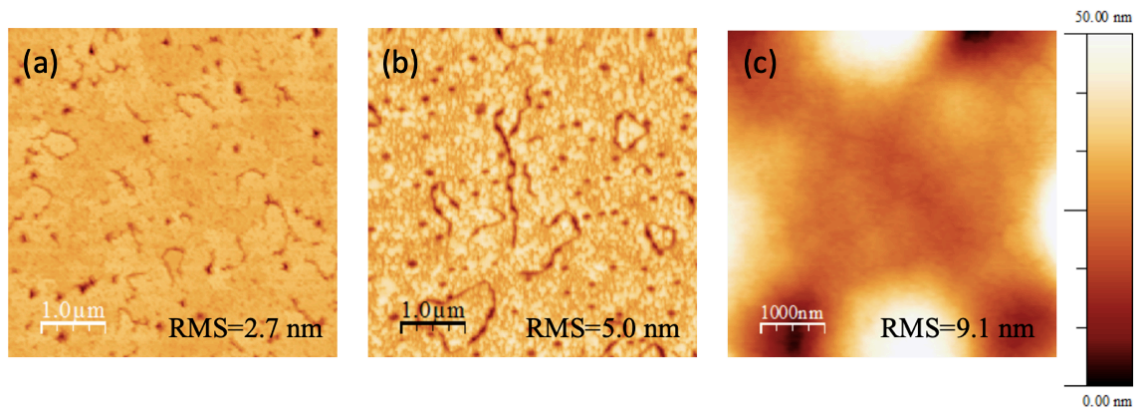


FIG. 4.17. Surface morphology of InN template (a) irradiated with N radical for 60 minutes (b) annealed for 10 minutes and (c) annealed for 60 minutes

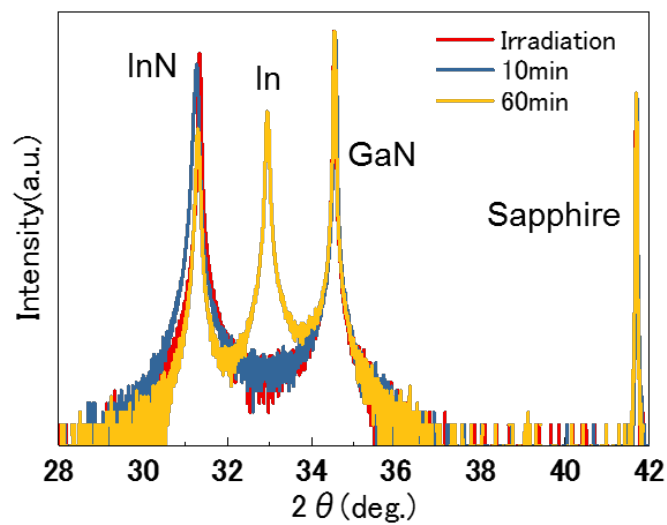


FIG. 4.18. ω - 2θ measurement result of InN template irradiated with N radical for 60 minutes and InN templates annealed for 10 and 60 minutes

4.2.6 Summary

In this section, N radical beam irradiation was performed on the InN templates with different plasma power, substrate temperature and irradiation time. For the template irradiated with plasma power of 200 W at substrate temperature of 330 °C, there was no change in the surface morphology by AFM, but the change in RHEED pattern from the streak to spotty streak pattern and the increase in carrier concentration were observed. On the other hand, for the sample irradiated at substrate temperature of 435 °C, it was found that the change in RHEED pattern was faster than during the substrate temperature of 330 °C, and the change in surface morphology was more remarkable. Furthermore, when the template was irradiated with a higher plasma power of 600 W, smaller grains were formed on the template and deterioration of electrical characteristics was obviously observed. In addition, it was found that as the N radical irradiation time increased, the electrical characteristics were also deteriorated. Therefore, for the aim of surface modification of the InN template and considering the minimal deterioration of electrical characteristics of the template, we considered that N radical irradiation at substrate temperature of 435 °C with plasma power of 200 W for 60 minutes might be the most appropriate.

In addition, comparison between N radical irradiation and annealing resulted in different changes in surface morphology. From XRD ω -2 θ measurement, the peak of In was found only in the template annealed for 60 minutes and it is considered that the template was thermally decomposed. However, no In peak was observed from the template irradiated with N radical and thus, suggesting that the N radical irradiation on the InN template not only able to modify the surface morphology of the template but also suppress the InN thermal decomposition.

4.3 InN regrowth on N radical irradiated InN template

It was confirmed that the N radical beam irradiation able to modify the surface morphology of InN template. We also considered that N radical irradiation at substrate temperature of 435 °C with plasma power of 200 W for 60 minutes might be the most appropriate for the aim of surface modification with the minimal deterioration of electrical characteristics of the InN template. In this section, we will describe the regrowth of InN on the InN template irradiated with N radical under the conditions mentioned above. Furthermore, the regrowth of InN on InN templates irradiated under different N radical conditions and on annealed InN templates are also studied.

4.3.1 Experimental method

As in the previous section, InN samples were grown under the same conditions as shown in Table 4.3 on MOCVD-grown (0001) GaN/sapphire substrates. The growth time chart is shown in Fig. 4.19. After growing InN for 60 minutes, N radical beam irradiation or annealing was carried out on the InN template for 60 minutes, then InN was regrown again on the template for 60 minutes. Table 4.5 shows N radical beam irradiation conditions for samples S2127, S2202 and S2203, and annealing conditions for sample S2248. Furthermore, as for comparison, another InN film was regrown on flat InN template (sample S2188). The sample was grown conventionally for 60 minutes plus 60 minutes (total growth time 120 minutes) without N radical irradiation or annealing in between the growth process. Threading dislocation behaviors in the samples grown under all these conditions were observed and characterized by cross-sectional TEM.

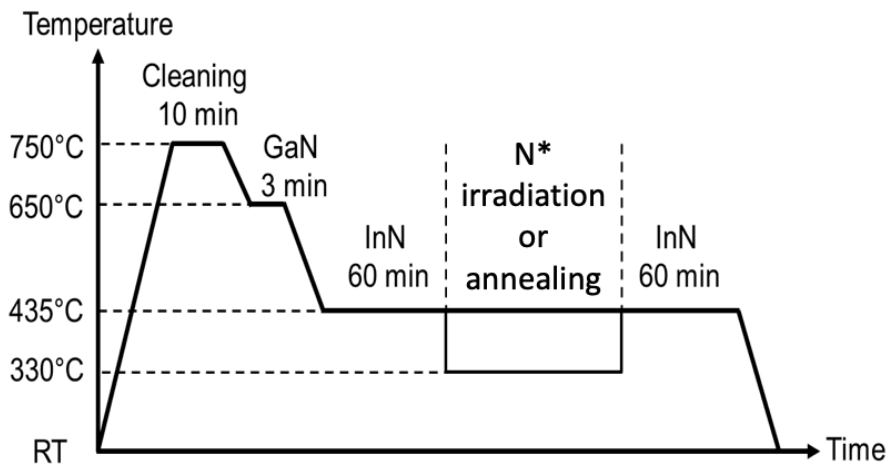


FIG. 4.19. Growth time chart

TABLE 4.5. N radical irradiation or annealing conditions in between the growth process

	Sample	Substrate temperature (°C)	Plasma power (W)
N radical irradiation	S2127	330	200
	S2202	435	200
	S2203	435	600
Annealing	S2248	435	—
Conventional	S2188	—	—

4.3.2 Threading dislocation behaviors by cross-sectional TEM observation

Figure 4.20 shows cross-sectional TEM images of InN regrown on the template irradiated with N radical at substrate temperature of 435 °C with plasma power of 200 W (S2202), and conventionally grown InN (S2188). Figures 4.20(a) and (b) show TEM images with diffraction vector, $\mathbf{g} = 0002$ which show screw dislocation while Fig. 4.20(c) and Fig.4.20(d) with $\mathbf{g} = 1-100$ which show edge dislocation in the samples. From these images, we found that both templates and regrown InN layers have dramatically low screw dislocation density, around $1 \times 10^9 \text{ cm}^{-2}$. As can be seen, screw dislocation propagated straightforwardly up to the top surface of regrown InN layers in both samples. More importantly, no additional screw dislocation was generated at the interface of regrown InN and irradiated template. A high density of edge dislocations around $2 \times 10^{10} \text{ cm}^{-2}$ can be seen in both templates' regions. Owing to this, edge dislocations in the flat InN template propagated to the top surface of the regrown InN layer, and no reduction of edge dislocation density in the regrown InN layer can be seen. This is similar to the general report of conventional heteroepitaxial InN film [18]. In contrast, the regrown InN layer on the irradiated InN template has much lower edge dislocation density and obviously the edge dislocations were reduced at the interface as shown in Fig. 4.20(d). This was not observed in the conventionally grown InN as shown in Fig. 4.20(c), and this is thought to be due to the N radical beam irradiation process. We confirmed that the edge dislocation density decreased by a factor of 3 from about 2×10^{10} to $6 \times 10^9 \text{ cm}^{-2}$ in the InN regrown on the irradiated InN template.

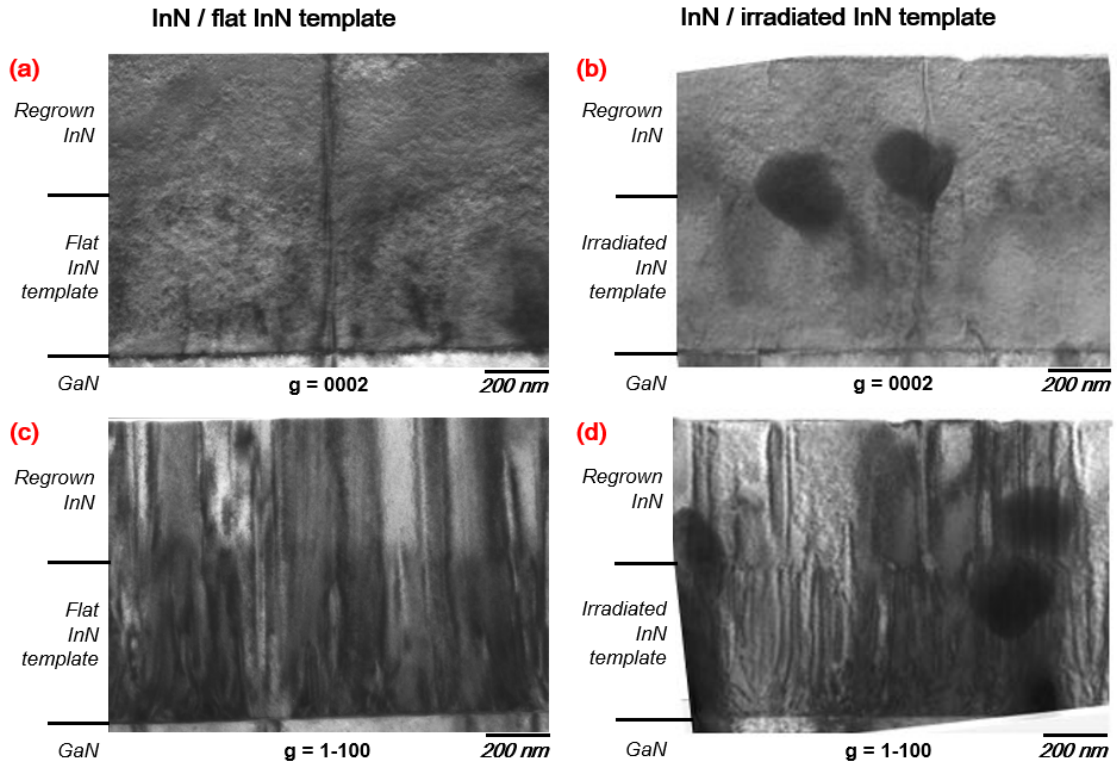


FIG. 4.20. Cross-sectional TEM images of InN regrown on flat and irradiated InN template: (a, b) $g = 0002$ and (c, d) $g = 1-100$ [8]

Next, Fig. 4.21 shows cross-sectional TEM images of InN samples (S2127, S2203, and S2248) which were regrown on the templates irradiated with N radical under different conditions and annealed InN template as described in Table 4.5. Figure 4.21(a) shows InN regrown on the template irradiated at substrate temperature of 330 °C with plasma power of 200 W. Several edge dislocations bendings can be seen at the regrowth interface. However, there was no reduction of threading dislocations in the regrown InN layer, and it has the same density as in the template. Next, Fig. 4.21(b) shows InN regrown on the template irradiated at substrate temperature of 435 °C with plasma power of 600 W. From this cross-sectional TEM image, similar to the plasma power of 200 W (Fig. 4.20 (d)), several edge dislocations disappeared at the regrowth interface but threading dislocations bunching was also observed in the regrown InN layer. Furthermore, Fig. 4.21(c) shows InN regrown on the annealed template (without N radical irradiation). Edge dislocations bending and a region where dislocation disappeared in a part of the regrown InN layer can also be seen. However, in all these three samples, the edge dislocation density estimated from the cross-sectional TEM images was $\sim 10^{10} \text{ cm}^{-2}$, and no significant

reduction of edge dislocation density was observed.

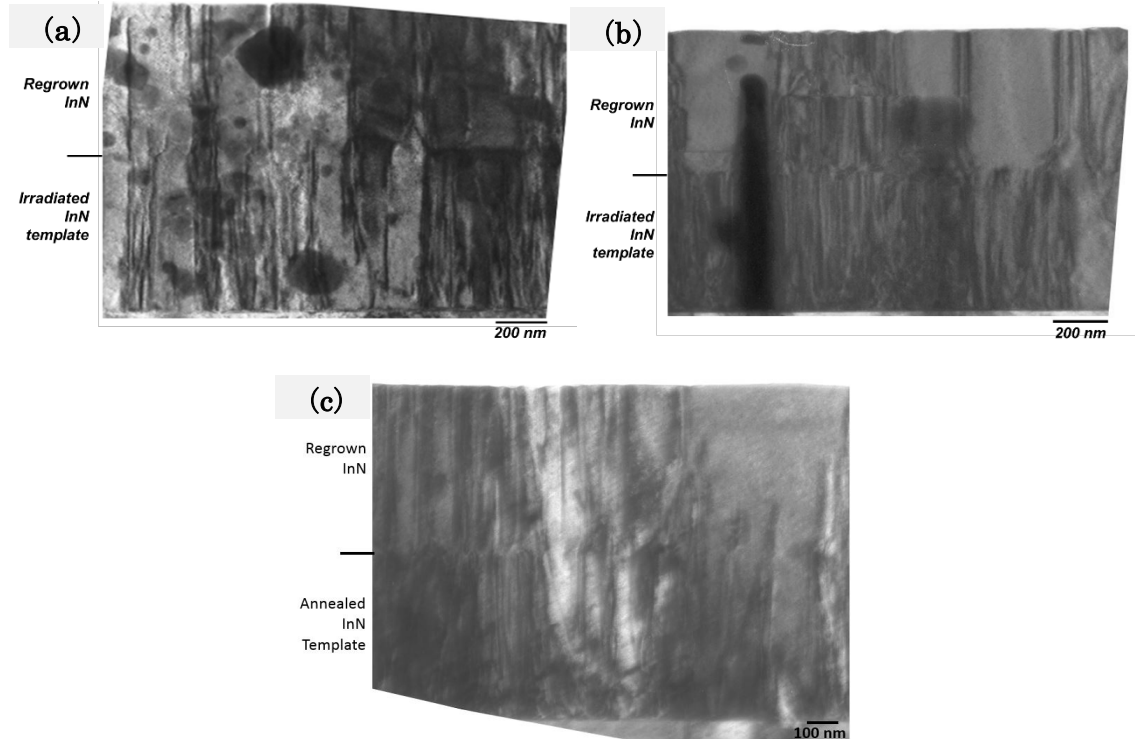


FIG. 4.21. Cross-sectional TEM images with diffraction vector, $\mathbf{g}=1-100$
(a) S2127 (b) S2203 (c) S2248

4.3.3 Mechanisms of threading dislocation reduction ^[8]

In these experiments, InN regrown on the template irradiated at substrate temperature of 435 °C with plasma power of 200 W (S2202) showed a more significant reduction of threading dislocation density compared to other samples. The edge dislocation density decreased by a factor of 3 from about 2×10^{10} to 6×10^9 cm⁻². Enlarged images of some regrowth interface regions from Fig. 4.20(d) are shown in Fig. 4.22. There are three types of edge dislocations behaviors that can be seen. In most cases, the dislocations showed a clear deviation from the original growth direction as shown in A. These dislocations bent or tilted only by a small angle then propagated straightforwardly up to the top surface of regrown InN layer. We observed a relatively large number of edge dislocations with this behavior in different regions of the sample. However, this behavior was not so effective to reduce the dislocation density, and thus no significant reduction of dislocation density can be seen in this region. Besides, dislocation bending with a large angle nearly by 90° were also observed. These dislocations bent, then joined other

dislocations and annihilated finally by forming dislocation loops as shown in B. Furthermore, several dislocations fused and produced a single resulting dislocation as shown in C. Both of these dislocation behaviors (B and C) led to a significant reduction of dislocation density in the regrown InN layer in this region.

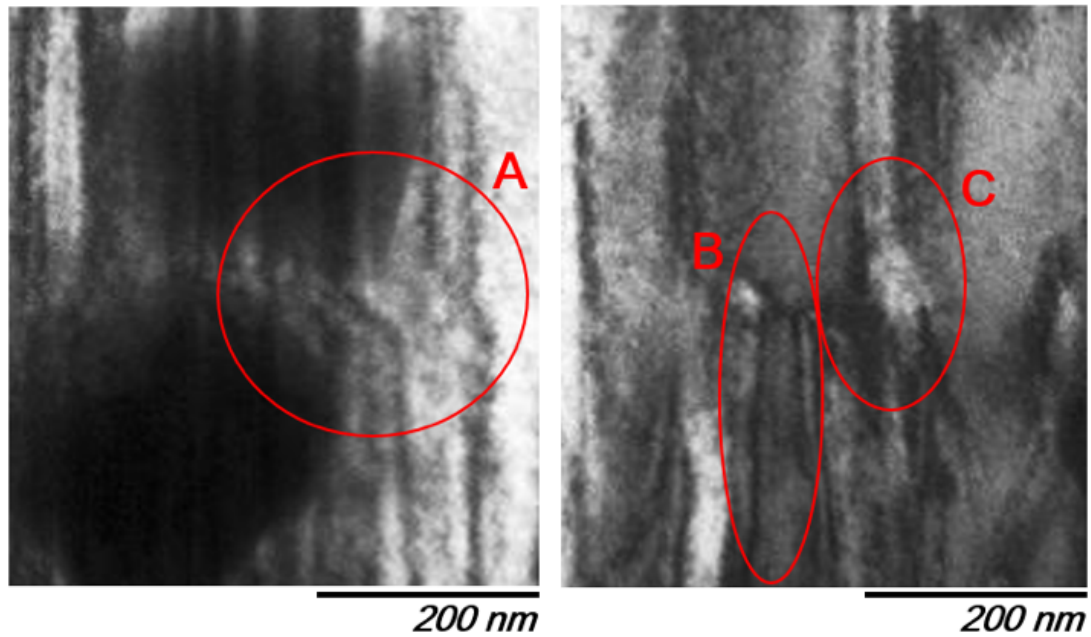


FIG. 4.22. Edge type dislocation behavior in InN/irradiated InN template. A: Dislocations bent or tilted by a small angle then propagated straightforwardly up to the top surface of regrown InN region. B: Dislocation bending with a large angle nearly by 90° and annihilated finally by forming dislocation loops. C: Dislocations fused and produced a single resulting dislocation. [8]

To understand the mechanism behind, TEM specimen of the irradiated InN template was also prepared and the corresponding cross-sectional TEM image is as shown in Fig. 4.23. This InN template was irradiated with a plasma power of 200 W at 435°C for 60 min. InN film was not regrown on this template in order to study the effect of in situ N radical beam irradiation on dislocation behavior before the regrowth of InN film. It can be seen from the TEM image that the dislocations propagated straightforwardly from the substrate up to the top surface of the template. However, it was difficult to discern the actual dislocation behavior on the superficial layer of the template. The template appears to have blunt pyramid-like shapes on its top surface and this is believed to influence the dislocation behavior in the bottom part of the regrown InN layer as shown in Fig. 4.23.

Therefore, the annihilation of dislocations is likely to be initiated by dislocations bending at the onset of InN regrowth and not right after the N radical beam irradiation on the InN template. The mechanisms considered for reduction of threading dislocation density with the surface modification by N radical beam irradiation are described below.

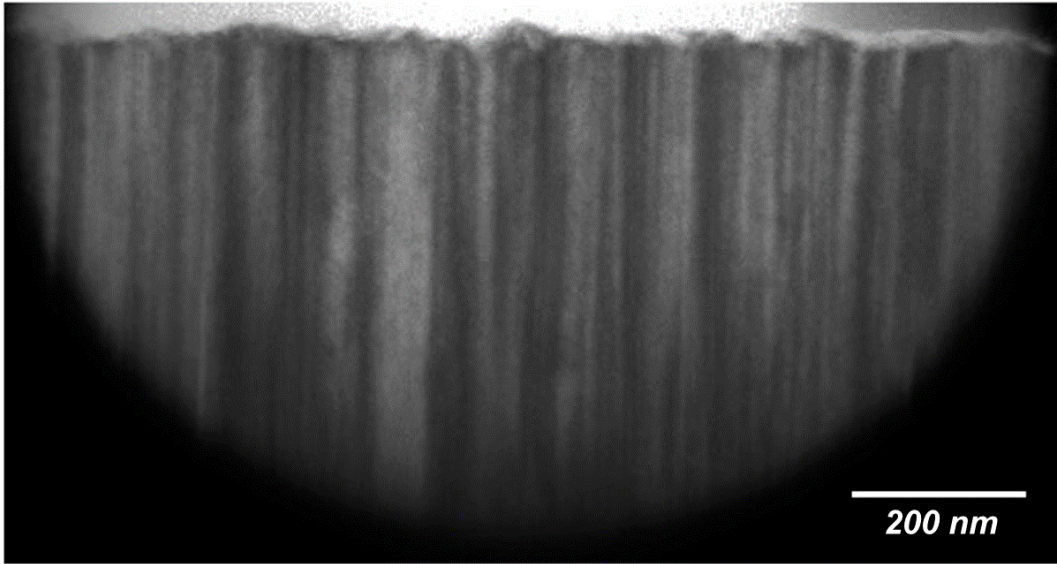


FIG. 4.23. Cross-sectional TEM image with $g = 1-100$ of the InN template after irradiated with N radical beam at 435 °C for 60 min. [8]

The mechanism of the threading dislocation density by this method are discussed from the following points. Generally, dislocation lines may end only at free surfaces, high-angle grain boundaries, or other dislocations, and threading dislocation densities are reduced by either annihilation of threading segments with antiparallel Burgers vectors or by reactions in which two threading dislocations combine to form one threading dislocation [19]. This can be achieved through various paths such as bending at the surface, merging of dislocations, and interaction with other defects. When we focus on the proposed in situ surface modification by N radical beam irradiation growth method, firstly, dislocation bending can be included because of the presence of the interface between the irradiated InN template and the regrown InN region. To date, it is well known that faceted surfaces are effective for threading dislocation bending at the interfaces in III-nitride semiconductors [20-23]. When compare with our proposed method, the faceted surface morphology was not obtained on the irradiated InN template. On the other hand, the surface changed from atomically flat surface to three-dimensional rough surface [8]. The change in surface morphology by N radical irradiation have also been reported by another groups [9, 10]. It is also known that low-energy ion irradiation in a regime where the surface

stays crystalline during the irradiation, strongly influences the surface morphology due to mass transport of the thermally activated diffusing adatoms or/and vacancies [24]. However, according to our observations, the threading dislocation inclination can be seen at the regrowth interface. This might be the result of an increased surface roughness of the irradiated InN template that had a definite correlation with increased stress relaxation of the template layers. Cantu et al. reported that the surface roughness of the stressed layer during growth helped diminish the energy barrier during the initial stage of threading dislocation inclination and they illustrated threading dislocation inclination due to the rough surfaces as shown in Fig. 4.24 [25].

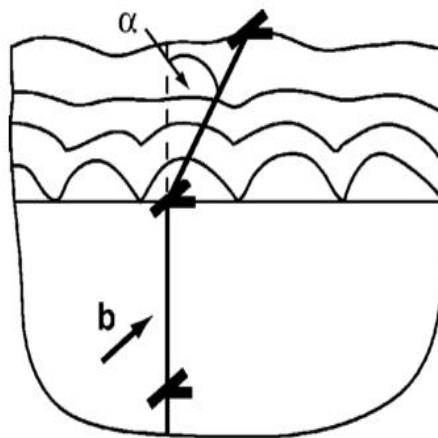


FIG. 4.24. Illustration of threading dislocation inclination due to the rough surfaces [25]

Secondly, the inclination of the threading dislocations may lead to merging of dislocations. These merging of dislocations will be enhanced when a film contains a high density of dislocations, especially when two-dimensional growth happens at a high enough growth temperature. Since threading dislocation density in InN template is high which is around 10^{10} cm^{-2} [26-29], merging of dislocations at the interface of the irradiated InN template and the regrown InN film could play the dominant role in the reduction of the threading dislocation density. We have confirmed by TEM [8] that several threading dislocations merged at the regrowth interface and resulted in one single dislocation as shown in Fig. 4.22.

Thirdly, the threading dislocation motion is strongly affected by the interaction with point defects^[30]. We found that the InN template has a higher carrier density after the N radical irradiation as discussed in Sections 4.2.3 and 4.2.4. In addition, when we regrew InN on InN template which was irradiated with a higher plasma power (600 W), the threading dislocation reduction at several part of the sample was more obvious compared to that of 200 W, as shown in Fig. 4.21(b). This might be the result of increased point defects due to the higher plasma power during the N radical irradiation^[11, 12]. Besides, there is a report showing that the InGaN surface crystalline structure has mixed with amorphous alloys after the N radical irradiation at elevated temperature^[10] and the annihilation of threading dislocation at the porous region of AlN buffer layer^[31]. Hence, we also consider the interaction between threading dislocations with point defects and amorphous region might also be one of the threading dislocation reduction mechanisms.

4.3.4 Summary

In situ surface modification was introduced in between of InN growth process to reduce threading dislocation density in InN films. N radical beam irradiation was investigated as a method to modify the surface morphology of the InN templates and compared with annealing. The threading dislocation behaviors of the InN films were observed by a cross-sectional TEM. For conventional InN growth, bending or disappearance of edge dislocations was not observed. However, the bending or/and annihilation of threading dislocations was observed in InN grown with in situ surface modification method under all conditions, and the lowest edge dislocation density obtained was $6 \times 10^9 \text{ cm}^{-2}$ with N radical irradiation performed at the substrate temperature of 435 °C and the plasma power of 200 W. In addition, it is considered that the annihilation of dislocations was likely to be initiated by dislocations bending at the onset of InN regrowth, and the most influential factor for the behavioral changes of the edge dislocations were the three-dimensional structures at the regrowth interface.

4.4 Conclusion

In this chapter, firstly, in situ surface modification of InN film by N radical beam irradiation was investigated. In this study, different plasma power, substrate temperature and irradiation time were examined to find the most appropriate N radical irradiation conditions. It was confirmed that the N radical beam irradiation able to modify the surface morphology of InN template. We also considered that N radical irradiation at substrate temperature of 435 °C with plasma power of 200 W for 60 minutes might be the most appropriate for the aim of surface modification with the minimal deterioration of electrical characteristics of the InN template. Furthermore, comparison with annealing was made, and it was also clarified that N radical irradiation on the InN template suppress the InN thermal decomposition.

Secondly, InN regrowth was performed on the modified InN surface, and the behavior of threading dislocation was investigated. From cross-sectional TEM observation, there was no change in the behavior of screw dislocations, but several edge dislocations were found to be bent and annihilated at the regrowth interface. The edge dislocation density obtained in the regrown InN region was $6 \times 10^9 \text{ cm}^{-2}$ with N radical irradiation performed at the substrate temperature of 435 °C and the plasma power of 200 W. It is assumed that the reduction of threading dislocation obtained in this study was resulted from dislocations bending at the regrowth interface, merging of dislocations and probably interaction with other defects.

References

- [1] K. Wang, T. Araki, T. Yamaguchi, Y.T. Chen, E. Yoon, and Y. Nanishi, *J. Cryst. Growth*, 430, 93 (2015).
- [2] S. Harui, H. Tamiya, T. Akagi, H. Miyake, K. Hiramatsu, T. Araki, and Y. Nanishi, *Jpn. J. Appl. Phys.* 47, 5330 (2008).
- [3] S. Nishikawa, Y. Nakao, H. Naoi, T. Araki, H. Na, and Y. Nanishi, *J. Cryst. Growth*, 301, 490 (2007).
- [4] H. Murakami, H. Cho, Y. Kumagai, and A. Koukitu, *Phys. Status Solidi C* 7, 2019 (2010).
- [5] K. Wang, T. Araki, M. Takeuchi, E. Yoon, and Y. Nanishi, *Appl. Phys. Lett.* 104, 032108 (2014).
- [6] J. Kamimura, K. Kishino, and A. Kikuchi, *Appl. Phys. Lett.* 97, 141913 (2010).
- [7] D. Muto, H. Naoi, T. Araki, S. Kitagawa, M. Kurouchi, H. Na, and Y. Nanishi, *Phys. Status Solidi A* 203, 1691 (2006).
- [8] F. B. Abas, R. Fujita, S. Mouri, T. Araki, and Y. Nanishi, *Jpn. J. Appl. Phys.* 57, 035502 (2018).
- [9] S. Gangopadhyay, T. Schmidt, C. Kruse, S. Figge, D. Hommel, and J. Falta, *J. Vac. Sci. Technol., A* 32, 051401 (2014).
- [10] J. Xue, Q. Cai, B. Zhang, M. Ge, D. Chen, J. Zheng, T. Zhi, Z. Tao, J. Chen, L. Wang, R. Zhang, Y. Zheng, *Appl. Surf. Sci.* 423, 219 (2017).
- [11] J. Sakaguchi, T. Araki, T. Fujishima, E. Matioli, T. Palacios, and Y. Nanishi, *Jpn. J. Appl. Phys.* 52, 08JD06 (2013).
- [12] A. R. Arehart, C. Poblenz, J. S. Speck, and S. A. Ringel, *J. Appl. Phys.* 107, 054518 (2010).
- [13] S. X. Li, K. M. Yu, J. Wu, R. E. Jones, W. Walukiewicz, J. W. Ager III, W. Shan, E. E. Haller, H. Lu, and W. J. Schaff, *Phys. Rev. B* 71, 161201 (2005).
- [14] R. E. Jones, S. X. Li, E. E. Haller, H. C. M. van Genuchten, K. M. Yu, J. W. Ager, Z. Liliental-Weber, W. Walukiewicz, H. Lu, and W. J. Schaff, *Appl. Phys. Lett.* 90, 162103 (2007).
- [15] C. S. Gallinat, G. Koblmüller, and J. S. Speck, *Appl. Phys. Lett.* 95, 022103 (2009).
- [16] S. Fernández-Garrido, G. Koblmüller, E. Calleja, and J. S. Speck, *J. Appl. Phys.* 104, 033541 (2008).
- [17] B. Loitsch, F. Schuster, M. Stutzmann, and G. Koblmüller, *Appl. Phys. Lett.* 102, 051916 (2013).
- [18] S. M. Islam, V. Protasenko, S. Rouvimov, H. Xing, and D. Jena, *Jpn. J. Appl. Phys.* 55, 05FD12 (2016).
- [19] J. S. Speck, M. A. Brewer, G. Beltz, A. E. Romanov, and W. Pompe, *J. Appl. Phys.* 80, 7

- (1996).
- [20] A. Usui, H. Sunakawa, A. Sakai, A. Yamaguchi, *Jpn. J. Appl. Phys.* 36, L899 (1997).
- [21] W. Luo, W. Luoa, L. Li, Z. Li, X. Xu, J. Wu, X. Liu, G. Zhang, *Appl. Surf. Sci.* 286, 358 (2013).
- [22] K. Hiramatsu, K. Nishiyama, M. Onishi, H. Mizutani, M. Narukawa, A. Motogaito, H. Miyake, Y. Iyechika, T. Maeda, *J. Cryst. Growth* 221, 316 (2000).
- [23] S. R. Xu, P.X. Li, J.C. Zhang, T. Jiang, J.J. Ma, Z.Y. Lin, Y. Hao, *J. Alloys Compd.* 614, 360 (2014).
- [24] A. Finzel, J.W. Gerlach, J. Lorbeer, F. Frost, and B. Rauschenbach, *Appl. Surf. Sci.* 317, 811 (2014).
- [25] P. Cantu, F. Wu, P. Waltereit, S. Keller, A. E. Romanov, S. P. DenBaars, and J. S. Speck, *J. Appl. Phys.* 97, 103534 (2005).
- [26] T. Araki, Y. Saito, T. Yamaguchi, M. Kurouchi, Y. Nanishi, and H. Naoi, *J. Vac. Sci. Technol. B* 22, 2139 (2004).
- [27] C. J. Lu, L. A. Bendersky, H. Lu, and W. J. Schaff, *Appl. Phys. Lett.* 83, 2817 (2003).
- [28] H. Nozawa, Y. Takagi, S. Harui, D. Muto, T. Yamaguchi, T. Araki, and Y. Nanishi, *Phys. Status Solidi C* 6, S429 (2009).
- [29] C. S. Gallinat, G. Koblmuller, F. Wu, and J. S. Speck, *J. Appl. Phys.* 107, 053517 (2010).
- [30] J. F. Justo, M. Koning, W. Cai, and V. V. Bulatov, *Mater. Sci. Eng. A* 309, 129 (2001).
- [31] J. Bai, T. Wang, P. J. Parbrook, and A. G. Cullis, *Appl. Phys. Lett.* 89, 131925 (2006).

Chapter 5

InN growth with in situ surface modification by radical beam irradiation (2)

Chapter 5

InN growth with in situ surface modification by radical beam irradiation (2)

5.1 Introduction

In Chapter 4, InN regrown on the template irradiated with N radical beam under the condition of plasma power of 200 W and substrate temperature of 435 °C for 60 minutes showed decrease in edge dislocation density. Therefore, in this chapter, we investigated the InN growth with in situ surface modification by N radical irradiation under the same conditions but with different irradiation time, as will be described in Section 5.2. We also studied the InN regrowth on different thickness of irradiated InN template in order to realize further improvement in crystallographic quality and electrical properties of the grown InN films, as will be described in Section 5.3. In addition, the repeatability of this method was also studied by repeating the N radical irradiation process several times during the growth process, as will be described in Section 5.4.

5.2 InN regrown on templates irradiated with different N radical irradiation time

In this section, further N radical irradiation condition optimization will be discussed using the condition of the substrate temperature of 435 °C and the plasma power of 200 W at which the threading dislocation density was reduced the most in Section 4.3. The N radical irradiation time, which is an important parameter for surface modification of the InN template was varied. As described in Section 4.2.4, we observed an increase in roughness of the surface morphology and point defects in the InN template when the irradiation time increased. Therefore, we believe that the effect of N radical irradiation time on the edge dislocations behavior will also change after the regrowth of InN on the templates. In this study, the crystallographic quality, dislocation behaviors, surface morphology, electrical characteristics and optical properties of the InN regrown on the template irradiated with N radical under different irradiation time will be described.

5.2.1 Experimental method

As in the previous chapter, InN samples were grown under the same conditions as shown in Table 4.2 on MOCVD-grown (0001) GaN/sapphire substrates. The growth time chart is shown in Fig. 5.1. After growing InN for 60 minutes, N radical beam irradiation was carried out on the InN template. Table 5.1 shows N radical beam irradiation conditions for samples S2188 (0 min), S2214 (30 min), S2202 (60 min), S2189 (120 min) and S2213 (180 min). Then, InN was regrown again on the template for 60 minutes. The samples were then characterized by XRD, TEM, AFM, Hall effect measurement and PL spectroscopy.

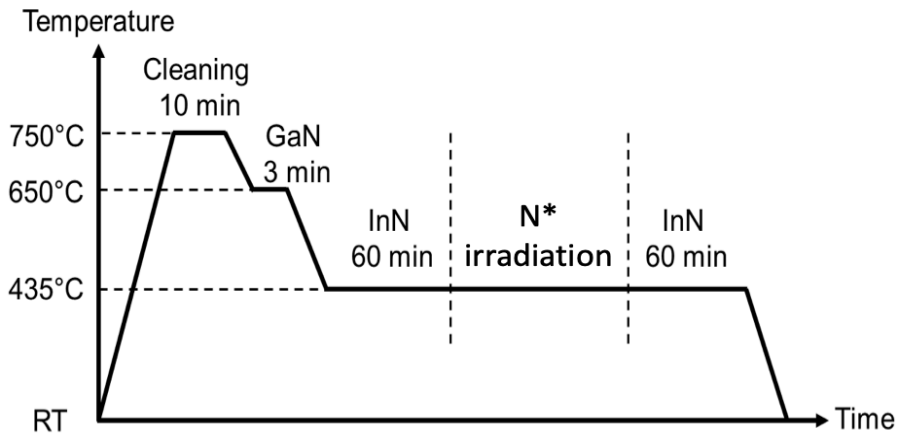


FIG. 5.1. Growth time chart

TABLE 5.1. N radical irradiation conditions with different irradiation time

Substrate temperature (°C)	435
In beam flux (Torr)	1.40×10^{-6}
N ₂ flux (sccm)	2.0
Plasma power (W)	200
N radical beam irradiation time (min)	0 (S2188)
	30 (S2214)
	60 (S2202)
	120 (S2189)
	180 (S2213)

5.2.2 Effects on threading dislocation behaviors

The XRC measurement which is an effective method for estimating threading dislocation density was carried out on five faces which are (002), (103), (102), (101), and (302) of the samples. The XRC results and fitting [1] results are as shown in Fig. 5.2. There was no large difference in measured values in any of the samples. The full width at half maximum of the (100) plane obtained from this fitting and threading dislocation density estimated by calculation are shown in Table 5.2. The estimated screw dislocation densities were around 10^8 to 10^9 cm^{-2} and the estimated edge dislocation densities were around 10^{10} cm^{-2} . From this result, there was no significant effect on reduction of screw dislocation and edge dislocation density in the samples could be observed.

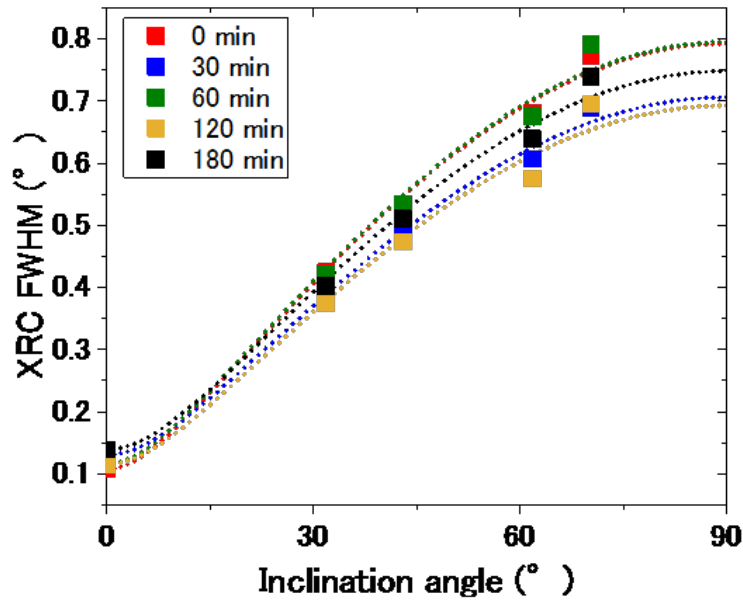


FIG. 5.2. Symmetrical and non-symmetrical XRC-FWHM

TABLE 5.2. FWHM and threading dislocation density estimated from XRC

Irradiation time (min)	(002) FWHM (arcsec)	(100) FWHM (arcsec)	Screw dislocation (cm^{-2})	Edge dislocation (cm^{-2})
0	390	2850	6×10^8	8×10^{10}
30	470	2540	9×10^8	6×10^{10}
60	420	2860	7×10^8	8×10^{10}
120	410	2490	7×10^8	6×10^{10}
180	500	2690	1×10^9	7×10^{10}

Figure 5.3 shows cross-sectional TEM images with diffraction vector, $\mathbf{g} = 1-100$ of InN samples (S2188, S2214, S2202, S2189 and S2213) which were regrown on the templates irradiated with N radical under different irradiation time as described in Table 5.2. The behavior of the edge dislocations in the sample grown on non-irradiated template (0 min irradiation) showed only straight propagation and reaching the sample surface straightforwardly. For other samples grown on the irradiated samples (30, 60, 120, 180 minutes irradiation), the N radical beam irradiation showed an effect on the propagation of edge dislocations where the dislocations showed bending propagation. The edge dislocation density obtained from the TEM image was around 10^{10} cm^{-2} for 0 min irradiation as shown in Fig. 5.3(a). For 60 minutes irradiation, the threading dislocation density reduced to $6 \times 10^9 \text{ cm}^{-2}$ as shown in Fig. 5.3(c). In the other three samples, as shown in Figs. 5.3(b), (d) and (e), although a decrease in dislocation density could be observed, the reduction was not large enough and it was found that around 10^{10} cm^{-2} edge dislocations still existed in the samples. The differences in scale of reduction of the threading dislocation density in these samples might be related to the mechanisms proposed in Section 4.3.3.

In addition, these dislocations behaviors observed by TEM were not reflected in the XRC measurement results as shown previously in Table 5.2. We suggested that the results of XRC measurements were influenced by the interface of the regrown InN and the irradiated InN template since the XRC profiles values appear to have resulted from the average properties of the entire sample including the template. In situ RHEED monitoring and ex-situ AFM confirmed that the irradiated InN templates had three-dimensional rough structures on the surface as described in Section 4.2. On the other hand, we could differentiate clearly the differences in density of threading dislocation in the irradiated template and the regrown InN regions by TEM observation. TEM observation also confirmed that the threading dislocation density in the irradiated InN template was higher than in the regrown InN region. Therefore, the evaluation of threading dislocation density by TEM is considered to be more reliable.

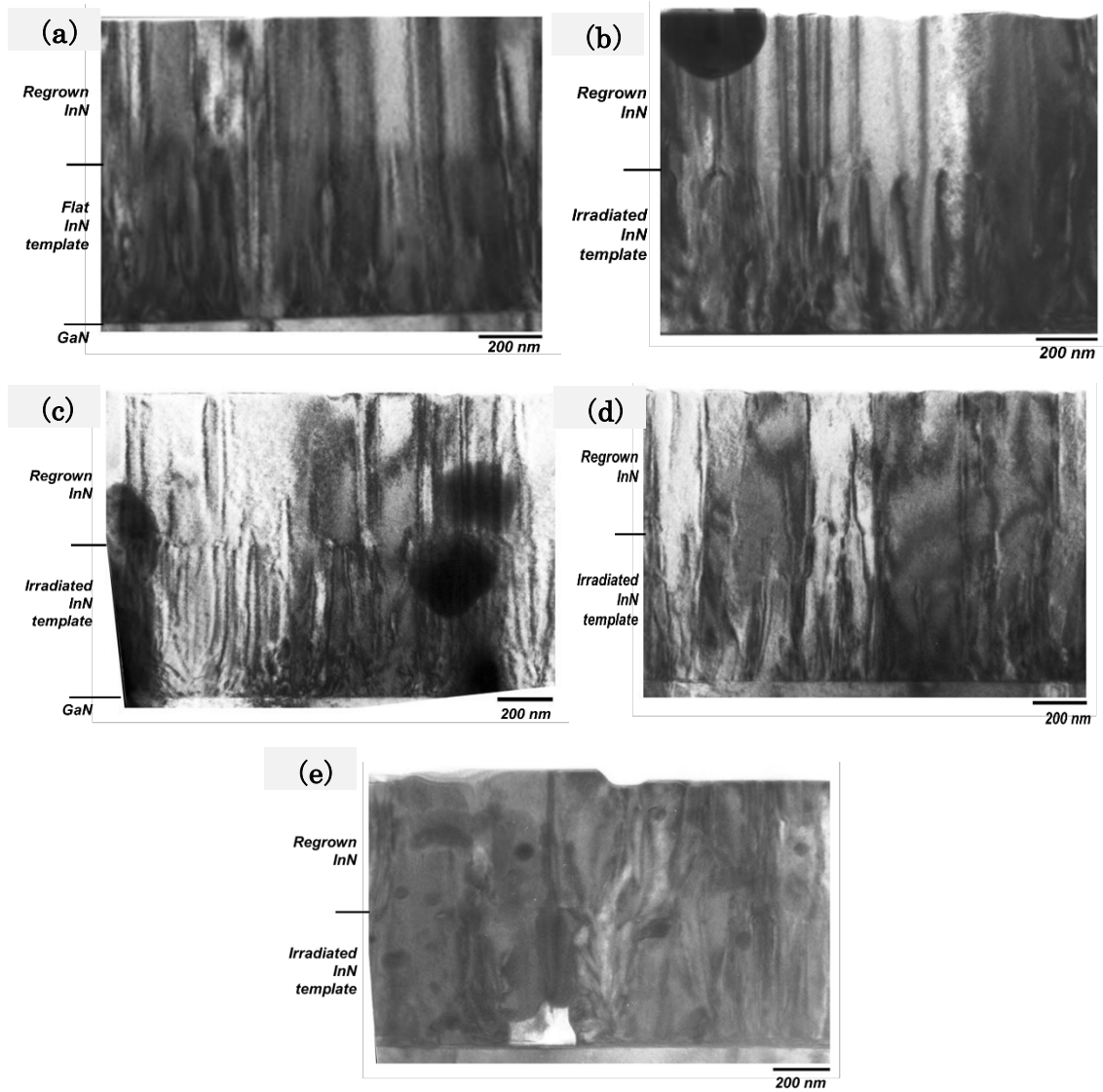


FIG. 5.3. Cross-sectional TEM images with diffraction vector, $\mathbf{g} = 1-100$ of InN samples regrown on the templates irradiated with N radical under different irradiation time as described in TABLE 5.2: (a) S2188, (b) S2214, (c) S2202, (d) S2189 and (e) S2213

5.2.3 Surface morphology, electrical characteristics and optical properties

Figure 5.4 shows RMS roughness values measured using AFM of the surface morphology of the InN samples regrown on the templates irradiated with N radical under different irradiation time. As can be seen, the samples with the irradiation time of 0 to 60 minutes have relatively flatter surfaces with RMS values below 2.5 nm. Therefore, it is considered that averagely, the surface morphology of the regrown InN layers was not influenced by the irradiated template for irradiation time below 60 minutes. However, with the irradiation time of 120 minutes and 180 minutes, the RMS values tended to increase. In addition, it can be seen that the surface morphologies are greatly different between (a) 0 minutes and (b) 180 minutes in the AFM images shown in Fig. 5.4. In figure Fig. 5.4(a), although the pits are present, the sample has two-dimensional structure surface and relatively flat. On the other hand, for Fig. 5.4(b), small grains with three-dimensional structures can be observed on the sample surface. We believe that the difference in surface morphology of the regrown InN layer was caused by the large differences of surface morphology of the irradiated InN templates. It was observed that the RMS roughness values of the irradiated templates increased with N radical beam irradiation time increased from 60 minutes to 120 minutes, as previously shown in Section 4.2.4. The RMS values of the regrown InN layers also showed the same trend. Therefore, it is considered that the surface roughness of the InN template affects the regrown InN layer surface morphology.

Next, we will discuss about the electrical characteristics and optical properties of the InN samples regrown on the templates irradiated with N radical under different irradiation time. Figure 5.5 shows carrier concentration and mobility of the samples. From the TEM observation described in Section 5.2.2, the edge dislocation density was decreased in the regrown InN region. Therefore, reduction of residual carrier concentration ^[2] and the improvement in mobility ^[3] were expected. However, no significant improvement in carrier concentration and mobility depending on the N radical beam irradiation time was observed. In the Hall effect measurement, the measurement of carrier concentration and mobility included not only the regrown InN region but also the irradiated InN template region. Since the irradiated InN templates had three-dimensional rough structures on the surface as described in Section 4.2, and higher dislocation density compared to the regrown InN layer as described in Section 5.2.2, it is considered that the carrier concentration and mobility obtained from the Hall effect measurement were

affected by the irradiated InN template layer, and thus, no significant improvement in the electrical characteristics can be observed.

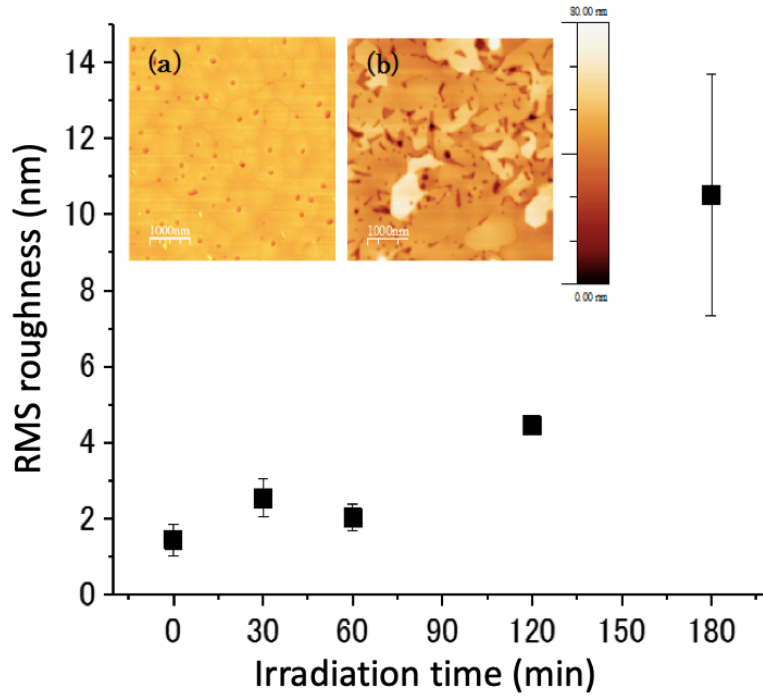


FIG. 5.4. RMS surface roughness of InN samples regrown on the templates irradiated with N radical under different irradiation time
 (a) Irradiation time of 0 min (b) Irradiation time of 180 min

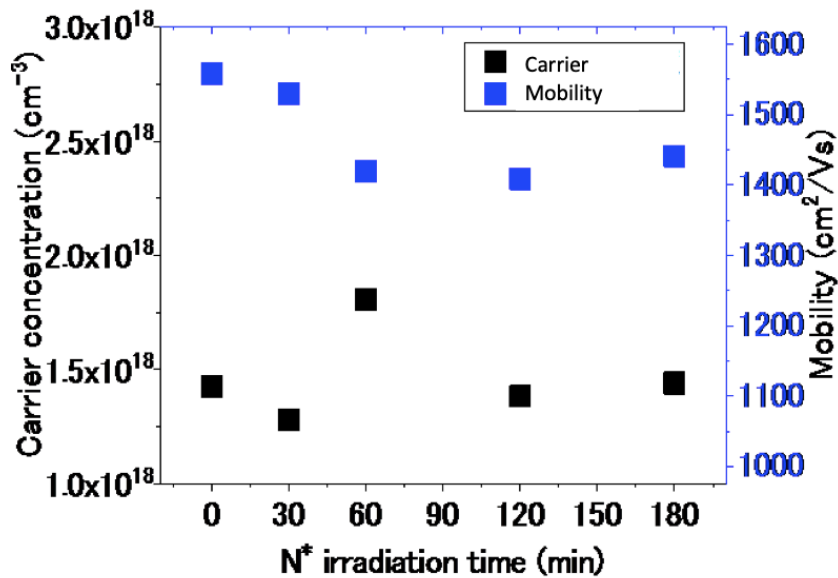


FIG. 5.5. Electrical properties of InN samples regrown on the templates irradiated with N radical under different irradiation time

To study the crystalline quality of the top regrown InN layer without the influence of the regrowth interface, PL spectroscopy was performed. The InN films were optically excited using an Ar ion laser line at 514 nm. A liquid nitrogen cooled InGaAs photodiode and a lock-in amplifier was used for phase sensitive detection. The samples were set in a cryostat coupled with a He compressor and the temperature was set at 10 K. The laser penetration length in InN is considered to be about 200 nm^[4]. Therefore, it is possible to measure only the regrown InN region of the samples. PL spectroscopy was performed at five different regions on each sample and the average values of the measurements are compared as shown in Fig. 5.6. As expected, all InN samples regrown on the templates irradiated with N radical although under different irradiation time showed not only lower peak energy but also smaller FWHM and higher PL intensity compared to the InN regrown on non-irradiated template (0 min irradiation). Average FWHM values of PL spectra improved from 51 meV for the InN regrown on non-irradiated template to 28 meV for the InN regrown on the irradiated template (60 min).

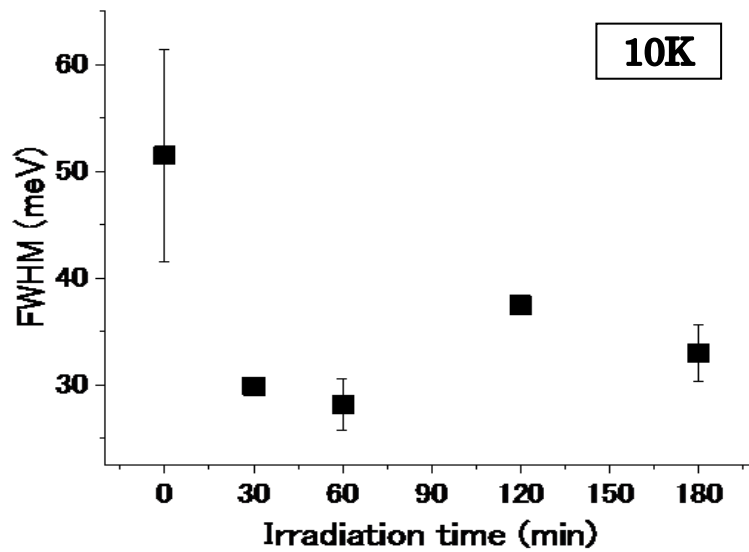


FIG. 5.6. FWHM of PL of InN regrown on the templates irradiated with N radical under different irradiation time

Furthermore, Fig. 5.7 shows the comparison of PL spectrum of the InN regrown on non-irradiated template (0 min) and the InN regrown on the irradiated template (60 min). In view of the results obtained, the peak of PL spectrum for the InN regrown on the irradiated template (60 min) was clearly shifted to lower energy region and closer to 0.65 eV compared to the InN regrown on non-irradiated template. It also showed sharper PL spectrum and higher PL intensity. This suggests that the InN layers regrown on the irradiated templates have lower defects density compared to the InN layer regrown on

non-irradiated template [5, 6]. The results showed good agreement with the reduction of threading dislocation density observed by TEM as previously discussed.

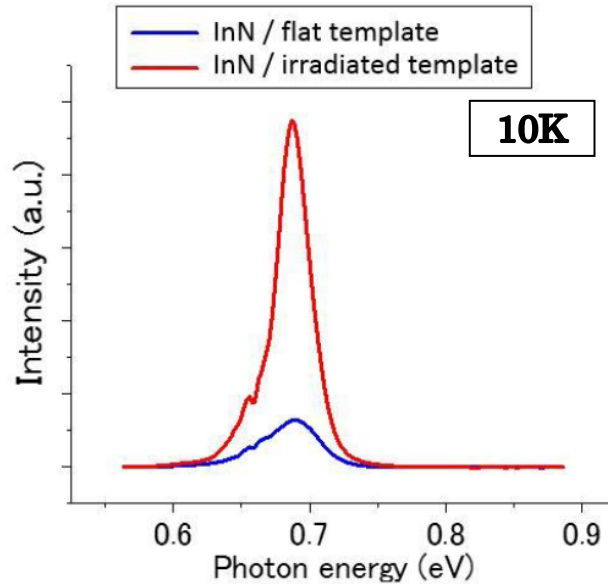


FIG. 5.7. Comparison of PL spectrum of the InN regrown on non-irradiated template and the InN regrown on the irradiated template (60 min) [7]

5.2.4 Summary

InN growth with in situ surface modification by N radical irradiation under the same conditions but with different irradiation time was investigated. InN samples were regrown on the template irradiated under N radical irradiation time from 0 to 180 minutes and evaluated. TEM revealed that threading dislocation density in InN regrown on the template irradiated with plasma power of 200 W and substrate temperature of 435 °C for 60 minutes reduced from about $2 \times 10^{10} \text{ cm}^{-2}$ to $6 \times 10^9 \text{ cm}^{-2}$ in certain regions. The results showed good agreement with the results from PL spectroscopy, although no obvious improvement was seen from XRD analysis and Hall effect measurement. Therefore, for future works, the irradiated InN template thickness is suggested to be taken into account to minimize the effect of regrowth interface on crystallographic quality and electrical properties of the entire InN film. In addition, the surface roughness of the regrown InN layer measured by AFM tended to increase with irradiation time of 120 minutes and above, and thus, 60 minutes of N radical beam irradiation is considered to be the most optimum irradiation time in this study.

5.3 Relationship between the thickness of irradiated template with crystallographic quality and electrical properties of InN film ^[8]

In Section 5.1, TEM observation revealed that the threading dislocation density in 450 nm thick InN film regrown on 450 nm thick irradiated InN template decreased by a factor of 3, from $2 \times 10^{10} \text{ cm}^{-2}$ to $6 \times 10^9 \text{ cm}^{-2}$ in certain regions and showed good agreement with the results from PL spectroscopy. However, no significant improvement was seen in crystallographic quality and electrical properties measured by XRD and Hall effect measurement. We suggested that these results are influenced by the interface of the regrown InN and the irradiated InN template since the XRC profiles and Hall effect measurement values appear to have resulted from the average properties of the entire sample including the template. In situ RHEED monitoring and AFM confirmed that the irradiated InN template had three-dimensional rough structures on the surface. In addition, TEM observation also confirmed that the threading dislocation density in the irradiated InN template was higher than in the regrown InN region. It was suggested that the thickness of irradiated InN template should be minimized to reduce its influences on crystallographic and electrical properties of the entire InN film. Therefore, in this section, we studied the relationship between the thickness of N radical irradiated InN template with crystallographic quality and electrical properties of InN film grown with this method.

5.3.1 Experimental method

As in the previous chapter, InN samples (A, B, C and D) were grown under the same conditions as shown in Table 4.2 on MOCVD-grown (0001) GaN/sapphire substrates. Figure 5.8 shows the growth time chart. Prior to growth, the substrates were thermally cleaned at 750 °C for 10 min, and thin GaN layers were deposited at 650 °C for 3 min. Then, InN templates were grown at 435 °C for 12 min, 20 min, 60 min and 90 min for sample A, B, C and D respectively. The templates were then irradiated with N radical beam at 435 °C with plasma power of 200 W for 60 min. Finally, InN films were regrown on the irradiated templates at 435 °C for 108 min, 100 min, 60 min and 30 min for sample A, B, C and D respectively. The resultant total thickness of each sample was ~900 nm and the schematic diagrams of the sample structures are shown in Fig. 5.9. After growth, the crystalline structure, electrical properties and threading dislocation behaviors of the samples were examined by XRD, Hall effect measurement and TEM. The TEM specimens were prepared by FIB etching.

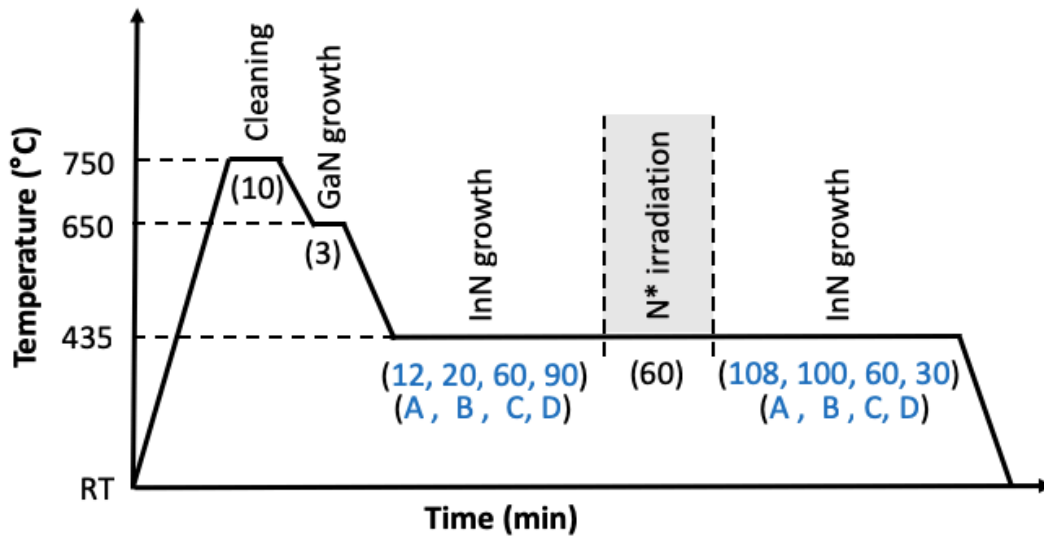
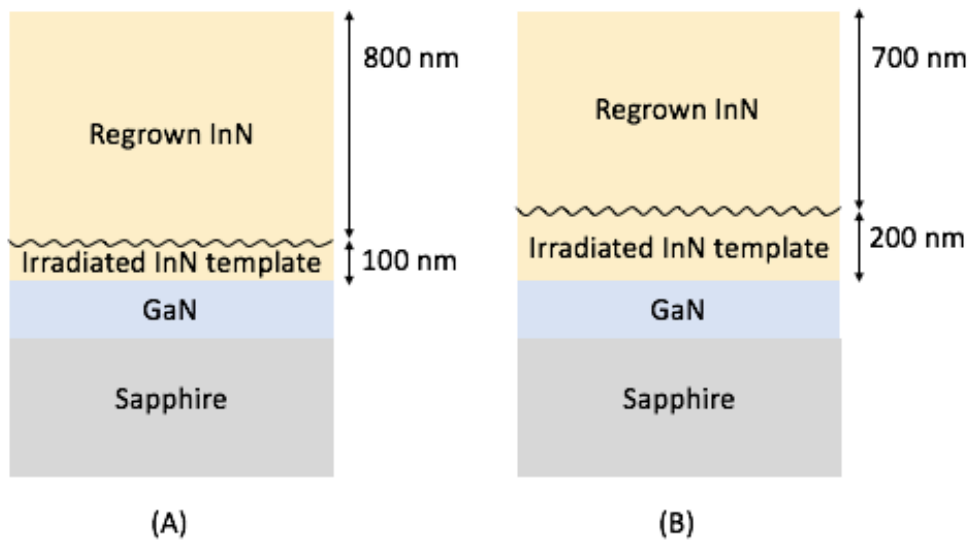


FIG. 5.8. Growth time chart of each sample (A: 12 min/108 min InN growth, B: 20 min/100 min InN growth, C: 60 min/60 min InN growth, D: 90 min/30 min InN growth)



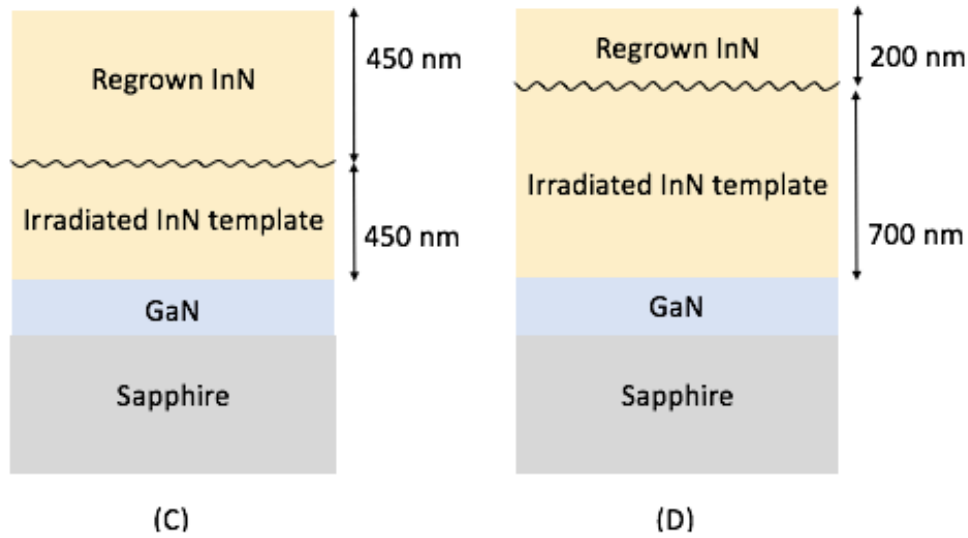


FIG. 5.9. Schematic diagrams of the sample structures (A: 800 nm thick InN/100 nm thick irradiated InN template, B: 700 nm thick InN/200 nm thick irradiated InN template, C: 450 nm thick InN/450 nm thick irradiated InN template, D: 200 nm thick InN/700 nm thick irradiated InN template)

5.3.2 Experimental results and discussion

XRC for (002) and (302) reflections were measured to characterize the crystalline quality of the grown InN films. Figure 5.10 shows the FWHM for (002) and (302) reflections. Comparison of XRC profiles showed that all samples had FWHM of ~ 400 arcsec to ~ 500 arcsec for (002) reflections. However, for (302) reflections, although no significant improvement can be seen from sample B, C and D, a striking contrast was observed in sample A with FWHM of 1100 arcsec. The FWHM was even smaller compared to the InN grown on flat InN template as also shown in Fig. 5.10 for comparison. It is well known that FWHM of (0002) and (302) reflections correspond to tilt distributions and twist distributions respectively. Since screw dislocation density in InN is comparatively lower than edge dislocation density, a significant reduction of screw dislocation by proposed growth method might be difficult to obtain, and thus no distinct improvement of (002) reflection was observed. On the other hand, the reduction of edge dislocation by this method has been confirmed [7]. The improved FWHM of (302) reflection obtained in this experiment for InN regrown on a thinner irradiated InN template i.e. 100 nm thick, confirmed the importance of minimizing the thickness of

irradiated InN template to be as thin as possible for a higher crystallographic quality of entire InN film.

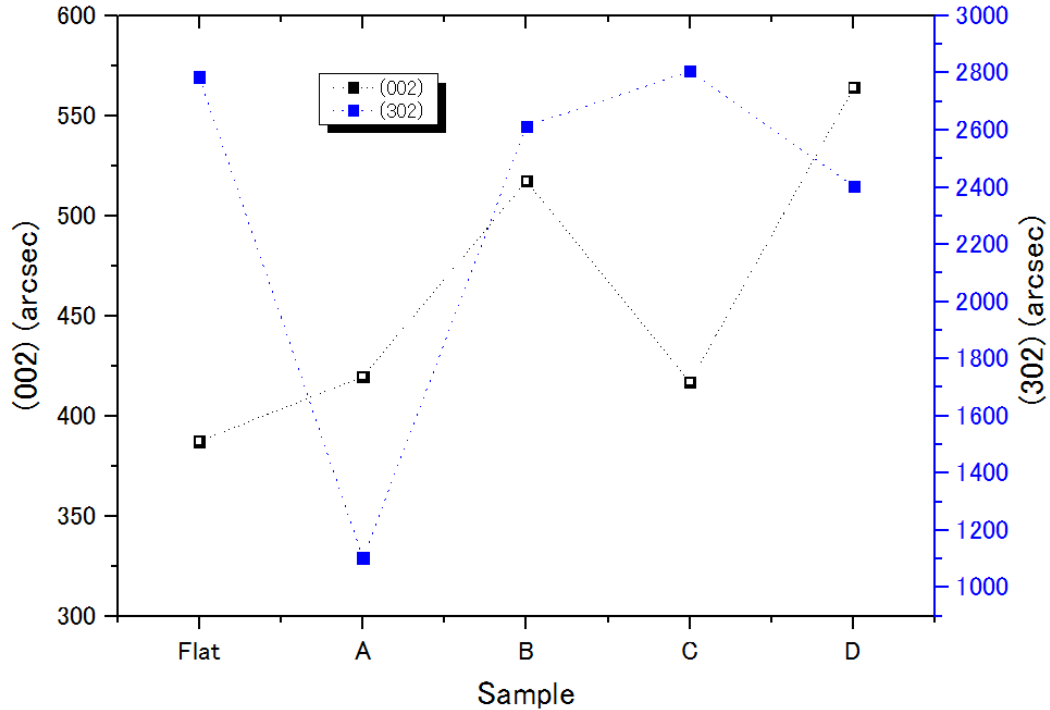


FIG. 5.10. XRC-FWHM of (002) and (302) reflections for sample A, B, C and D compared to the InN regrown on flat template.

Next, the irradiated InN template thickness dependence of the entire InN film electrical properties was studied by Hall effect measurement at room temperature. Figure 5.11 shows carrier concentration and mobility of the grown InN films. It is noted that a lower carrier concentration was obtained with a thinner irradiated InN template, i.e. sample A which was decreased drastically to $1.06 \times 10^{18} \text{ cm}^{-3}$. This might be due to the larger region of regrown InN layers with fewer threading dislocations and thus, smaller residual carrier concentration was obtained [9-13]. On the other hand, no significant improvement on mobility can be seen from sample A, B, C and D. This might be influenced by the current path by Hall effect measurement. As shown in Fig. 5.12, the carrier concentration at the interface of InN and substrate vicinity is high due to a high density of threading dislocations [14, 15]. In addition, from the results in Chapter 4, the carrier concentration was increased when the InN template was irradiated by N radical beam due to the introduction of point defects [16-18], and thus, it is also considered that the irradiated interface vicinity has a high carrier concentration. To put it briefly, since the carrier concentration is higher at these two regions (vicinity of substrate interface and N radical irradiated interface)

compared to the regrown InN region, it is considered that the current path by Hall effect measurement is dominant. Therefore, in the Hall effect measurement, further analysis that consider the three areas of the substrate interface (high carrier concentration, high dislocation density), N radical beam irradiation interface (high carrier concentration, high point defect density) and regrown region (low carrier concentration, low dislocation density) is necessary. Comparison with KOH etching which introduces fewer point defects is also considered to be one effective means for these investigations.

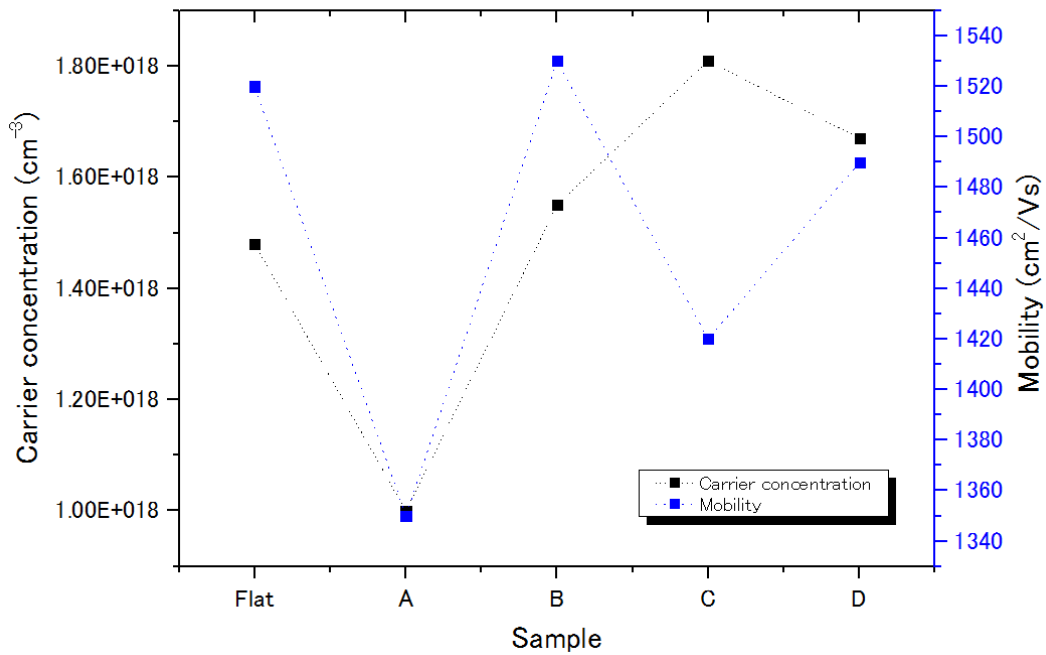


FIG. 5.11. Electrical properties by Hall effect measurement of sample A, B, C and D compared to the InN regrown on flat template.

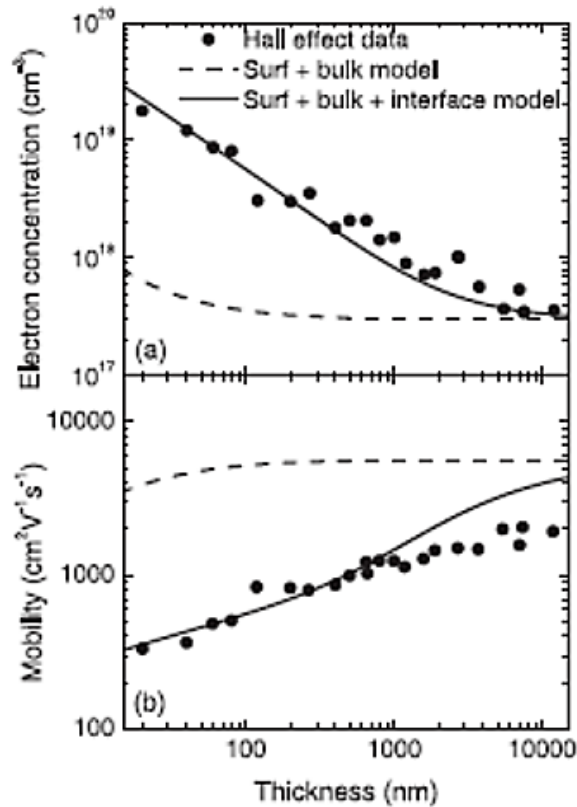


FIG. 5.12. Relationship between InN film thickness with electron concentration and mobility by Hall effect measurement ^[14]

Figure 5.13 shows cross-sectional TEM images with diffraction vector, $g=1-100$ of the grown InN samples A, B, C and D with different thickness of irradiated InN template of 100, 200, 450 and 700 nm, respectively. The interface between InN template irradiated with N radical beam and the regrown InN region of samples C and D can be identified and threading dislocations can also be clearly observed, as shown in Figs. 5.13(c) and (d). However, for samples A and B, the interface between InN template irradiated with N radical beam and the regrown InN region cannot be identified and threading dislocations also cannot be clearly observed, as shown in Figs. 5.13(a) and (b). This probably might be due to the deterioration of the templates after the N radical irradiation since the thickness of each template in samples A and B were relatively thin. However, the edge dislocation density in the regrown InN regions estimated from these TEM images were $4.6 \times 10^9 \text{ cm}^{-2}$ for sample A, $5.5 \times 10^9 \text{ cm}^{-2}$ for sample B, $6.0 \times 10^9 \text{ cm}^{-2}$ for sample C and $8 \times 10^9 \text{ cm}^{-2}$ for sample D. These values are smaller than the edge dislocation density of 10^{10} cm^{-2} in conventional InN growth, and it is considered that there is an effect of N radical beam irradiation on reduction of threading dislocation density in the regrown InN region regardless of the irradiated template thickness.

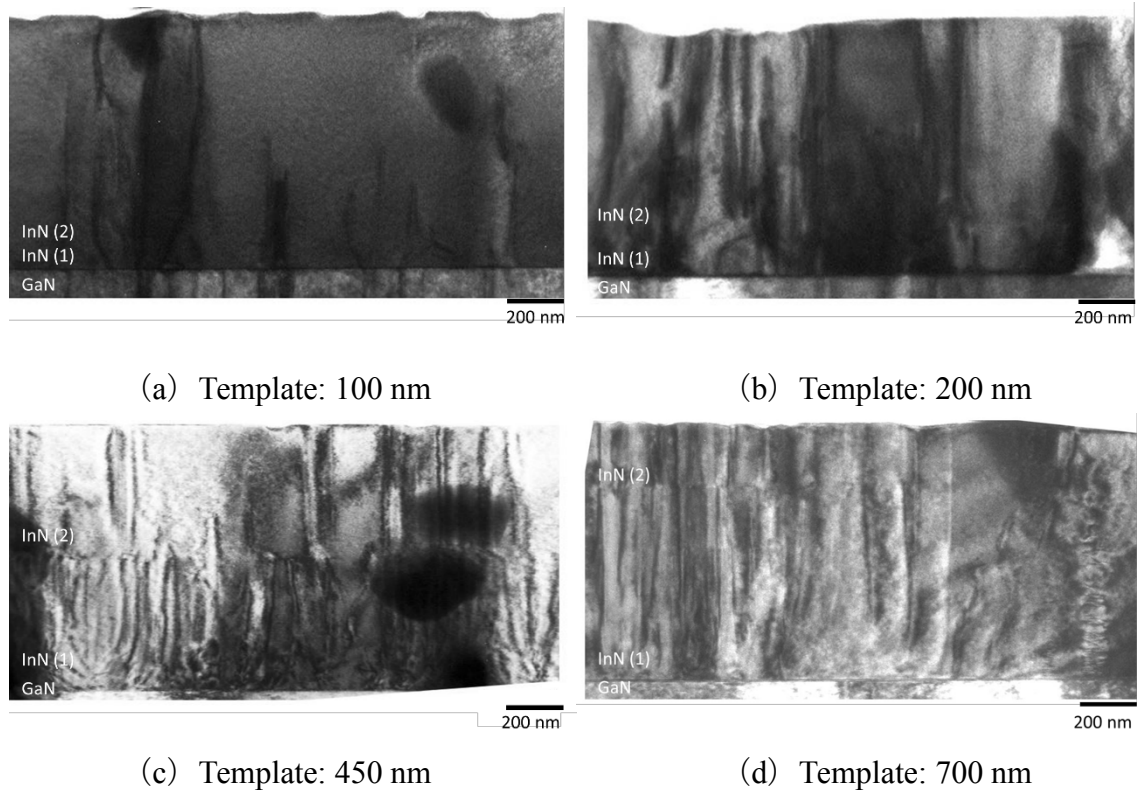


FIG. 5.13. Cross-sectional TEM images of the InN samples (A: 800 nm thick InN/100 nm thick irradiated template, B: 700 nm thick InN/200 nm thick irradiated template, C: 450 nm thick InN/450 nm thick irradiated template, D: 200 nm thick InN/700 nm thick irradiated template).

Figure 5.14 shows the FWHM of the PL measurement at 10 K of the InN samples. As mentioned previously, since Ar ion laser line at 514 nm was used, the laser penetration length in InN is considered to be about 200 nm^[4]. Therefore, it is possible to measure only the regrown InN region of the samples. For InN samples regrown on the irradiated template with thickness of 100, 200 and 450 nm (samples A, B and C), the FWHM obtained were as low as less than 30 meV, which can be considered to be high quality. On the other hand, for InN sample regrown on the irradiated template with thickness of 700 nm (sample D), the FWHM obtained was about 50 meV, which is almost similar to the InN sample regrown on flat template. This result is suggested to be related to the penetration length of Ar ion laser used for PL measurement. PL measurement in sample D which consists of only 200 nm thick regrown InN layer as shown in Fig. 5.13(d), is thought to include not only the regrown InN layer but also the irradiated InN template region, since the laser penetration length was about 200 nm.

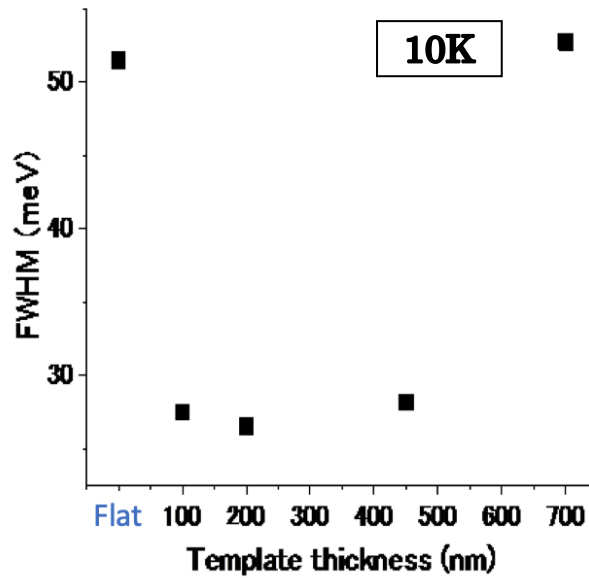


FIG. 5.14. FWHM of PL spectrum at 10 K of InN samples regrown on different thickness of irradiated InN template

5.3.3 Summary

In this section, we have tried to improve the crystallographic quality and electrical characteristics of the grown InN samples by varying the film thickness of the InN template. FWHM of X-ray rocking curves and carrier concentration for InN film regrown on the thinnest irradiated template i.e. 100 nm thick, improved more distinctly compared to InN films regrown on 200, 450 and 700 nm thick irradiated template, and showed good agreement with the results from TEM observation with edge threading dislocation density of $4.6 \times 10^9 \text{ cm}^{-2}$ in the regrown InN layer. In addition, since the FWHM of PL spectrums showed small values of less than 30 meV from the samples with the template thickness of 100 to 450 nm, threading dislocation is considered to be decreased regardless of the template thickness. These results suggest that this method is possible for reduction of threading dislocation density and confirmed the importance of minimizing the thickness of irradiated InN template to be as thin as possible for higher crystallographic quality. On the other hand, although the lowest carrier concentration obtained was $1.06 \times 10^{18} \text{ cm}^{-3}$ from the InN samples regrown on the 100 nm thick template, the mobility was not improved. Therefore, in the Hall effect measurement, analysis that consider the substrate interface, N radical beam irradiation interface and regrowth region is necessary. Comparison with KOH etching which introduces fewer point defects is also considered to be one effective means for these investigations.

5.4 Repeatability of in situ surface modification by radical beam irradiation to reduce threading dislocation density in InN

In Section 5.2, it was observed that threading dislocation density decreased the most when the N radical beam irradiation was performed at substrate temperature of 435 °C with plasma power of 200 W and irradiation time of 60 minutes. The FWHM in the PL measurement was also small indicating that the quality of the regrown InN layer was improved and showed good agreement with the results from TEM observation. We believe that further reduction of the threading dislocation density can be expected by re-irradiating N radical on the InN layer with reduced edge dislocation density and then regrowing another InN layer on top of it. This is one of the expected advantages of surface modification by in situ N radical beam irradiation compared to the KOH etching method as described in Section 4.1. Therefore, in this section, we investigated the repeatability of in situ surface modification by N radical beam irradiation to further reduce threading dislocation density in InN film and we show cross-sectional view TEM evidence of the two stages of threading dislocation reduction.

5.4.1 Experimental method

As in the previous chapter, InN samples were grown on MOCVD-grown (0001) GaN/sapphire substrate in a conventional RF-MBE system under the same conditions as shown in Table 4.2. The growth time chart is as shown in Fig. 5.15. After the substrate was inserted into the MBE growth chamber, (1) the substrate was thermally cleaned at 750 °C for 10 min. (2) Then, a thin GaN layer was deposited at 650 °C for 3 min. (3) Next, InN layer was grown at 435 °C for 30 min. (4) The InN layer was then irradiated with N radical beam at 435 °C with a N₂ gas supply of 2.0 sccm and plasma power of 200 W for 60 min. Steps (3) to (4) were then repeated. Finally, InN film was regrown on the irradiated template at 435 °C for 60 min. The growth rate was about 450 nm/h and the resultant total thickness of the sample was ~900 nm as shown in Fig. 5.16. In addition, another experiment with five repetitions of N radical irradiation process have also been carried out as shown in Fig. 5.17. In this experiment, in order to keep the total thickness of the sample constant at ~900 nm, the thickness of each irradiated InN layer was reduced to ~90 nm and the top regrown InN layer was kept constant at ~450 nm as shown in Fig. 5.18.

After the growth, TEM has been used to study dislocation behavior in the irradiated InN layers and the regrown InN film. Cross-sectional view specimens which is transparent for electrons with the thickness of ~ 100 nm have been prepared by FIB etching. A TEM with an accelerating voltage of 200 kV was used in these studies. The sample was characterized with diffraction vectors, $\mathbf{g}=1-100$ and $\mathbf{g}=0002$ to determine the edge-type dislocation and screw-type dislocation, respectively.

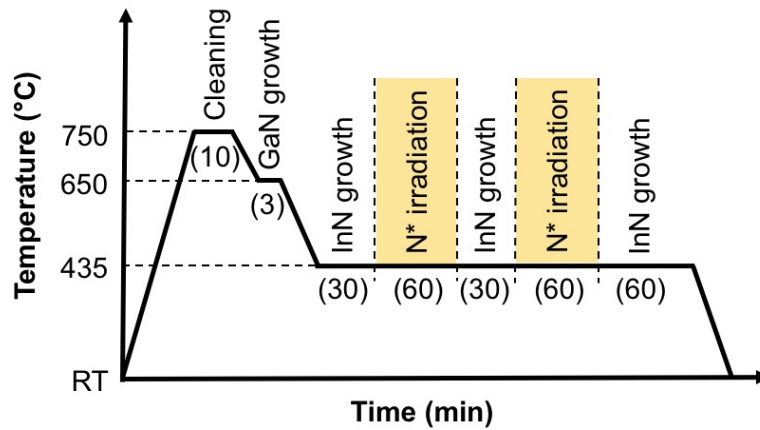


FIG. 5.15. Growth time chart (2 repetitions of N radical irradiation)

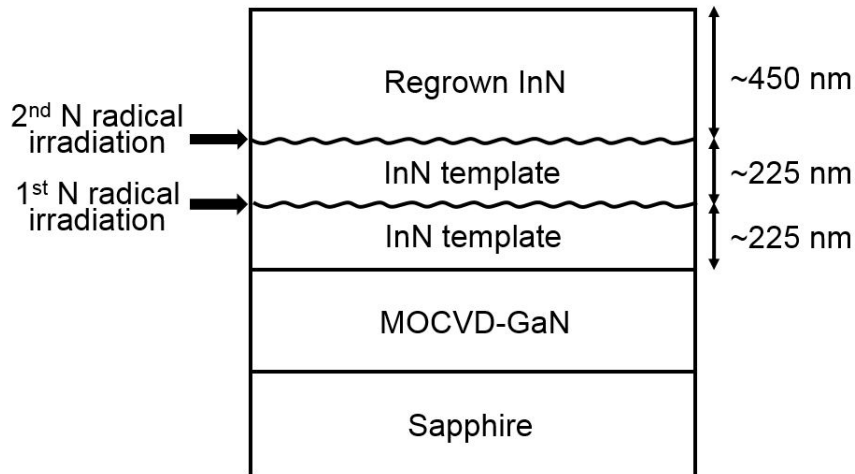


FIG. 5.16. Illustration of sample structure grown with in situ surface modification by radical beam irradiation method (2 repetitions of N radical irradiation)

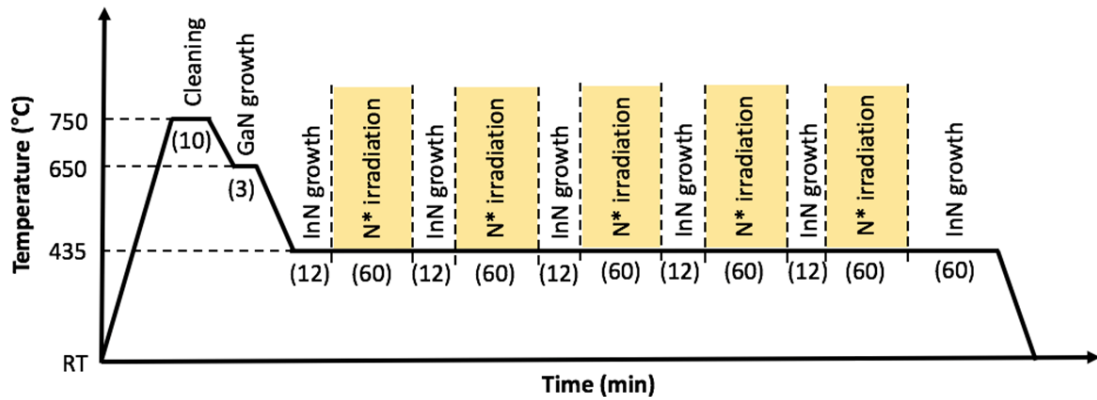


FIG. 5.17. Growth time chart (5 repetitions of N radical irradiation)

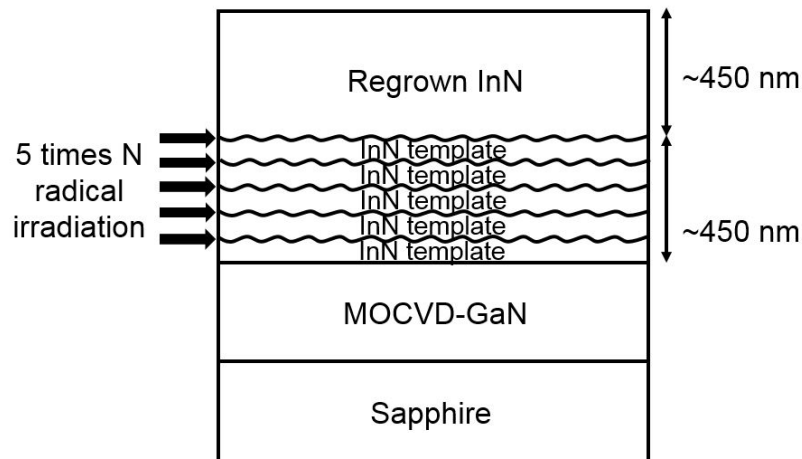


FIG. 5.18. Illustration of sample structure grown with in situ surface modification by radical beam irradiation method (5 repetitions of N radical irradiation)

5.4.2 Experimental results and discussion

Figure 5.19 shows a representative cross-sectional TEM image of InN grown with two repetitions of N radical irradiation. The thickness of the first irradiated InN layer was ~225 nm, the second irradiated InN layer was ~225 nm and the top regrown InN layer was 450 nm, as estimated from the TEM image. Note that threading dislocations are the only extended defect that grew through to the free surface of the InN layer. Threading dislocations observed in this figure should have the edge component as diffracton vector of TEM observation, $\mathbf{g}=1-100$. As can be seen, a high density of threading dislocations were generated at the interface of GaN and InN, and these dislocations propagated into

the InN layers. It is important to realize that these dislocations were clearly bent and some of them merged at the regrowth interfaces. The density of the edge dislocations in the first irradiated InN layer was estimated to be about $2.8 \times 10^{10} \text{ cm}^{-2}$. The dislocation density reduced step by step to about $2.0 \times 10^{10} \text{ cm}^{-2}$ in the second InN irradiated layer, and then to about $1.3 \times 10^{10} \text{ cm}^{-2}$ in the top regrown InN layer. This means that the two stages of threading reduction can be clearly observed. From the TEM observation results, clearly, repeating the N radical irradiation process on the InN template properly could further reduce threading dislocation density in the top regrown InN layer.

On the other hand, for the five repetitions of N radical irradiation, flat surface was not obtained starting from the second layer of the InN template as confirmed by in situ RHEED monitoring during growth process. As a consequence, the flat surface could not be obtained at the top regrown InN layer. Fig. 5.20 shows a cross-sectional TEM image of the grown InN sample. As can be seen, the interfaces between each irradiated layers and the regrown layer could not be identified. This phenomenon was also observed previously in the cross-sectional TEM images as shown in Figs. 5.13(a) and (b). What is common in these three samples is that the InN templates growth time are short. The templates of the samples in Figs. 5.13(a) and (b) were grown for 12 and 20 minutes, respectively. In the five repetitions of N radical irradiation experiment, each re-growth time of the template layers was also 12 minutes. These growth time were found to be less than the growth time of the template in the two repetitions of N radical irradiation experiment as shown in Fig. 5.15. Therefore, we considered that the reason why the irradiation interface could not be observed in the cross-sectional TEM image was probably due to the deterioration of the template surface morphology after the N radical irradiation since the thickness of each re-grown template layer was relatively thin.

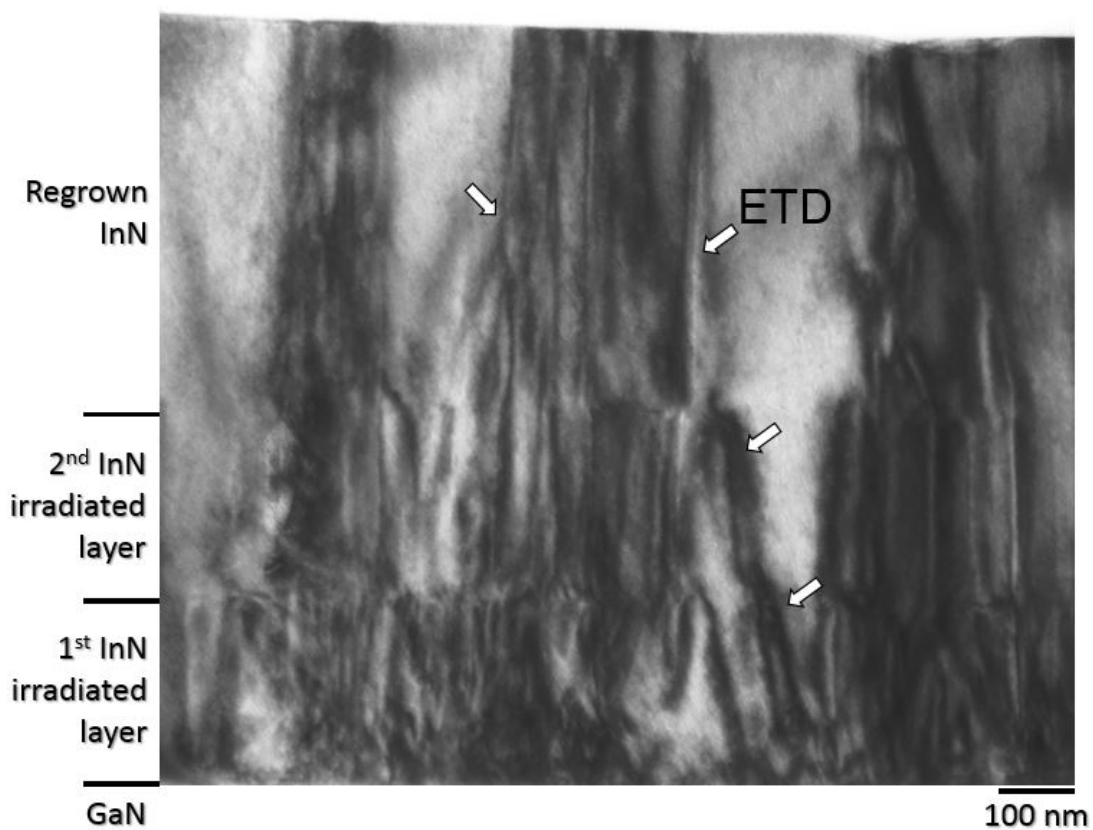


FIG. 5.19. Cross-sectional TEM image of InN sample grown with two repetitions of N radical irradiation ($g=1-100$)

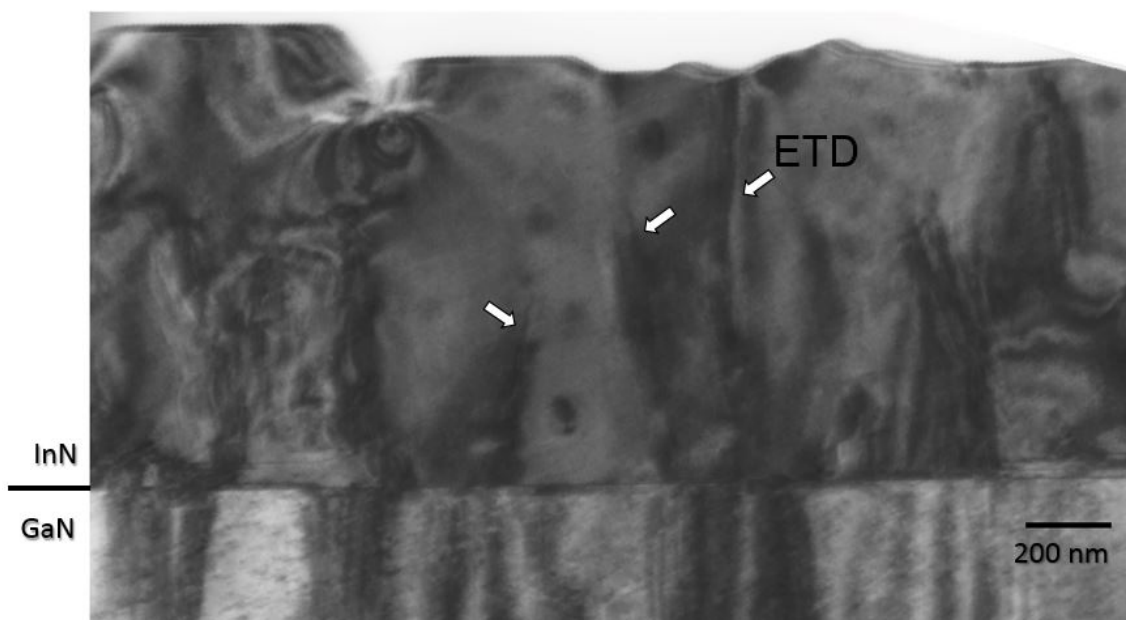


FIG. 5.20. Cross-sectional TEM image of InN sample grown with five repetitions of N radical irradiation ($g=1-100$)

Figure 5.21 shows electrical characteristics of the samples measured by Hall effect measurement. The carrier concentration tends to be slightly reduced or almost no difference in InN grown with two repetitions of N radical irradiation compared to the one repetition. However, the carrier concentration seems largely deteriorated to $3.2 \times 10^{18} \text{cm}^{-3}$ for the InN grown with five repetitions of N radical irradiation. Furthermore, as the number of N radical irradiation repetitions increased, the deterioration of mobility could also be seen. The mobility deteriorated from $1420 \text{cm}^2/\text{Vs}$ for the sample grown with one repetition to $1270 \text{cm}^2/\text{Vs}$ for the sample grown with two repetitions and then to $1020 \text{cm}^2/\text{Vs}$ for the sample grown with five repetitions of N radical irradiation.

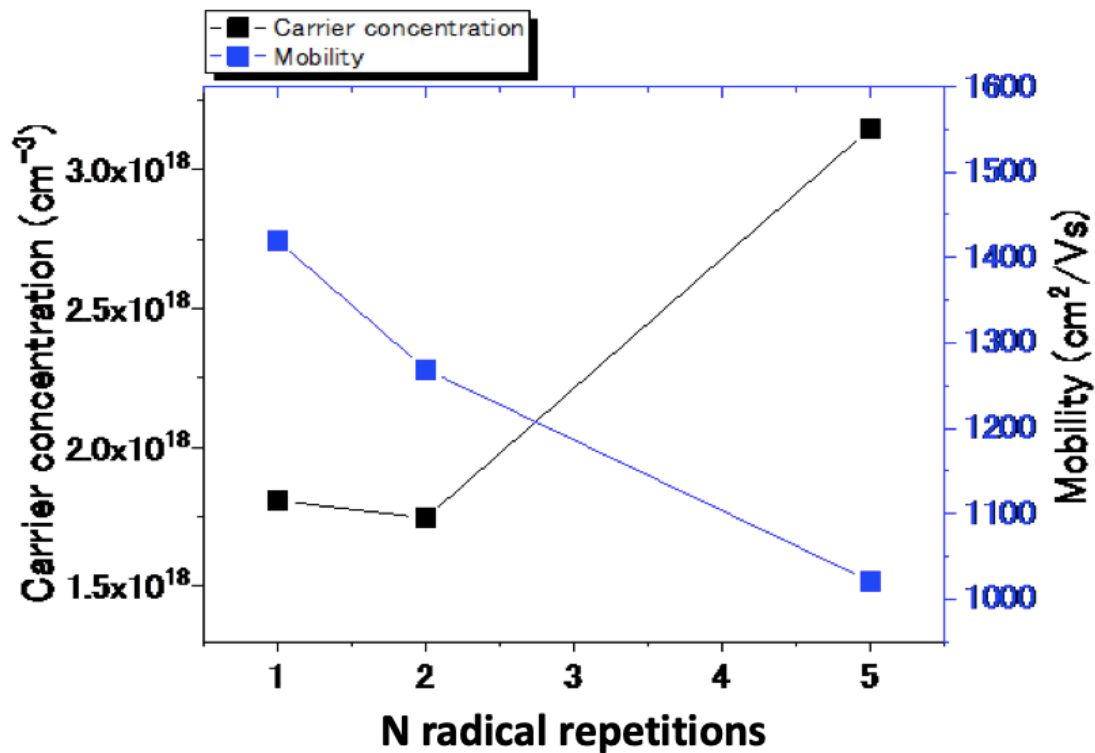


FIG. 5.21. Irradiation repeatability dependence of electrical characteristics

As described in previous Section 5.2.3, we suggested that these results are influenced by the interface of the regrown InN and the irradiated InN template since the Hall effect measurement values appear to have resulted from the average properties of the entire sample including the template. In addition, as described in Section 4.2.3, the carrier concentration was increased when the InN template was irradiated by N radical beam due to the introduction of point defects ^[16-18], and thus, it is considered that the irradiated interface vicinity has a high carrier concentration. Furthermore, formation of an amorphous layer by irradiation of N radical beam in InGaN has also been reported ^[19].

Although the structural analysis of the formation of the amorphous layer at the InN regrowth interface cannot be performed at this time, there might be a possibility of the formation of an amorphous layer. The amorphous layer has many dangling bonds and the layer is thought to increase scattering of electrons, which causes an increase in carrier concentration and a decrease in mobility. However, since the regrown InN region has a better crystalline quality, it seems that the formation of the amorphous layer may exist only in part of the sample. Last but not least, the InN sample grown with five repetitions of N radical irradiation in this experiment has a large deterioration in surface morphology as shown in Fig. 5.20 and Fig. 5.22(c), probably due to the failure of recovery to flat surface because of the short re-growth time of the templates after N radical irradiation. This also might influence the electrical properties obtained from the sample ^[8].

Next, Fig. 5.22 shows the AFM images and RMS values of the InN samples grown with one, two and five repetitions of N radical irradiation. The surface of InN grown with one repetition of N radical irradiation was relatively flat, and the RMS value obtained was 1.7 nm. However, it can be seen that the surface roughness increased as the number of irradiation repetition increased. The InN sample grown with two repetitions of N radical irradiation showed an RMS value of 2.6 nm while the InN sample with five repetitions showed an RMS value of 25.7 nm. As previously mentioned, this may be related to the thickness of regrown template layers. For two repetitions experiment, after the first N radical irradiation, regrowth of the template was performed for 30 minutes, and then the second N radical irradiation was performed. On the other hand, for the five repetitions experiment, regrowth of the template was performed only for 12 minutes and then the N radical beam irradiation was performed. As the regrowth time was shorter, the film thickness became thinner. It is considered that the surface roughness was accumulated because the N radical irradiation was performed in a state where a flat surface was not obtained on the film. Therefore, it is suggested that the optimum template thickness should also be taken into consideration before the N radical irradiation.

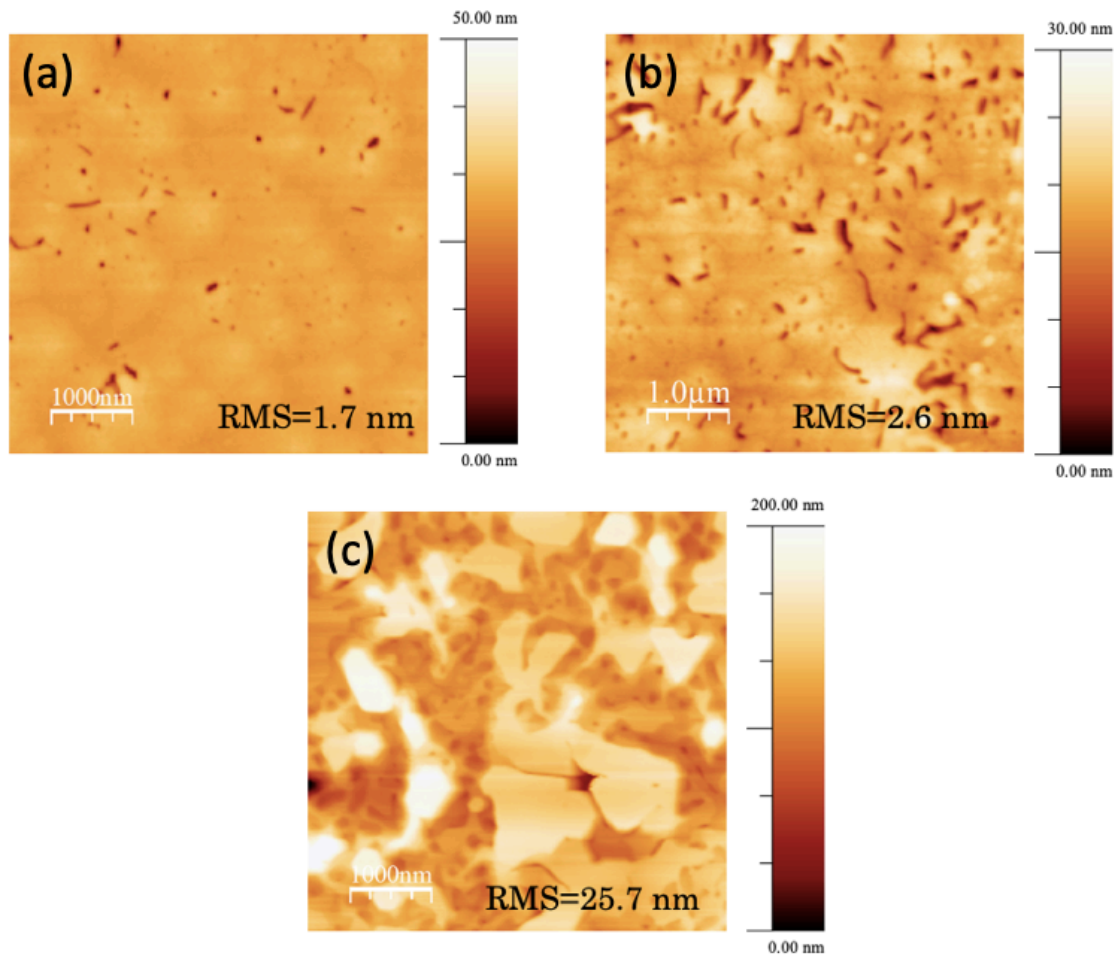


FIG. 5.22. Surface morphology of InN samples grown with (a) one (b) two and (c) five repetitions of N radical irradiation

5.4.3 Additional experiments

Additional thick InN growth experiments were performed to study the repeatability and limit of threading dislocation reduction with this method. The InN growth conditions are as shown in Table 5.3 and the InN growth rate in this experiment was 250 nm/h. Figure 5.23(a) shows an illustration of the thick InN film grown with in situ surface modification by radical beam irradiation while Fig. 5.23(b) shows an illustration of the thick InN film grown with conventional method (without in situ surface modification by radical beam irradiation) as for comparison. For sample (a), after the substrate was inserted into the MBE growth chamber, (1) the substrate was thermally cleaned at 750 °C for 10 min. (2) Then, a thin GaN layer was deposited at 650 °C for 3 min. (3) Next, InN layer was grown at 435 °C for an hour. (4) The InN layer was then irradiated with N radical beam at 435 °C with a N₂ gas supply of 2.0 sccm and plasma power of 200 W for an hour. Steps (3) to (4)

were then repeated six times. Finally, InN film was regrown on the irradiated template at 435 °C for an hour. For sample (b), the sample was regrown under the same condition but without N radical irradiation process for 8 hours.

TABLE 5.3. InN growth condition

Substrate temperature (°C)	435
In beam flux (Torr)	$1.36 \sim 1.40 \times 10^{-6}$
N ₂ flow (sccm)	2.0
Plasma power (W)	100

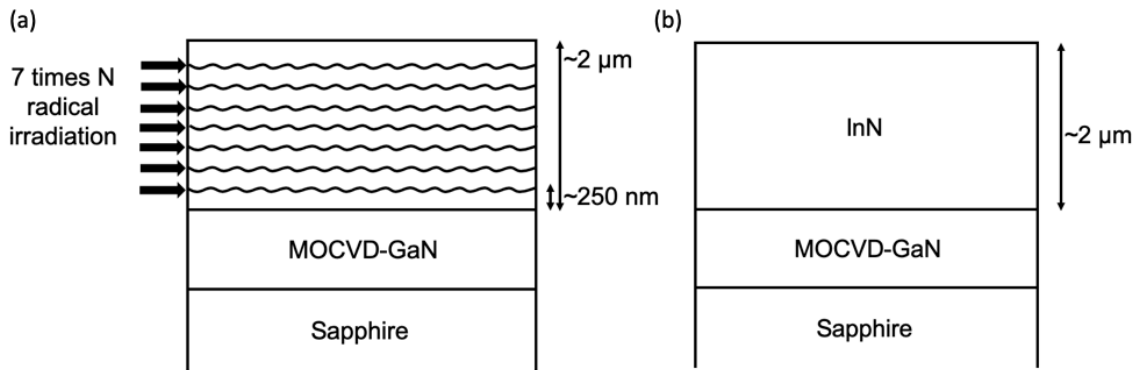


FIG. 5.23. Illustration of thick InN films grown (a) with seven repetitions of N radical irradiation (S2389), (b) without in situ surface modification (S2412)

RHEED patterns during the growth of sample (S2389) are as shown in Fig. 5.24. After the first InN layer was grown, streak pattern could be observed indicating that atomically flat surface was obtained. Next, after the N radical irradiation was performed on the first InN layer, the RHEED pattern changed to spotty streak pattern indicating that the layer surface was modified to three-dimensional structures. Then, after the second InN layer was regrown on the irradiated layer, streak RHEED pattern was regained indicating that the surface of the regrown layer was recovered to flat surface. Until the end of experiments, spotty streak patterns were obtained after each N radical irradiation process and streak patterns were regained after each InN regrowth process, indicating that the InN surface was modified after each N radical irradiation and the InN surface recovered to atomically flat at the end of the experiment. RHEED patterns during the growth of sample (S2412) are as shown in Fig. 5.25. 16 DERI cycles^[20] could be clearly observed and the RHEED pattern at the end of the growth process showed slightly streak pattern indicating that the surface morphology obtained was relatively flat.

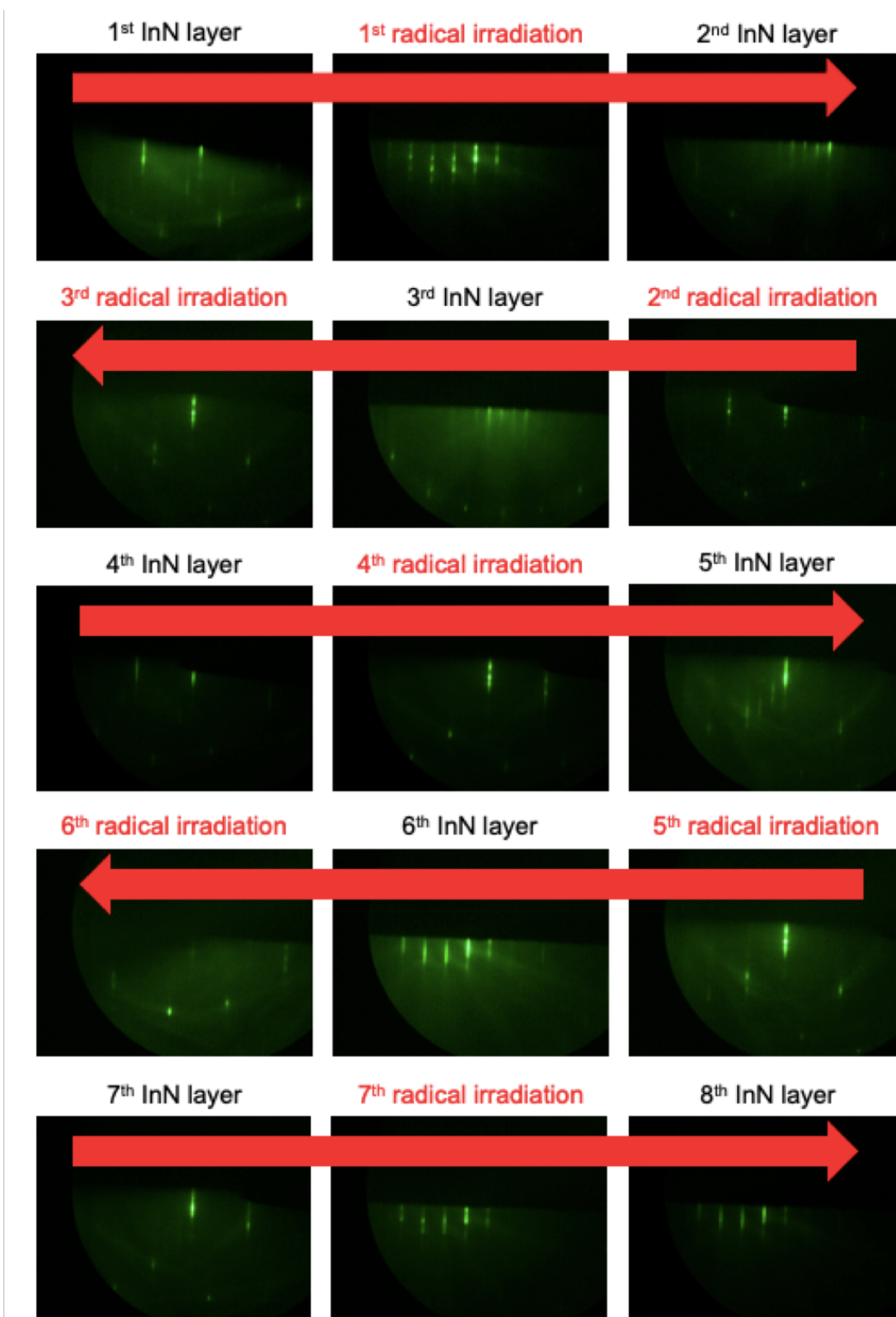


FIG. 5.24. RHEED patterns of InN grown with in situ surface modification by seven repetitions of N radical irradiation

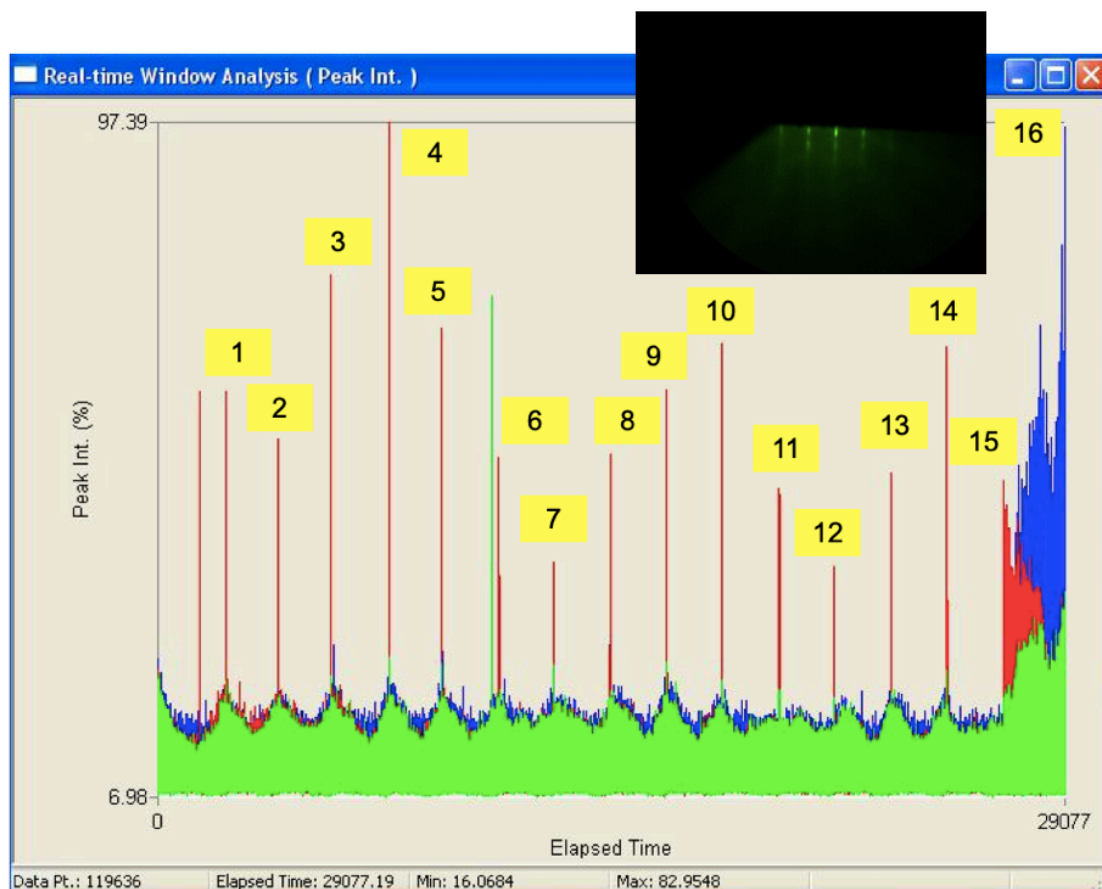


FIG. 5.25. DERI cycles ^[20] and RHEED pattern of conventionally grown InN film (without in situ surface modification)

SEM images of surface morphology obtained from both samples are as shown in Fig. 5.26. For sample (S2389), in spite of streak RHEED pattern was obtained, the surface morphology of the sample was not so flat but it has a better surface morphology compared to the results obtained from five times repetitions of N radical irradiation in the previous experiment as shown in Fig. 5.22(c). This might be the result of longer time of regrowth process performed in each layer in this experiment which allowed a better recovery of flat surface morphology to occur. For sample (S2412), as expected, atomically flat surface morphology was obtained. In addition, cross-sectional SEM image of sample (S2389) is as shown in Fig. 5.27. The thickness of the InN layer grown was confirmed to be around $\sim 2 \mu\text{m}$.

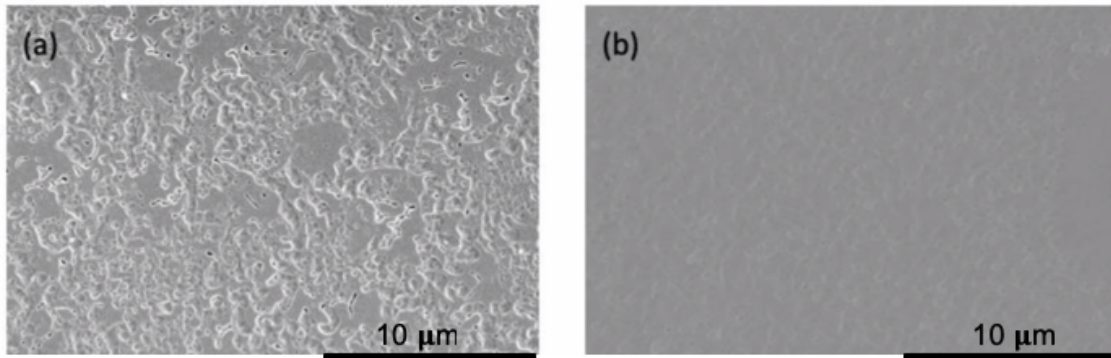


FIG. 5.26. SEM images (a) InN grown with in situ surface modification (S2389), (b) Conventional InN growth (S2412)

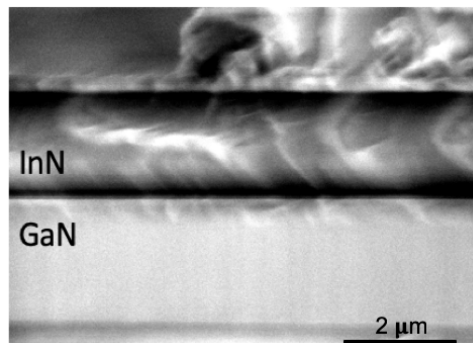


FIG. 5.27. Cross-sectional SEM image of sample (S2389)

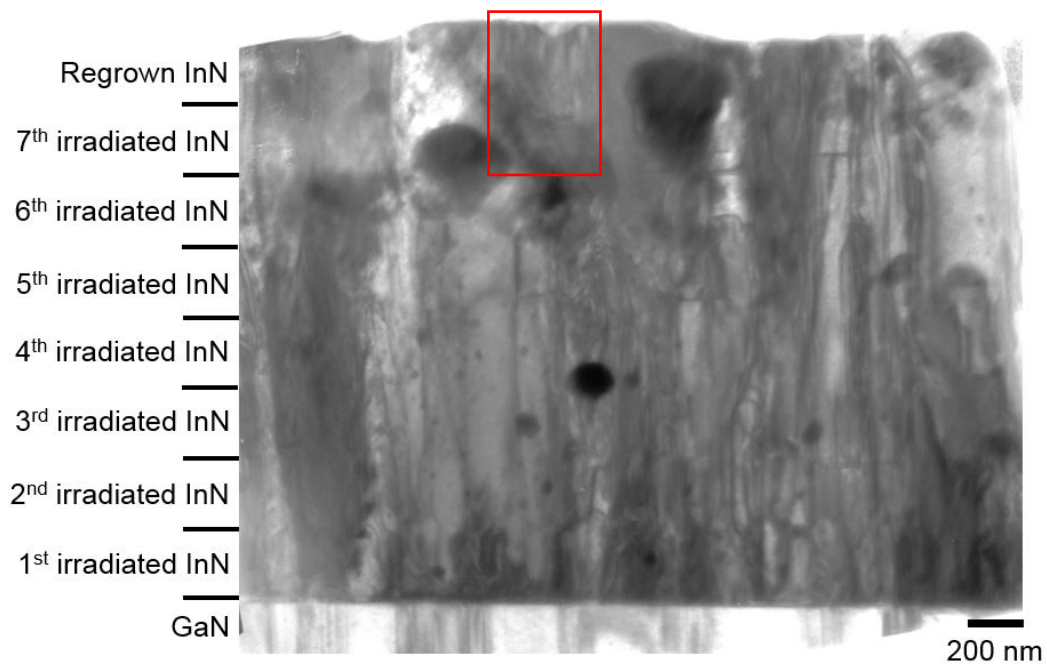


FIG. 5.28. Cross-sectional TEM image of sample (S2389) with $g=1-100$

Cross-sectional TEM image of sample (S2389) is as shown in Fig. 5.28. The interfaces of each N radical irradiated surfaces were predicted by the growth time of each layer. As can be seen, inclination of edge dislocation occurred repetitively at each interface. Several regions with less threading dislocations also can be seen clearly in the top regrown layer. Most of the threading dislocations annihilated at the interface of the first irradiated layer and the second irradiated layer. Threading dislocation density in the first irradiated layer was estimated to be around $2 \times 10^{10} \text{ cm}^{-2}$ and reduced to around $5 \times 10^9 \text{ cm}^{-2}$ in the top regrown layer. The estimated threading dislocation density in the top regrown layer could be lower than that if without the threading dislocations bunching as shown in the red rectangle in Fig. 5.28.

The results of XRD and Hall effect measurement of these samples compared to the samples in the previous experiments are as shown in Table 5.4. Both of these two samples showed a lower FWHM for both (002) and (302) reflections compared to previously experiments. It is well known that FWHM of (002) and (302) reflections correspond to tilt distributions and twist distributions respectively. For sample (S2412), this is assumed to be the result of lower threading dislocation density due to a thicker film of InN grown [21]. However, for sample (S2389), it showed a slightly lower FWHM for (002) reflection but an ultimately lower FWHM for (302) reflections compared to not only in the previous experiments but also to the sample (S2412). The FWHM of (302) which correspond to edge-type dislocation density of sample (S2389) was 1783 arcsec and it is the lowest value obtained so far in our study. This showed that the crystallographic quality of the InN film grown with in situ surface modification could be improved. On the other hand, there was no significant improvement on the electrical properties in both samples grown in this experiment. Variable temperature Hall effect measurement was also performed on both samples by varying the measurement temperature from around 100 K to 300 K, as shown in Fig. 5.29. For sample (S2389), the highest mobility obtained was $1510 \text{ cm}^2/\text{Vs}$ at 120 K and the lowest mobility obtained was $1300 \text{ cm}^2/\text{Vs}$ at 297 K. For sample (S2412), the highest mobility obtained was $1590 \text{ cm}^2/\text{Vs}$ at 133 K and the lowest mobility obtained was $1360 \text{ cm}^2/\text{Vs}$ at 297 K. Both samples showed similar trends of the change in mobility and no significant difference can be observed.

TABLE 5.4. Summary of results

Total film thickness (~ μm)	N radical repetitions (times)	XRC-FWHM		Hall effect measurement at RT	
		002 (arcsec)	302 (arcsec)	Carrier concentration (cm^{-3})	Mobility (cm^2/Vs)
1	0	390	2790	1.5×10^{18}	1520
	1	420	2810	1.8×10^{18}	1420
	2	410	2510	1.8×10^{18}	1270
	5	480	2730	3.2×10^{18}	1020
2	0 (s2412)	390	2370	1.1×10^{18}	1360
	7 (s2389)	380	1780	1.9×10^{18}	1300

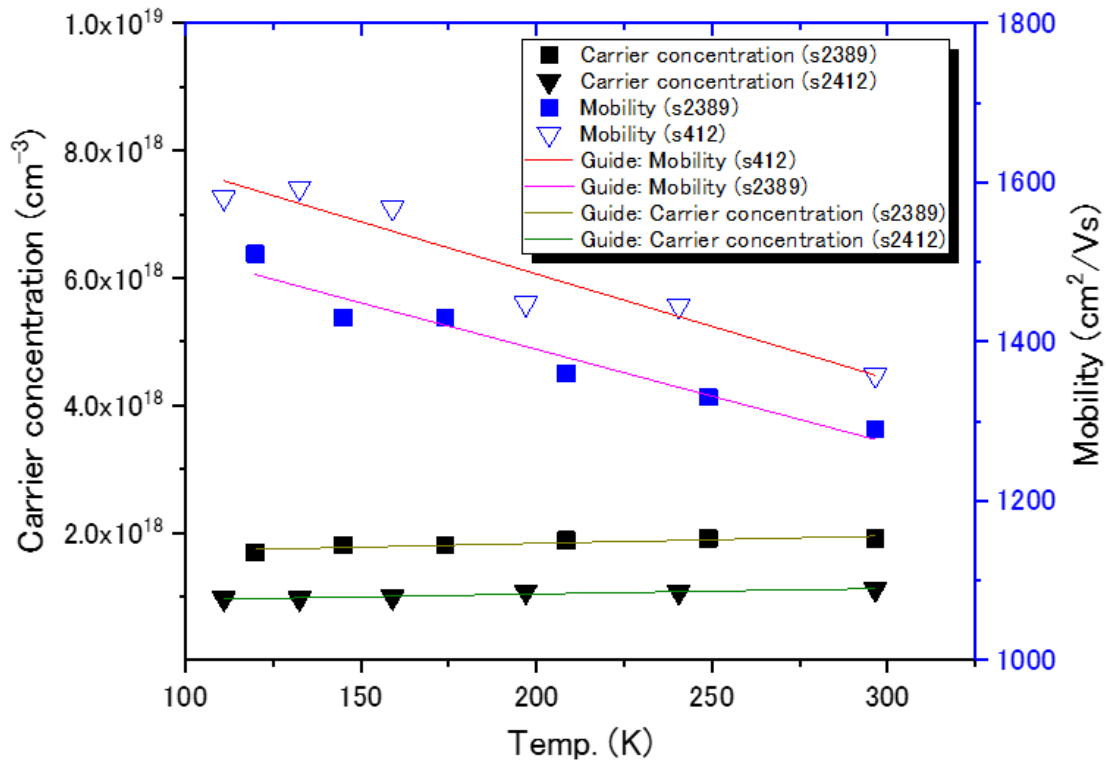


FIG. 5.29. Variable temperature Hall effect measurement of InN grown with in situ surface modification (s2389) and conventionally grown InN (s2412)

5.4.4 Summary

We have investigated the repeatability of in situ surface modification by N radical beam irradiation method to further reduce threading dislocation density in InN. InN films were grown with two, five and finally seven repetitions of N radical irradiation process. We showed cross-sectional view TEM evidence of the two stages of threading dislocation reduction for InN grown with two repetitions of N radical irradiation. However, for the five times repetitions, the interfaces between each irradiated layer and the regrown layer could not be identified and reduction of threading dislocation was difficult to be seen. We suggested that this might be due to the deterioration of the template after the N radical irradiation since the thickness of each regrown layer was relatively thin which is around 90 nm. Therefore, for seven repetitions, we increased the thickness of each layer to 250 nm and 2 μm thick InN was grown with in situ surface modification. For the thick InN growth, InN grown with in situ surface modification showed a large improvement in crystallographic quality measured by XRD compared to the conventionally 2 μm thick InN grown without in situ surface modification. The inclination of edge dislocation occurred repetitively at each interface and several regions with less threading dislocations also can be seen clearly in the top regrown layer of the sample.

5.5 Conclusion

In this chapter, firstly, InN growth with in situ surface modification by N radical irradiation under the same conditions but with different irradiation time was investigated. InN samples were regrown on the template irradiated under N radical irradiation time from 0 to 180 minutes and evaluated. TEM revealed that threading dislocation density in InN regrown on the template irradiated with plasma power of 200 W and substrate temperature of 435 °C for 60 minutes reduced from about $2 \times 10^{10} \text{ cm}^{-2}$ to $6 \times 10^9 \text{ cm}^{-2}$ in certain regions, and it is the smallest density obtained in this study. The result showed good agreement with the results from PL spectroscopy, although no obvious improvement was seen from XRD analysis and Hall effect measurement.

Secondly, we have tried to improve the crystallographic quality and electrical characteristics of the grown InN samples by varying the thickness of the irradiated template. FWHM of X-ray rocking curves and carrier concentration for InN film regrown on the thinnest irradiated template i.e. 100 nm thick, improved more distinctly compared to InN films regrown on 200, 450 and 700 nm thick irradiated template, and showed good agreement with the results from TEM observation with edge threading dislocation density of $4.6 \times 10^9 \text{ cm}^{-2}$ in the regrown InN layer. In addition, since the FWHM of PL spectrums showed a small value of less than 30 meV from the samples with the template thickness of 100 to 450 nm, threading dislocation density is considered to be decreased regardless of the template thickness. These results suggest that this method is possible for reduction of threading dislocation density and confirmed the importance of minimizing the thickness of irradiated InN template for higher crystallographic quality. On the other hand, although the lowest carrier concentration obtained was $1.06 \times 10^{18} \text{ cm}^{-3}$ from the InN samples regrown on the 100 nm thick template, the mobility was not improved.

Thirdly, we have investigated the repeatability of in situ surface modification by radical beam irradiation method to further reduce threading dislocation density in InN. InN films were grown with two, five and finally seven repetitions of N radical irradiation process. We showed cross-sectional view TEM evidence of the two stages of threading dislocation reduction for InN grown with two repetitions of N radical irradiation. For the five times repetitions, the interfaces between each irradiated layer and the regrown layer could not be identified and reduction of threading dislocation was difficult to be seen. We suggested that this might be due to the deterioration of the template after the N radical irradiation since the thickness of each regrown layer is relatively thin which is around 90

nm. Therefore, for seven repetitions, we increased the thickness of each layer to 250 nm and 2 μm thick InN was grown with in situ surface modification. The results showed a large improvement in crystallographic quality measured by XRD compared to the conventionally 2 μm thick InN grown without in situ surface modification and other samples in previous experiment. The inclination of edge dislocation occurred repetitively at each interface and several regions with less threading dislocations also can be seen clearly in the top regrown layer of the sample.

References

- [1] C. S. Gallinat, G. Koblmüller, F. Wu, and J. S. Speck, *J. Appl. Phys.* 107, 053517 (2010).
- [2] X. Wang, S.-B. Che, Y. Ishitani, and A. Yoshikawa, *Appl. Phys. Lett.* 90, 151901 (2007).
- [3] X. Wang, S. Liu, N. Ma, L. Feng, G. Chen, F. Xu, N. Tang, S. Huang, K. J. Chen, S. Zhou, and B. Shen, *Appl. Phys. Express* 5, 015502 (2012).
- [4] K. S. A. Butcher, M. Wintrebert-Fouquet, P. P. -T. Chen, H. Timmers, and S. K. Shrestha, *Mat. Res. Soc. Symp. Proc.* 6, 351 (2003).
- [5] T. Akagi, K. Kosaka, S. Harui, D. Muto, H. Naoi, T. Araki, and Y. Nanishi, *J. Electron. Mater.* 37, 603 (2008).
- [6] F. Chen, A. N. Cartwright, H. Lu, and W. J. Schaff, *Physica E*, 20, 308 (2004).
- [7] F. B. Abas, R. Fujita, S. Mouri, T. Araki, and Y. Nanishi, *Jpn. J. Appl. Phys.* 57, 035502 (2018).
- [8] F. B. Abas, R. Fujita, S. Mouri, T. Araki, and Y. Nanishi, *MRS Adv.* 3, 18, 931 (2018).
- [9] V. Lebedev, V. Cimalla, J. Pezoldt, M. Himmerlich, S. Krischok, J. A. Schaefer, O. Ambacher, F. M. Morales, J. G. Lozano, and D. Gonzalez, *J. Appl. Phys.* 100, 094902 (2006).
- [10] C. S. Gallinat, G. Koblmüller, and J. S. Speck, *Appl. Phys. Lett.* 95, 022103 (2009).
- [11] L. F. J. Piper, T. D. Veal, C. F. McConville, L. Hai, and W. J. Schaff, *Appl. Phys. Lett.* 88, 252109 (2006).
- [12] W. Walukiewicz, *Physica B* 302, 123 (2001).
- [13] X. Wang, S.-B. Che, Y. Ishitani, and A. Yoshikawa, *Appl. Phys. Lett.* 90, 151901 (2007).
- [14] P. D. C. King, T. D. Veal, and C. F. McConville, *J. Phys.: Condens. Matter* 21, 174201 (2009).
- [15] H. Lu, W. J. Schaff, L. F. Eastman, J. Wu, W. Walkiewicz, D. C. Look, and R. J. Molnar, *Mat. Res. Soc. Symp. Proc.* 743, L4.10.1 (2003).
- [16] A. R. Arehart, C. Poblenz, J. S. Speck, and S. A. Ringel, *J. Appl. Phys.* 107, 054518 (2010).
- [17] S. X. Li, K. M. Yu, J. Wu, R. E. Jones, W. Walukiewicz, J. W. Ager III, W. Shan, E. E. Haller, H. Lu, and W. J. Schaff, *Phys. Rev. B* 71, 161201 (2005).
- [18] R. E. Jones, S. X. Li, E. E. Haller, H. C. M. van Genuchten, K. M. Yu, J. W. Ager, Z. Liliental-Weber, W. Walukiewicz, H. Lu, and W. J. Schaff, *Appl. Phys. Lett.* 90, 162103 (2007).
- [19] J. Xue, Q. Cai, B. Zhang, M. Ge, D. Chen, J. Zheng, T. Zhi, Z. Tao, J. Chen, L. Wang, R. Zhang, and Y. Zheng, *Appl. Surf. Sci.* 423, 219 (2017).
- [20] T. Yamaguchi, and Y. Nanishi, *Appl. Phys. Express* 2, 051001 (2009).
- [21] X. Wang, S. Liu, N. Ma, L. Feng, G. Chen, F. Xu, N. Tang, S. Huang, K. J. Chen, S. Zhou,

Chapter 5 InN growth with in situ surface modification by radical beam irradiation (2)

and B. Shen, Appl. Phys. Express 5, 015502 (2012).

Chapter 6

Summary

This dissertation was devoted to investigating the applicability of InN growth with in-situ surface modification by RF-MBE to reduce threading dislocation density in InN film. In this section, each chapter in this dissertation are summarized.

Since we are living in a phenomenal time of electronics era, the development of new materials is required to support our modern society in various applications fields. InN and its related alloys of group III-nitride semiconductors is a very promising material for various applications ranging from electronic devices to optical devices. However, the hetero-epitaxial InN films have an extremely high density of threading dislocations (10^{10} – 10^{11} cm⁻²) which leads to high residual carrier concentration and low mobility and thus, hindered the realization of InN-based device applications. Therefore, in this research, a new approach which provides a simple but effective growth process for threading dislocation reduction in InN film, “InN growth with in situ surface modification by radical beam irradiation” was studied. The surface modification of InN film and its effect on threading dislocation behaviors, surface morphology, electrical characteristics and optical properties were investigated.

Details of each chapter are described below.

In Chapter 1, we described the expectations for III-nitride semiconductors in our modern society and the attractive features of InN. Furthermore, the issues of threading dislocation density in InN and the purpose of this research were also discussed.

In chapter 2, we described the features of RF-MBE method used in this study. In addition, crystal growth technique for nitride semiconductors and InN were also discussed.

In chapter 3, we described the principles and features of equipment used in the characterization and evaluation of the samples grown in this study.

In chapter 4, we studied the in situ surface modification of InN templates by N radical beam irradiation and regrowth of InN on the irradiated templates. The results

obtained are summarized as follows.

For in situ surface modification of InN template, the substrate temperature, plasma power, and irradiation time were varied, and the change in surface morphology and the influence on electrical characteristics were examined. It was revealed that the substrate temperature during the N radical irradiation plays an important role for surface modification and the surface morphology changed to a three-dimensional structure at 435 °C. The influence on electrical characteristics was depending on the plasma power, and the carrier concentration was largely increased with a plasma power of 600 W, suggesting a higher introduction of point defects. Furthermore, as the irradiation time increased, the surface morphology and the electrical characteristics tended to deteriorate. In addition, as a result from comparison with annealing, it was found that N radical beam irradiation suppresses thermal decomposition of InN and considered to be an effective method for surface modification of InN.

For regrowth of InN on the irradiated templates, the effect on threading dislocation behaviors was investigated using cross-sectional TEM. Bending and disappearance of edge dislocation was observed at the regrowth interface in the sample grown on the template irradiated with plasma power of 200 W and substrate temperature of 435 °C for 60 minutes. The edge dislocation density reduced by a factor of 3 from about 2×10^{10} to 6×10^9 cm⁻² in the regrown InN region. The annihilation of dislocations is likely to be initiated by dislocations bending at the onset of InN regrowth and not right after the N radical beam irradiation on the InN template. The mechanisms of threading dislocation reduction were also discussed.

In Chapter 5, we investigated InN growth with in situ surface modification under different N radical irradiation time, InN growth on different thickness of irradiated template, and the repeatability of the proposed method. The results obtained are summarized as follows.

For InN growth with in situ surface modification under different N radical irradiation time, N radical was performed for 0 to 180 minutes before the regrowth of InN film. For the sample regrown on non-irradiated template, edge dislocations propagated straightforwardly up to the surface, and the dislocation density was found to be around 10^{10} cm⁻². On the other hand, bending and annihilation of edge dislocations were observed for the sample regrown on the templates irradiated for 30 to 180 minutes. The samples also showed a small value of PL spectrum FWHM about 30 meV, and thus clarified that the quality in the regrown region was improved.

Next, for InN growth on different thickness of irradiated template, four samples

were prepared and the crystallographic quality and electrical properties obtained were compared. FWHM of X-ray rocking curves and carrier concentration for InN film regrown on the thinnest irradiated template i.e. 100 nm thick, improved more distinctly compared to InN films regrown on 200, 450 and 700 nm thick irradiated template, and showed good agreement with the results from TEM observation with edge threading dislocation density of $4.6 \times 10^9 \text{ cm}^{-2}$ in the regrown InN layer. In addition, since the FWHM of PL spectrums showed a small value of less than 30 meV from the samples with the template thickness of 100 to 450 nm, threading dislocation is considered to be decreased regardless of the template film thickness.

For the repeatability of the proposed method to further reduce threading dislocation density, InN films were grown with two, five and seven repetitions of N radical irradiation process. We showed cross-sectional view TEM evidence of the two stages of threading dislocation reduction for InN grown with two repetitions of N radical irradiation. For the five times repetitions, the interfaces between each irradiated layer and the regrown layer could not be identified and reduction of threading dislocation was difficult to be seen. We suggested that this might be due to the deterioration of the template after the N radical irradiation since the thickness of each regrown layer is relatively thin which is around 90 nm. Therefore, for seven repetitions, we increased the thickness of each layer to 250 nm and 2 μm thick InN was grown. The results showed a large improvement in crystallographic quality compared to the conventionally grown 2 μm thick InN and other samples in the previous experiments, but no significant changes in electrical properties measured by Hall effect measurement was observed.

Expectation for the future

We have confirmed that InN growth with in situ surface modification by N radical irradiation is applicable for reducing threading dislocations. Further investigation on the N radical irradiation conditions should be carried out in order to further reduce the threading dislocations density and at the same time, to improve the electrical characteristic of InN grown with this method. We hope that this research will contribute to further reduction of threading dislocation density in InN and thus open up new possibilities in realization of future optoelectronic and electronic device applications.

Research achievements

Scientific journals publication

- [1] Faizulsalihin Bin Abas, Ryoichi Fujita, Shinichiro Mouri, Tsutomu Araki and Yasushi Nanishi, “*Threading Dislocation Reduction in InN Grown with in situ Surface Modification by Radical Beam Irradiation*”, Japanese Journal of Applied Physics, **57**, 035502 (2018).
- [2] Faizulsalihin Bin Abas, Ryoichi Fujita, Shinichiro Mouri, Tsutomu Araki and Yasushi Nanishi, “*Reduction of Threading Dislocation Density in InN Film Grown with in situ Surface Modification by Radio-frequency Plasma-excited Molecular Beam Epitaxy*”, MRS Advances **3**, 18, 931 (2018).

International conference presentation

- [1] Faizulsalihin Bin Abas, Ryoichi Fujita, Shinichiro Mouri, Tsutomu Araki, Yasushi Nanishi, “*Effects of Nitrogen Radical Irradiation on InN Growth by RF-MBE*”, International Symposium on Growth of III-Nitrides (ISGN-7), Warsaw University, Warsaw, Poland (2018).
- [2] Faizulsalihin Bin Abas, Ryoichi Fujita, Shinichiro Mouri, Tsutomu Araki, Yasushi Nanishi, “*Epitaxial InN Growth with in situ Surface Reformation by Radical Beam Irradiation*”, International Symposium on Advanced Plasma Science and its Applications for Nitrides and Nanomaterials/International Conference on Plasma-Nano Technology & Science (ISPlasma/IC-PLANTS), Meijo University, Nagoya, Aichi, Japan (2018).
- [3] Faizulsalihin Bin Abas, Ryoichi Fujita, Shinichiro Mouri, Tsutomu Araki, Yasushi Nanishi, “*Reduction of Threading Dislocation Density in InN Film Grown with in situ Surface Reformation by Radio-frequency Plasma-excited Molecular Beam Epitaxy*”, Materials Research Society (MRS) Fall Meeting & Exhibit, Hynes Convention Center & Sheraton Boston Hotel, Boston, Massachusetts, U.S.A. (2017).
- [4] Faizulsalihin Bin Abas, Ryoichi Fujita, Shinichiro Mouri, Tsutomu Araki, Yasushi Nanishi, “*Threading Dislocation Behavior in InN Grown with In-situ Surface Reformation by Radical Beam Irradiation*”, 29th International Conference on Defects in Semiconductors (ICDS), Kunibiki Messe, Shimane Prefectural Convention Center, Matsue, Shimane, Japan (2017).

Domestic conference presentation

- [1] Faizulsalihin Bin Abas, Hirokazu Omatsu, Ryoichi Fujita, Shinichiro Mouri, Tsutomu Araki, Yasushi Nanishi, “*InN growth with in situ surface modification*”, 11th Joint Workshop of Nitride Semiconductors Growth and Characterization, Ritsumeikan Univ., Japan, Sept. 13-14 (2018).
- [2] Faizulsalihin Bin Abas, Ryoichi Fujita, Shinichiro Mouri, Tsutomu Araki and Yasushi Nanishi, “*Threading Dislocations Behavior in InN Films Regrown on N Radical Irradiated InN Template*”, The 36th Electronic Materials Symposium, Nagahama Royal Hotel, Shiga, Japan, Nov. 8-11 (2017).
- [3] Faizulsalihin Bin abas, Ryoichi Fujita, Nur Liyana Binti Zainol Abidin, Shinichiro Mouri, Tsutomu Araki, Yasushi Nanishi, “*The Reduction of Threading Dislocation Density in InN by Radical-beam Irradiation*”, Ritsumeikan University IEEE Student Branch English Presentation, Shiga, Japan, Oct. 20 (2017).
- [4] Faizulsalihin Bin Abas, Ryoichi Fujita, Shinichiro Mouri, Tsutomu Araki, Yasushi Nanishi, “*Dislocation Reduction in InN Film Grown with in situ Surface Reformation by Radical Beam Irradiation*”, The 10th Joint Workshop of Nitride Semiconductors Growth and Characterization, Ritsumeikan Univ., Japan, Sept. 13-15 (2017).
- [5] Faizulsalihin Bin Abas, Ryoichi Fujita, Shinichiro Mouri, Tsutomu Araki, Yasushi Nanishi, “*Dislocation Reduction in InN Film Grown with in situ Surface Modification by Radical Beam Irradiation*”, The 78th Japan Society of Applied Physics (JSAP) Fall Meeting, Fukuoka Convention Center, Fukuoka, Japan Sept. 5-8 (2017).
- [6] Faizulsalihin Bin Abas, Nur Liyana Binti Zainol Abidin, Ryoichi Fujita, Shinichiro Mouri, Tsutomu Araki, Yasushi Nanishi, “*TEM Study of InN Films Grown with In-situ Surface Reformation by Radical Beam Irradiation*”, The 64th Japan Society of Applied Physics (JSAP) Spring Meeting, Pacifico Yokohama, Kanagawa, Japan, March 14-17 (2017).
- [7] Hirokazu Omatsu, Faizulsalihin Bin abas, Ryoichi Fujita, Shinichiro Mouri, Tsutomu Araki, Yasushi Nanishi, “*In-situ Surface Modification of InN Films by Nitrogen Radical Irradiation and Thermal Annealing*”, The 37th Electronic Materials Symposium, Nagahama Royal Hotel, Shiga, Japan, Oct. 10-12 (2018).
- [8] Ryoichi Fujita, Faizulsalihin Bin Abas, Atsushi Katagiri, Shinichiro Mouri, Tsutomu Araki, Yasushi Nanishi, “*In-situ Surface Modification of InN by N radical Beam Irradiation*”, The 9th Nanostructure/Epitaxial Growth Meeting, Hokkaido University, Hokkaido, Japan, July 13-15 (2017) [in Japanese].
- [9] Ryoichi Fujita, Faizulsalihin Bin Abas, Nur Liyana Binti Zainol Abidin, Shinichiro Mouri, Tsutomu Araki, Yasushi Nanishi, “*Effect of In-situ Surface Reformation by N Radical Beam Irradiation on InN Growth*”, The 64th Japan Society of Applied Physics (JSAP) Spring Meeting, PACIFICO Yokohama, Kanagawa, Japan, March 14-17 (2017) [in Japanese].

- [10] Ryoichi Fujita, Faizulsalihin Bin Abas, Nur Liyana Binti Zainol Abidin, Shinichiro Mouri, Tsutomu Araki, Yasushi Nanishi, “*The Reduction of Threading Dislocation Density in InN by Radical-beam Irradiation*”, Ritsumeikan University IEEE Student Branch English Presentation, Shiga, Japan, Oct. 7 (2016).

Honors and Awards

- [1] Best Presentation Award, International Symposium on Advanced Plasma Science and its Applications for Nitrides and Nanomaterials / International Conference on Plasma-Nano Technology & Science (ISPlasma/IC-PLANTS) (2018).
- [2] Excellent Award, Ritsumeikan University Research Proposal Contest (2017).
- [3] Excellent Award, Ritsumeikan University IEEE Student Branch English Presentation (2017).
- [4] International Conference Paper Presentation Grant from The NEC C&C Foundation (2017).
- [5] GAKKAI Scholarships from Ritsumeikan University (2014~2018).
- [6] Yayasan Pelajaran MARA Scholarship for Doctoral Program (2016-2019).
- [7] Advanced TEM characterization and TEM sample preparation training course sponsored by Nanotech Career-up Alliance (CUPAL) at National Institute of Materials Science (NIMS), Tsukuba, Japan (2017).
- [8] TEM training course of Nanotechnology Platform Program by Japan Science and Technology Agency at Tokyo University, Japan (2016).
- [9] Research Presentation Excellent Award, Ritsumeikan University (2016).
- [10] Yayasan Pelajaran MARA Scholarship for Master’s Program (2014-2016).
- [11] Yayasan Pelajaran MARA Scholarship for Japanese Associate Degree Program (2009-2014).

Acknowledgements

Firstly, I would like to express my sincere gratitude to my advisor Prof. Dr. Tsutomu Araki for the continuous support of my Ph.D study and related research, for his patience, motivation, and immense knowledge. His guidance helped me in all the time of research and writing of this thesis. I could not have imagined having a better advisor and mentor for my Ph.D study.

Besides my advisor, I would like to thank the rest of my thesis committees: Prof. Dr. Shigeru Imai and Prof. Dr. Takashi Minemoto for their support and assistance for the examination and public hearing of this doctoral thesis.

My sincere thanks also go to Emeritus Prof. Dr. Yasushi Nanishi, Associate Prof. Dr. Shinichiro Mouri, Visiting Prof. Takashi Fujii and Dr. Junjiro Kikawa for their insightful comments and encouragement, but also for the hard questions during our lab research progress meetings which incited me to widen my research from various perspectives.

I am very much indebted to Yayasan Pelajaran MARA (Malaysia) for their financial support for my doctoral study, and Ritsumeikan University for providing research facilities and sponsorships for me to present my research works at domestic/international conferences in Japan, U.S.A., Poland, Czech Republic, and Portugal.

I thank my fellow labmates for the stimulating discussions, for the sleepless nights we were working together before deadlines, and for all the fun we have had in the last three years. In particular, I am grateful to Mr. Ryoichi Fujita and Mr. Hirokazu Omatsu. Without their precious support, it would not be possible to conduct this research.

Last but not the least, I would like to thank my family: my wife, my parents and to my brothers and sisters for supporting me emotionally and spiritually throughout writing this thesis and my life in general.

Above all, I owe it all to Almighty God for granting me the wisdom, health and strength to undertake this research task and enabling me to its completion.

This research work was supported by Japan Society for the Promotion of Science (JSPS) Grants-in-Aid for Scientific Research (KAKENHI) Grant Numbers JP16H03860, JP16H06415, and JP15H03559 and SEI Group CSR Foundation.

